

DA C: 429.5  
60  
1979  
④

ANOMALOUS ANALYZING POWERS FOR STRONG  
(p,t) GROUND-STATE TRANSITIONS

by

SHUICHIRO KUNORI

Dissertation submitted to the Faculty of the Graduate School  
of the University of Tsukuba in partial fulfilment  
of the requirements for the degree of  
Doctor of Science  
January, 1980

## ABSTRACT

Strong ground-state (p,t) transitions in nuclei of neutron number  $\approx 50-82$  are found to show anomalous analyzing powers which cannot be reproduced by direct one-step distorted-wave Born-approximation calculations at all. The anomalies are explained as an interference between (p,d) (d,t) sequential processes and the one-step process. The cross section of the sequential processes is as large as that of the one-step process in the  $L=0$  (p,t) reactions. The neutron-number dependence of the anomalies is interpreted.

## CONTENTS

Chapter 1	Introduction.....	1
Chapter 2	Experimental Procedures.....	4
Chapter 3	Experimental Results.....	7
Chapter 4	Analyses in Terms of the First- and Second-Order Distorted-Wave Born-Approximation (DWBA).....	9
4.1	Formalism for the first- and second-order DWBA.....	10
4.2	Definition of analyzing power.....	18
4.3	BCS wave function.....	21
4.4	Spectroscopic amplitude.....	24
4.5	Procedure for calculations.....	27
4.6	Results of analyses.....	30
Chapter 5	Discussion.....	35
5.1	Isotope dependence of the analyzing power.....	35
5.2	Effect of the imaginary part of the deuteron optical potential.....	37
5.3	Effect of the spin-orbit terms of the optical potentials.....	39
5.4	Finite-range effect.....	41
5.5	Effect of the non-orthogonality term.....	43
5.6	Effect of inelastic two-step processes.....	44
5.7	Absolute values of the cross sections.....	46
Chapter 6	Conclusion.....	48
	Acknowledgements.....	50
	References.....	51

Tables

Figure captions

Figures

Appendix 1	Expression for the $A(\theta)$ in terms of the reduced amplitude $B$ .....	A - 1
Appendix 2	Derivative relation between the $A(\theta)$ and $\sigma(\theta)$ .	A - 4
Appendix 3	Numerical values of experimental analyzing powers and cross sections.....	A - 9

## Chapter 1 Introduction

The two-nucleon transfer reaction (p,t) and/or (t,p) has been recognized to be a very useful method in obtaining nuclear structure information, particularly on the correlations of the transferred pair in the nucleus. Actually, by using this reaction, collective modes associated with the pair correlations were observed and identified as BCS states<sup>1)</sup> in the ground states of medium- and heavy-mass nuclei.

So far most of the studies of two-nucleon transfer reactions have been carried out by measuring differential cross sections  $\sigma(\theta)$  for (p,t) and/or (t,p) transitions. Angular distributions of the cross sections  $\sigma(\theta)$  for these transitions between  $0^+$  ground states ( $0_g^+$ ) of medium- and heavy-mass nuclei are known to have diffractive patterns<sup>2)</sup> which can be explained by a direct transfer of two neutrons in a  $^1S_0$  state on the basis of the first-order distorted-wave Born approximation (DWBA) theory<sup>3-5)</sup>. In addition to the cross sections  $\sigma(\theta, 0_g^+)$ , vector analyzing powers  $A(\theta, 0_g^+)$  for the (t,p) ground-state transitions have been analyzed so far by the method of the first-order DWBA<sup>6)</sup> because anomalous analyzing powers  $A(\theta, 0_g^+)$  which are far beyond the predictions by this method have not been reported in two-neutron transfer experiments.

The present work, however, reports for the first time the existence of anomalous angular distributions of  $A(\theta, 0_g^+)$  for (p,t) reactions which cannot be reproduced by the first-order DWBA calculations at all. This work is the first

systematic study of analyzing powers for (p,t) ground-state transitions between medium-mass nuclei having neutron number of  $N \approx 50-82$ . So far published works of (p,t) analyzing power measurements for medium- and heavy-mass nuclei have been only the following two reactions:  $^{176}\text{Yb}(\vec{p},t)^{174}\text{Yb}$  at  $E_p = 16 \text{ MeV}$ <sup>7)</sup> and  $^{208}\text{Pb}(\vec{p},t)^{206}\text{Pb}$  at  $E_p = 40 \text{ MeV}$ <sup>8)</sup>.

From the definition of analyzing powers  $A(\theta)$  and cross sections  $\sigma(\theta)$  in terms of transition amplitudes (see eqs. 33 and 41 in chapter 4), it is obvious that an interference effect between various transition processes in (p,t) reactions plays a more dominant role in the analyzing powers than in the corresponding cross sections. As a consequence, measurements of analyzing powers for (p,t) reactions are of fundamental importance in understanding the reaction dynamics such as a competition between a one-step process and multistep processes in the (p,t) transitions.

In the present work, the analyzing powers  $A(\theta, 0_g^+)$  and cross sections  $\sigma(\theta, 0_g^+)$  for the ground-state transitions to fifteen nuclei of  $^{98,100,102}\text{Ru}$ ,  $^{102,104,106,108}\text{Pd}$ ,  $^{110,112,114}\text{Cd}$ ,  $^{116}\text{Sn}$ ,  $^{120,126,128}\text{Te}$  and  $^{142}\text{Nd}$  have been measured by using a polarized proton beam of  $E_p = 22.0 \text{ MeV}$ .

In Chapter 2, experimental procedures are described. In Chapter 3, experimental data of  $A(\theta, 0_g^+)$  and  $\sigma(\theta, 0_g^+)$  for the (p,t) reactions on the fifteen targets are given. Characteristic features of these experimental results are described. The anomalous analyzing powers  $A(\theta, 0_g^+)$  appear in the angular distributions around  $\theta \approx 20^\circ$  where the  $\sigma(\theta, 0_g^+)$  have a deep minimum.

The anomalies display distinguishable change in going one nucleus to the other. Chapter 4 is devoted to the theoretical analysis of the data by means of the first-order and  $(p,d)$   $(d,t)$  second-order DWBA. The anomalies can be accounted for as an interference effect between the  $(p,d)$   $(d,t)$  sequential processes and the direct one-step process. Chapters 5 and 6 are devoted to discussions and conclusion, respectively.

The essential point of the present results has been published in Phys. Rev. Letters (ref. 9).

## Chapter 2 Experimental Procedures

A polarized proton beam was accelerated with the University of Tsukuba 12 UD Pelletron at  $E_p=22.0$  MeV. The polarized beam was produced with a Lamb-shift-type ion source<sup>10)</sup>. The layout of the beam preparation system is illustrated in Fig. 1. The beam intensity on target was about 100 nA within a diameter of 2 mm. Emitted tritons were momentum analyzed with an ESP-90 magnetic spectrograph<sup>11)</sup> and detected with silicon position-sensitive detectors mounted in the focal plane.

The upper limit of the instrumental and geometrical asymmetries of the whole detection system was estimated by measuring an asymmetry for a  $H(\vec{p},p)H$  scattering at  $\theta_L=17.5^\circ$  and found to be zero<sup>12)</sup> within a statistical error of 1%.

Measurements of angular distributions of the analyzing powers  $A(\theta)$  and cross sections  $\sigma(\theta)$  were made from  $\theta_L=5^\circ$  to  $65^\circ$  in  $5^\circ$  steps with spin-up and spin-down runs taken at each angle. In addition refined measurements were made in smaller steps around the angles at which the corresponding  $\sigma(\theta)$  has a sharp minimum.

Reversal of the polarization of spin-up and spin-down at the target was accomplished by reversing magnetic fields of the spin filter and ionization region at the polarized-ion source. The degree of the proton-beam polarization was measured at the beginning and end of each run using the quench-ratio method<sup>13)</sup> and was found to be quite stable with an average value of  $(85\pm 1)\%$ . This value agreed with the one obtained

from a measurement of an asymmetry for a  ${}^4\text{He}(\vec{p},p){}^4\text{He}$  scattering<sup>14)</sup> within an experimental error of 1%.

The angular acceptance of the magnetic spectrograph was  $\Delta\theta_L=3.0^\circ$  or  $1.5^\circ$ , which corresponded to a solid angle of 2.0 msr or 1.0 msr. The measurement around the angles at which the cross section had a minimum was made by using the smaller acceptance of  $\Delta\theta_L=1.5^\circ$ . A monitor detector was placed normal to the scattering plane at  $\theta_L=155^\circ$  and was used to measure the elastic proton scattering, monitoring the target thickness and charge collection of a Faraday cup. The monitor detector was insensitive to the polarization of the incident protons with spin normal to the scattering plane.

A specially designed Faraday cup was used to monitor the geometrical condition of the beam in addition to the collection of the charge. As shown in Fig. 2, it consists of separated two cups: the forward cup with a hole of 3 mm in diameter and the backward one which stops the full beam. The current from the forward cup indicates the geometrical condition of the beam passing the hole. This current is measured continuously in the case of a long run. If the current changes anomalously during the run, the data accumulation is automatically stopped by an electrical monitoring system of the current.

In order to measure tritons leading to several levels of the residual nucleus and deuterons in (p,d) reaction simultaneously, several silicon position-sensitive detectors were aligned precisely on the focal plane by using a laser-beam. The active area of the detector was about 45 mm long and 8 mm

wide. The vertical spread of the particles on the focal plane was confirmed to be within 8 mm as shown in Fig. 4 . The position pulses from two detectors were fed to a multichannel pulse-height analyzer (MCA) after processing by the parallel electric circuits as shown in Fig. 3 .

Targets were made by several methods according to their chemical and physical property. All Pd,  $^{112}\text{Cd}$  and  $^{114}\text{Cd}$  targets were self-supporting metallic foils, while other targets had an aluminium backing which was 0.4 (or 7)  $\mu\text{m}$  in thick. The Pd targets were made by a press of ingot with a roller, and  $^{112}\text{Cd}$  and  $^{114}\text{Cd}$  targets were made by electroplating. Of the targets with the Al backing, the argon-sputtering method was used for all Te and  $^{116}\text{Cd}$  targets, while the centrifugal settling method was applied to all Ru,  $^{118}\text{Sn}$  and  $^{144}\text{Nd}$  targets.

The thickness of each target was determined by measuring its weight or an energy loss of  $\alpha$  particles from an  $^{241}\text{Am}$  source through each target. Uncertainties of the thickness were estimated to be within 20 % by comparing with the results in each method. However, the accuracy of the thickness for all Ru and  $^{116}\text{Cd}$  targets was limited to about 50 % mainly due to their non-uniformity.

A measurement to determine the relative cross sections among isotopes was made for four Pd isotopes.

A summary of types, thicknesses and enrichments of the targets used is presented in Table 1.

### Chapter 3 Experimental Results

Typical momentum spectra of tritons taken at  $\theta_L=20^\circ$  for fifteen targets are shown in Fig. 5 . The energy resolutions are tabulated in Table 1, which are mainly due to the target thickness and the non-uniformity. Measured angular distributions of the analyzing power  $A(\theta)$  and the differential cross section  $\sigma(\theta)$  for the (p,t) transition to the ground state ( $0_g^+$ ) are shown in Figs. 7 and 8 , respectively. The numerical results with experimental errors are given in Appendix 3.

The absolute error in the  $A(\theta)$  was estimated to be less than 2 %, which was due to the geometrical asymmetry ( $\approx 1\%$ ) and the uncertainties of the beam polarization ( $\approx 1\%$ ) discussed in Chapter 2. However, the absolute values of  $\sigma(\theta)$  had rather large uncertainties (20 ~ 50 %) due to inaccuracies in the thickness of the targets used.

The observed  $A(\theta)$  and  $\sigma(\theta)$  have the following characteristic features. The most striking result for  $A(\theta)$  is observed in a pair of two isotopes of Ru and Pd as shown in Fig. 6 . A positive peak of  $A(\theta)$  around  $\theta \approx 20^\circ$  in  $^{98}\text{Ru}(^{102}\text{Pd})$  changes to a sharp negative dip in  $^{102}\text{Ru}(^{108}\text{Pd})$ . On the other hand, all the  $\sigma(\theta)$  have a deep minimum around  $\theta \approx 20^\circ$  and do not show such a drastic change.

As is easily seen in Fig. 7 , the  $A(\theta)$  display distinguishable change in going from one nucleus to the other in the angular distributions around  $\theta \approx 20^\circ$ . However, they are very similar with each other over an angular range of  $25^\circ \leq \theta \leq 65^\circ$ .

This feature is clearly shown in Fig. 9 . A hatched area covers the all data points after correcting the effect due to the nuclear radius.

An interesting comparison can be made for three pairs of nuclei which have the same neutron number:  $^{100}\text{Ru}$ ,  $^{102}\text{Pd}$  with  $N=56$ ,  $^{102}\text{Ru}$ ,  $^{104}\text{Pd}$  with  $N=58$  and  $^{108}\text{Pd}$ ,  $^{110}\text{Cd}$  with  $N=62$ . The sign of the  $A(\theta)$  is opposite with each other around  $\theta \approx 20^\circ$  for the latter two pairs, while no such a change is observed for the first pair.

It is easily recognized that the several properties mentioned above cannot be explained simply by the differences of  $Q$ -values (Table 2) because the results of  $A(\theta)$  for  $^{108}\text{Pd}$  and  $^{114}\text{Cd}$  which have almost the same  $Q$ -value ( $-6.5$  MeV) are quite different with each other.

It seems to have a relation between the derivative of the measured  $\sigma(\theta)$  and the corresponding  $A(\theta)$  in the angular range of  $25^\circ \leq \theta \leq 65^\circ$ . As will be discussed in section 4.5, the experimental results approximately satisfy the following relation:

$$A(\theta) \propto \frac{d}{d\theta} \sigma(\theta) / \sigma(\theta) .$$

On the contrary, all the nuclei except  $^{102}\text{Ru}$  and  $^{108}\text{Pd}$  do not obey this simple relation in the forward angular region of  $\theta \leq 25^\circ$  where the  $A(\theta)$  are expected to be negative since the corresponding cross section  $\sigma(\theta)$  decreases steeply with increasing  $\theta$ .

## Chapter 4 Analyses in Terms of the First- and Second- Order Distorted-Wave Born-Approximation

In (p,t) reactions the importance of successive neutron transfer processes has been pointed out especially for the so-called "forbidden" transitions in which the direct one-step process is strongly inhibited<sup>15)</sup>. The cross section for unnatural-parity transitions is such a case and has been well reproduced on the basis of the (p,d)(d,t) two-step processes<sup>16)</sup>.

It has been also pointed out that the (p,d)(d,t) mechanism has a significant effect on the allowed (p,t) reactions such as our experiments. The results of calculation<sup>17)</sup> have suggested that the (p,d)(d,t) process is as strong as the one-step process.

However, the comparison between the calculated results and the data has been made only for the differential cross sections. The purpose of the present analysis is to investigate the effect of the two-step mechanism on the analyzing power for strong ground-state (p,t) transitions. The main analysis for the present experimental results is made by considering (p,d)(d,t) process as a two-step mechanism and will be discussed in this chapter. The effect of the two-step process involving inelastic scattering processes will be discussed in sect. 5.6.

#### 4.1 Formalism for the first- and the second-order DWBA

In the last ten years, there has been success for the method of coupled-channel (CC) calculations<sup>18)</sup> and it has been found that CC reaction mechanism plays an important role in various type of reactions.

In this section, one- and two-step distorted-wave Born-approximation (DWBA) theory is reviewed, which is derived from the iterative approximate solution of coupled channel equations.

The coupled channel theory is based upon a wave function for the total system:

$$\Psi = \phi_{\alpha}(i_{\alpha})\chi_{\alpha}(\vec{r}_{\alpha}) + \sum_{\gamma} \phi_{\gamma}(i_{\gamma})\chi_{\gamma}(\vec{r}_{\gamma}) + \phi_{\beta}(i'_{\beta})\chi_{\beta}(\vec{r}_{\beta}) , \quad (1)$$

where  $\alpha, \beta, \gamma$ , which are described by a symbol  $c$  in general, denote the incident, final and intermediate channel, respectively. The  $\phi_c$  is the normalized internal wave function of the channel  $c$  and is described by the internal coordinate  $i_c$ . The  $\phi_c$  is a solution of a Shroedinger equation

$$H_c \phi_c = \epsilon_c \phi_c , \quad (2)$$

where  $H_c$  is the internal Hamiltonian in channel  $c$  and  $\epsilon_c$  is the corresponding eigen value. The  $\chi_c$  is a wave function describing the relative motion and is expressed by a relative coordinate  $\vec{r}_c$ . The  $\psi$  satisfies a Shroedinger equation for the total system:

$$H\psi = E\psi \quad , \quad (3)$$

where  $H$  is a Hamiltonian for the total system and has a total energy  $E$  as its eigenvalue. The  $H$  is written as

$$H = H_c + T_c + V_c \quad , \quad (4)$$

where  $T_c$  describes the kinematic energy of the relative motion in the channel  $c$  and  $V_c$  is the interaction in each channel  $c$ . Eq. (3) can be written as

$$\langle \phi_c | E - H | \psi \rangle_{i_c} = 0 \quad , \quad (5)$$

where the subscript  $i_c$  stands for the coordinate for integration. By inserting eq. (1) into eq. (5), we obtain coupled channel equations

$$(E_c - T_c - U_c) \chi_c = \sum_{c \neq c'} V_{cc'} \chi_{c'} \quad , \quad (6)$$

where

$$E_c = E - \epsilon_c \quad , \quad (7)$$

$$U_c \equiv \langle \phi_c | V_c | \phi_c \rangle_{i_c} \quad , \quad (8)$$

and  $V_{cc'}$  is defined by

$$V_{cc'} \chi_{c'} \equiv \langle \phi_c | H - E | \phi_{c'} \chi_{c'} \rangle_{i_c} \quad (9)$$

and will be discussed later.

By putting  $\alpha, \beta, \gamma$  into  $c$  or  $c'$  in eq. (6), we obtain the explicit form of the coupled equations:

$$\begin{aligned} (E_\alpha - T_\alpha - U_\alpha) \chi_\alpha &= \sum_{\gamma} V_{\alpha\gamma} \chi_\gamma + V_{\alpha\beta} \chi_\beta, \\ (E_\gamma - T_\gamma - U_\gamma) \chi_\gamma &= V_{\gamma\alpha} \chi_\alpha + \sum_{\gamma' \neq \gamma} V_{\gamma\gamma'} \chi_{\gamma'} + V_{\gamma\beta} \chi_\beta, \\ (E_\beta - T_\beta - U_\beta) \chi_\beta &= V_{\beta\alpha} \chi_\alpha + \sum_{\gamma} V_{\beta\gamma} \chi_\gamma. \end{aligned} \quad (10)$$

These equations can be solved by an iterative approximate way.

By treating up to the second order of  $V_{cc'}$ , we have the solution for the final channel  $\beta$ :

$$\chi_\beta^{(2)} = G_\beta^{(+)} V_{\beta\alpha} f_\alpha^{(+)} + \sum_{\gamma} G_\beta^{(+)} V_{\beta\gamma} G_\gamma^{(+)} V_{\gamma\alpha} f_\alpha^{(+)} \quad (11)$$

The  $G_c$  is a Green operator which describes propagation of a particle in the field  $U_c$  and has a form of

$$G_c^{(\pm)} = (E_c - T_c - U_c \pm i\varepsilon)^{-1}, \quad (12)$$

where the sign of the superscript indicates the well-known boundary condition. The  $f_c^{(+)}$  is the distorted wave of outgoing boundary condition and is given by

$$f_c^{(+)} = (1 + G_c^{(+)} U_c) \xi_c, \quad (13)$$

where  $\xi_c$  is a plane wave:

$$\xi_c = (2\pi)^{-3/2} \exp(i \vec{k}_c \cdot \vec{r}_c). \quad (14)$$

Here  $\vec{k}_c$  is the wave number in the channel  $c$ .

The transition amplitude which corresponds to the transition from the incident channel  $\alpha$  to the final channel  $\beta$  can be obtained from eq. (11) and has the form of

$$T_{\beta\alpha} = T_{\beta\alpha}^{(1)} + T_{\beta\alpha}^{(2)}, \quad (15)$$

where

$$T_{\beta\alpha}^{(1)} = \langle f_\beta^{(-)} | V_{\beta\alpha} | f_\alpha^{(+)} \rangle, \quad (16)$$

$$T_{\beta\alpha}^{(2)} = \sum_\gamma \langle f_\beta^{(-)} | V_{\beta\gamma} G_\gamma^{(+)} V_{\gamma\alpha} | f_\alpha^{(+)} \rangle. \quad (17)$$

The first term  $T_{\beta\alpha}^{(1)}$  corresponds to the first-order DWBA and the second term  $T_{\beta\alpha}^{(2)}$  to the second-order DWBA.

The  $V_{cc}$  defined in eq. (9) can be represented in terms of the various channel. For example,  $V_{\beta\alpha}$  in eq. (16) can be described more explicitly as

$$V_{\beta\alpha}^{(c)} f_\alpha^{(+)} = \langle \phi_\beta | H_c + T_c + V_c - E | \phi_\alpha f_\alpha^{(+)} \rangle \quad (18)$$

If  $c = \alpha$  ( $\beta$ ), the above expression is called the prior form (post form). It is well known that the first-order transition amplitude does not depend on the representation of  $V_{\beta\alpha}^{(c)}$ . Eq. (16) is written as

$$T_{\beta\alpha}^{(1)} = \langle f_{\beta}^{(-)} | V_c - U_c | f_{\alpha}^{(+)} \rangle \quad c = \alpha \text{ or } \beta \quad (19)$$

When we consider the sequential pickup process, such as (p,d)(d,t) process,  $V_{\beta\gamma}$  and  $V_{\gamma\alpha}$  in eq. (17) are represented by the prior forms in order to make actual calculations easy.

Then eq. (17) becomes

$$\begin{aligned} T_{\beta\alpha}^{(2)} &= \sum_{\gamma} \langle f_{\beta}^{(-)} | V_{\beta\gamma}^{(\gamma)} G_{\gamma}^{(+)} V_{\gamma\alpha}^{(\alpha)} | f_{\alpha}^{(+)} \rangle \\ &= T_{\beta\alpha}^{vv} + T_{\beta\alpha}^{no} \end{aligned} \quad (20)$$

where

$$T_{\beta\alpha}^{vv} = \sum_{\gamma} \langle f_{\beta}^{(-)} \phi_{\beta} | V_{\gamma} - U_{\gamma} | \phi_{\gamma} G_{\gamma}^{(+)} \langle \phi_{\gamma} | V_{\alpha} - U_{\alpha} | \phi_{\alpha} f_{\alpha}^{(+)} \rangle \rangle, \quad (21)$$

$$T_{\beta\alpha}^{no} = - \sum_{\gamma} \langle f_{\beta}^{(-)} \phi_{\beta} | \phi_{\gamma} \langle \phi_{\gamma} | V_{\alpha} - U_{\alpha} | \phi_{\alpha} f_{\alpha}^{(+)} \rangle \rangle. \quad (22)$$

The first term having the superscript vv describes the transition which is caused by successive two interactions and the second one is due to the non-orthogonality between the different channels.

To carry out the calculations, we need the transformation of the coordinate for integration. The results are as follows:

$$T_{\beta\alpha}^{(1)} = J_{\beta\alpha} \langle f_{\beta}^{(-)} | F_{\beta\alpha}^{(\alpha)} | f_{\alpha}^{(+)} \rangle_{\vec{r}_{\alpha}, \vec{r}_{\beta}} , \quad (23)$$

$$T_{\beta\alpha}^{VV} = \sum_{\gamma} J_{\beta\gamma} J_{\gamma\alpha} \langle f_{\beta}^{(-)} | F_{\beta\gamma}^{(\alpha)} G_{\gamma} F_{\gamma\alpha}^{(\alpha)} | f_{\alpha}^{(+)} \rangle_{\vec{r}_{\alpha}, \vec{r}_{\beta}, \vec{r}_{\gamma}, \vec{r}_{\gamma}'} , \quad (24)$$

$$T_{\beta\alpha}^{n0} = - \sum_{\gamma} J_{\beta\gamma} J_{\gamma\alpha} \langle f_{\beta}^{(-)} | \langle \phi_{\beta} | \phi_{\gamma} \rangle F_{\gamma\alpha}^{(\alpha)} | f_{\alpha}^{(+)} \rangle_{\vec{r}_{\alpha}, \vec{r}_{\gamma}, \vec{r}_{\beta}} , \quad (25)$$

where  $J_{c',c}$  is the Jacobian for the transformation from the coordinate  $(\vec{r}_{c'}, i_{c'})$  to  $(\vec{r}_c, \vec{r}_{c'}, i)$ . Here  $i$  is the coordinate which is independent of both  $r_c$  and  $r_{c'}$ . The  $F_{c',c}^{(c)}$  is a form factor given by

$$F_{c',c}^{(c)} = \langle \phi_{c'} | \hat{V}_c | \phi_c \rangle_i , \quad (26)$$

where

$$\hat{V}_c = V_c - U_c , \quad (27)$$

and the superscript  $c$  denotes the channel in which the interaction is described.

If the incident and outgoing particle have spin  $s_i$  and  $s_f$ , and the target and residual nuclear spins are  $J_i$  and  $J_f$ , respectively, we define

$$\vec{j} = \vec{J}_f - \vec{J}_i , \quad \vec{S} = \vec{S}_i - \vec{S}_f , \quad \vec{l} = \vec{j} - \vec{S} . \quad (28)$$

The reduced amplitude  $\beta$  for the first-order DWBA is defined<sup>3)</sup> by

$$T^{(1)} = \sum_{\ell S j} (2j+1) \langle J_i j M_i, M_f - M_i | J_f M_f \rangle A_{\ell S j}^{J_f J_i} \beta_{\ell S j}^{m_f \sigma_f \sigma_i}, \quad (29)$$

where  $m_f = M_f - M_i + \sigma_f - \sigma_i$  and  $A_{\ell S j}^{J_f J_i}$  is a spectroscopic amplitude for the transition.

In a similar way, when the light and heavy particle in the intermediate channel have spin  $s_m$  and  $J_m$ , respectively, the reduced amplitude for the second-order DWBA is defined

$$T^{(2)} = \sum_j (2j+1) \langle J_i j M_i, M_f - M_i | J_f M_f \rangle \times \sum_{\substack{\ell_1 S_1 j_1 \\ \ell_2 S_2 j_2}} A_{\ell_1 S_1 j_1}^{J_m J_i} A_{\ell_2 S_2 j_2}^{J_f J_m} \beta_j^{m_f \sigma_f \sigma_i}{}_{\ell_1 S_1 j_1 \ell_2 S_2 j_2}, \quad (30)$$

where

$$\begin{aligned} \vec{j}_1 &= \vec{J}_m - \vec{J}_i, \quad S_1 = S_i - S_m, \quad \vec{\ell}_1 = \vec{j}_1 - S_1, \\ \vec{j}_2 &= \vec{J}_f - \vec{J}_m, \quad S_2 = S_m - S_f, \quad \vec{\ell}_2 = \vec{j}_2 - S_2. \end{aligned} \quad (31)$$

The total amplitude for the first- and the second-order DWBA is written as

$$B_j^{m_f \sigma_f \sigma_i} = \sum_{\ell S} A_{\ell S j}^{J_f J_i} \beta_{\ell S j}^{m_f \sigma_f \sigma_i} + \sum_{\substack{\ell_1 S_1 j_1 \\ \ell_2 S_2 j_2}} A_{\ell_1 S_1 j_1}^{J_m J_i} A_{\ell_2 S_2 j_2}^{J_f J_m} \beta_j^{m_f \sigma_f \sigma_i}{}_{\ell_1 S_1 j_1 \ell_2 S_2 j_2}. \quad (32)$$

The differential cross section for unpolarized projectiles and unpolarized target nuclei is given by

$$\sigma(\theta) = \frac{\mu_i \mu_f}{(2\pi k_i^2)^2} \cdot \frac{k_f}{k_i} \cdot \frac{2J_f + 1}{(2J_i + 1)(2S_i + 1)} \sum_{j m_f \sigma_f \sigma_i} |B_j^{m_f \sigma_f \sigma_i}|^2, \quad (33)$$

where  $\mu_i$  and  $\mu_f$  are the reduced masses of the incident and outgoing channel, respectively, and  $k_i$  and  $k_f$  are the relative momentum of the respective channels.

## 4.2 Definition of analyzing power

In discussing polarization phenomena, it is recommended to use the Madison Convention concerning notations and coordinate systems. According to this convention, the analyzing power is generally defined as the quantities which describe the effect of initial polarization of a beam on the differential cross section for a nuclear reaction.

The polarization of a beam is referred to a right-handed coordinate system in which the positive z-axis is along the direction of momentum  $\vec{k}_{in}$  of the incident particles and the positive y-axis is along  $\vec{k}_{in} \times \vec{k}_{out}$  for the nuclear reaction. To describe the state of spin orientation of an assembly of particles, it is recommended to use spherical tensor operators  $\tau_{kq}$  or Cartesian operators  $S_i$  associated with spin of the particles. The polarization of an incident beam is described as an expectation value of  $\tau_{kq}$ :

$$t_{kq} = \langle \tau_{kq} \rangle . \quad (34)$$

The analyzing power for a reaction induced by the polarized beam of the polarization  $\tau_{kq}$  is defined as<sup>18)</sup>:

$$T_{kq} \equiv \frac{\text{Tr}(M \tau_{kq} M^\dagger)}{\text{Tr}(M M^\dagger)} , \quad (35)$$

where M represents the transition matrix for the reaction.

The corresponding differential cross section is given by

$$\sigma(\theta) = \sigma_0(\theta) \left[ \sum_{kq} t_{kq} T_{kq}^*(\theta) \right] , \quad (36)$$

where  $\sigma_0(\theta)$  is the differential cross section for unpolarized particles. In the case of the incident particle with spin 1/2, the cross section in eq. (36) is easily written in terms of the Cartesian representation:

$$\sigma(\theta) = \sigma_0(\theta) [ 1 + p A(\theta) ] , \quad (37)^*$$

If the incident beam is purely polarized along the direction of the positive (negative) y-axis, the polarization  $p$  equals 1 (-1). Then the  $A(\theta)$  can be written from eq. (37) as

$$A(\theta) = \frac{[\sigma_{\uparrow\uparrow}(\theta) + \sigma_{\downarrow\uparrow}(\theta)] - [\sigma_{\uparrow\downarrow}(\theta) + \sigma_{\downarrow\downarrow}(\theta)]}{\sigma_{\uparrow\uparrow}(\theta) + \sigma_{\downarrow\uparrow}(\theta) + \sigma_{\uparrow\downarrow}(\theta) + \sigma_{\downarrow\downarrow}(\theta)} , \quad (38)$$

because we have the relations

$$\sigma_{\uparrow\uparrow}(\theta) + \sigma_{\downarrow\uparrow}(\theta) = \sigma_0(\theta) [ 1 + A(\theta) ] , \quad (39)$$

$$\sigma_{\uparrow\downarrow}(\theta) + \sigma_{\downarrow\downarrow}(\theta) = \sigma_0(\theta) [ 1 - A(\theta) ] , \quad (40)$$

where the  $\sigma_{\downarrow\uparrow}$ , for example, is the differential cross section from an initial state with the spin projection 1/2 (described as  $\uparrow$ ) of the incident particle ( $p$ ) to a final state with the

---

\*) In the present paper, we abbreviate the vector analyzing power  $A_y(\theta)$  to  $A(\theta)$ .

spin  $-1/2$  ( $\uparrow$ ) of the outgoing particle ( $t$ ) on the  $y$ -axis.

From eq. (38), the  $A(\theta)$  can be expressed in terms of the reduced scattering amplitude  $B_j^{m_f \sigma_f \sigma_i}$  defined in sect. 4.1:

$$A(\theta) = - \frac{\sum [(s_i + \sigma_i + 1)(s_i - \sigma_i)]^{1/2} \text{Im} [ B_j^{m_f \sigma_f \sigma_i} B_j^{m_f - 1, \sigma_f, \sigma_i + 1*} ]}{s_i \sum | B_j^{m_f \sigma_f \sigma_i} |^2} \quad (41)$$

The eq. (41) will be derived in Appendix 1.

### 4.3 BCS wave function

The BCS theory is well known as the powerful method to describe the wave function for nuclei in an unfilled shell<sup>1)</sup>. Detailed comparisons with experiments have been carried out successfully by many authors<sup>19-21)</sup>.

In this section, the BCS theory will be discussed briefly since we apply the BCS wave function to the ground state of the nuclei involved.

The model space consists of nucleons in the truncated shell-model orbits and the pairing force between like nucleons is introduced. The Hamiltonian for the system is given by<sup>19,20)</sup>

$$H = \sum_{j'm} \epsilon_j C_{jm}^+ C_{jm} - \frac{1}{4} G_0 \sum_{j'm'} (-1)^{j'-m'} C_{j'm'}^+ C_{j'-m'}^+ \chi \sum_{j'm} (-1)^{-j+m} C_{j-m} C_{jm} , \quad (42)$$

where  $C_{jm}^+$  and  $C_{jm}$  are the creation and annihilation operators of the shell model state with spin  $j$  and  $z$ -component  $m$ , respectively. The first term of the right-hand side represents the sum of single-particle energies while the second term represents the pairing interactions among nucleons. The  $\epsilon_j$  is the single-particle energy of the state  $j$ , and  $G_0$  is the strength of the pairing interaction.

Following the usual procedures of the BCS theory, the  $C_{jm}^+$  and  $C_{jm}$  are transformed by the Bogoliubov-Valatin transformation and the "quasi-particle" operators are introduced:

$$C_{jm}^+ = U_j a_{jm}^+ + V_j (-1)^{j-m} a_{j-m} \quad , \quad (43)$$

where  $U_j$  and  $V_j$  satisfy

$$U_j^2 + V_j^2 = 1 \quad . \quad (44)$$

As this transformation mixes states with different mass number, it is necessary to introduce the auxiliary Hamiltonian

$$H' = H - \lambda \sum_{jm} a_{jm}^+ a_{jm} \quad , \quad (45)$$

where  $\lambda$  is the chemical potential, serving as a Lagrange multiplier to take into account the constraint that the average occupation number equals the number  $n$  of nucleons in the unfilled shell. The coefficients  $U_j$  and  $V_j$  are chosen so that the new Hamiltonian in terms of  $a_{jm}$  and  $a_{jm}^+$  will not contain terms like  $a^+ a^+$  and  $aa$ . Therefore the following equations are obtained

$$\frac{1}{4} G_0 \sum_j \frac{2j+1}{[(\epsilon_j - \lambda)^2 + \Delta^2]^{1/2}} = 1 \quad , \quad (46)$$

where

$$\Delta = \frac{1}{2} G_0 \sum_j (2j+1) U_j V_j \quad , \quad (47)$$

and

$$U_j^2 = \frac{1}{2} \left[ 1 + \frac{\epsilon_j - \lambda}{[(\epsilon_j - \lambda)^2 + \Delta^2]^{1/2}} \right], \quad (48)$$

$$V_j^2 = \frac{1}{2} \left[ 1 - \frac{\epsilon_j - \lambda}{[(\epsilon_j - \lambda)^2 + \Delta^2]^{1/2}} \right]. \quad (49)$$

The number of nucleons is obtained as

$$n = \sum_j \frac{2j+1}{2} \left[ 1 - \frac{\epsilon_j - \lambda}{[(\epsilon_j - \lambda)^2 + \Delta^2]^{1/2}} \right]. \quad (50)$$

Equations (46) and (50) are the basic equations, and  $\Delta$  and  $\lambda$  will be obtained if  $\epsilon_j$ ,  $G_0$  and  $n$  are given. After  $\Delta$  and  $\lambda$  are derived,  $U_j$  and  $V_j$  may be calculated from eqs. (48) and (49). A physical meaning of  $V_j^2$  ( $U_j^2$ ) is the probability of occupation (nonoccupation) of the  $j$  level. Also one-half of the gap energy in the even-even nuclei approximately equals  $\Delta$  in this model.

The numerical values  $\epsilon_j$  and  $G_0$  are tabulated, for example, in Ref. 21) where a detailed study of nuclei from Ni to Pb has been made. The values of  $\epsilon_j$ ,  $\Delta$  and  $\lambda$  used in the present paper are given in Table 3.

#### 4.4 Spectroscopic amplitude

In reaction calculations, the spectroscopic amplitude is an important quantity which contains all information about the nuclear structure involved. The application of the BCS theory to the direct nuclear reaction has been made extensively by S. Yoshida for one-nucleon<sup>20)</sup> and two-nucleon<sup>22)</sup> transfer reactions. The expression for the spectroscopic amplitudes which are necessary to perform the calculation of (p,t) reaction including (p,d)(d,t) process can be obtained from his work.

If the second-quantization formalism is used, the spectroscopic amplitude for one-nucleon transfer is expressed as

$$A_1(j) = \sum_{M_l m} \langle I_l M_l j m | I_h M_h \rangle \\ \times \langle I_h M_h | C_{jm}^+ | I_l M_l \rangle .$$

Here we distinguish between the heavier nucleus (target nucleus in pick-up reactions) and the lighter nucleus (residual nucleus in pick-up reactions). The subscript h denotes the heavier nucleus and the l denotes the lighter one, and the I and M having subscript h or l are the total angular momentum and its Z component for the respective nucleus.

If the BCS wave function is assumed for the states  $|I_h M_h\rangle$  and  $|I_l M_l\rangle$ , the spectroscopic amplitudes are obtained easily in the following two cases:

(i) The heavier nucleus is in a zero quasi-particle state and the lighter one is a one quasi-particle state:

$$A_1(j) = \sqrt{2j+1} V_j(h) . \quad (52)$$

(ii) The heavier nucleus is in a one quasi-particle state and the lighter one is in a zero quasi-particle state:

$$A_1(j) = U_j(l) . \quad (53)$$

The case (i) corresponds to a (p,d) reaction on an even-even target and the case (ii) to a (d,t) reaction on an even-odd target.

In a similar way, the spectroscopic amplitude for the two-nucleon transfer is defined as

$$A_2(j_1 j_2) = \sum_{M_2 M} \langle I_l J M_2 M | I_h M_h \rangle \times \langle I_h M_h | [C_{j_1}^+ C_{j_2}^+]_M^J | I_l M_l \rangle , \quad (54)$$

where

$$[C_{j_1}^+ C_{j_2}^+]_M^J = \frac{1}{\sqrt{1 + \delta_{j_1 j_2}}} \sum_{m_1 m_2} \langle j_1 j_2 m_1 m_2 | JM \rangle C_{j_1 m_1}^+ C_{j_2 m_2}^+ , \quad (55)$$

which is a creation operator of a pair of nucleons coupled to total spin J. Then the spectroscopic amplitude for the transition between the BCS ground states is given as

$$A_2(0jj) = \sqrt{i + \frac{1}{2}} U_j(\ell) V_j(k) . \quad (56)$$

#### 4.5 Procedure for calculations

The numerical calculations of one-step and two-step DWBA were carried out by using the code TWOFNR<sup>23)</sup>. The zero-range approximation is used in this chapter for both the one-step (p,t) process and the two-step (p,d)(d,t) process. In addition the non-orthogonality term given by eq. (25) is neglected. The finite-range effect and the contribution of the non-orthogonality term will be discussed in sects. 5.4 and 5.5, respectively.

The form of the optical potential employed is

$$U(r) = -V_R f_V^{(R)}(r) - i [W_V f_V^{(I)}(r) + W_S f_S^{(I)}(r)] \\ + 4V_{LS} \frac{1}{r} \frac{d}{dr} f_{LS}^{(R)}(r) (\vec{l} \cdot \vec{s}) + f_C(r) ,$$

where

$$f_V^{(R)}(r) = [1 + \exp(r - R_R)/a_R]^{-1} ; R_R = r_R A^{1/3} , \\ f_V^{(I)}(r) = [1 + \exp(r - R_I)/a_I]^{-1} ; R_I = r_I A^{1/3} , \\ f_S^{(I)}(r) = 4 [\exp(r - R_I)/a_I] [1 + \exp(r - R_I)/a_I]^{-2} , \\ f_{LS}^{(R)}(r) = [1 + \exp(r - R_{LS})/a_{LS}]^{-1} ; R_{LS} = r_{LS} A^{1/3} , \\ f_C(r) = (Zz e^2 / 2R_C) [3 - (r/R_C)^2] , \text{ for } r \leq R_C ,$$

$$\text{or } \sum Z e^2 / r \quad , \text{ for } r > R_c \quad ,$$

$$; R_c = r_c A^{1/3} .$$

We first used the parameters listed in Table 4 which were determined by elastic scattering experiments. Those are obtained from the work of Becchetti and Greenlees<sup>24)</sup> for protons, that of Hjorth, Lin, and Johnson<sup>25)</sup> for deuterons, and that of Flynn et al.<sup>26)</sup> for tritons. As discussed later, calculations will be performed by using modified parameters for the deuteron optical potential. These parameters are listed in Table 5 together with those used in the discussion about the effect of the spin-orbit force; see sect. 5.3.

The radial shape of the form factor was calculated with the conventional methods of zero-range DWBA; the so-called separation energy method for the one-neutron transfer process, (p,d) and (d,t), and the method of Baymann and Kallio<sup>27)</sup> for the direct (p,t) process. The single-neutron wave function is calculated by assuming single-particle potentials of the form<sup>28)</sup>

$$U_n(r) = V_0 f_V^{(R)}(r) + 2V_{LS} \frac{1}{r} \frac{d}{dr} f_{LS}^{(R)}(r) (\vec{l} \cdot \vec{\sigma}) \quad ,$$

where  $V_0$  is determined to give an experimental separation energy of a bound neutron.

In the calculation of the BCS wave functions, we consider five neutron orbits  $1d_{5/2}$ ,  $0g_{7/2}$ ,  $2s_{1/2}$ ,  $1d_{3/2}$ , and  $0h_{11/2}$ ,

of which binding energies are taken from the table of Kisslinger and Sorensen<sup>21)</sup>. The pairing interaction strength  $G_0$  is taken as  $G_0=23/A$  MeV. By use of this force strength together with the single-particle energies, we calculate the spectroscopic amplitudes of eqs. (52) and (53) for each one-neutron transfer process in (p,d)(d,t) process and those of eq. (56) for one-step (p,t) process. The results of the calculation are given in Table 3, where  $A_{pt}(0jj)$  is a spectroscopic amplitude for one-step (p,t) process and  $A_{pdt}(j)$  is a product of the spectroscopic amplitude of a (p,d) process and that of a (d,t) process.

In the case of Nd isotopes, the nucleus  $^{144}\text{Nd}$  ( $^{143}\text{Nd}$ ) can be assumed to have a pure configuration  $f_{7/2}^2$  ( $f_{7/2}$ ) outside a core nucleus  $^{142}\text{Nd}$  of  $N=82$ . Then the spectroscopic amplitudes are simply given by  $A_{pt}(0, f_{7/2}, f_{7/2})=1$  and  $A_{pdt}(f_{7/2})=\sqrt{2}$ .

The normalization constants of the zero-range form factors are taken to be as follows:

$$D_0^2(p,d) = 1.53 \quad , \quad D_0^2(d,t) = 3.37$$

all in units of  $10^4 \text{MeV}^2 \text{fm}^3$ . These values have been widely used in DWBA analyses and taken from Ref. 17). The determination of  $D_0^2(p,t)$  is more ambiguous than the other two  $D_0^2$ 's. We use the value  $D_0^2(p,t)=22$  throughout all the relevant calculations, which is obtained by assuming a simple wave function for triton and the n-p interaction in the zero-range treatment of the Baymann and Kallio method.

#### 4.6 Results of analyses

First it should be emphasized that the observed  $A(\theta)$  cannot be interpreted by only one-step (p,t) process because it always predicts a sharp negative minimum at  $\theta \approx 20^\circ$  as shown in Fig. 10.

The analyzing powers  $A(\theta)$  which cannot be explained in terms of the direct one-step process are called anomalous in this paper. The calculated  $A(\theta)$  and  $\sigma(\theta)$  by the one-step process seem to obey a derivative relation  $A(\theta) \approx d[\ln\sigma(\theta)]/d\theta$  as indicated by dashed lines in Fig. 10, which connect a peak or valley of the cross section with a corresponding zero-cross point of the analyzing power. This relation, which is well known in the elastic scattering, can be obtained quite generally in the ground state  $0_g^+(p,t)0_g^+$  transition and is derived in Appendix 2 by the perturbation treatment of spin-orbit distortion. According to this relation, the sharp negative dip should always appear around  $\theta \approx 20^\circ$  because the corresponding  $\sigma(\theta)$  decreases steeply with increasing  $\theta$  from  $\theta \approx 0$ .

In consequence it can be concluded that other transition processes than the direct one-step process are essential to interpret the experimental  $A(\theta)$  around  $\theta \approx 20^\circ$ . Then (p,d) (d,t) processes are taken into account.

The calculated analyzing power  $A(\theta)$  and cross sections  $\sigma(\theta)$  in terms of the one- and two-step DWBA are shown in Figs. 11 and 12, respectively. The potential parameters in Table 4 are used as a first trial. It should be noticed that this optical potential for deuterons has a surface imaginary part

which depends linearly on the deformation parameter  $\beta_2$  of the nucleus. As is seen in Fig. 13, the strength of the (p,d) (d,t) process is comparable to that of the one-step process and the resultant magnitude of the cross section can reproduce the experimental results within a factor of about 3.

The variation of the  $A(\theta)$  around  $\theta \approx 20^\circ$  seems to be well reproduced for the Ru and Pd isotopes, although the characteristic negative dip in the one-step DWBA still remains slightly. These results are considered to be a success because the sharp negative dip is inevitably predicted by the one-step DWBA and no variation in  $A(\theta)$  is obtained around  $\theta \approx 20^\circ$  as far as the one-step DWBA is applied. However, the fitting to the experimental results becomes worse in going from Cd to Te both in the cross sections and the analyzing powers. Thus we cannot obtain overall fit to the measured angular distributions of the  $A(\theta)$  and  $\sigma(\theta)$  for the fifteen nuclei.

As the second stage, we made a calculation by using a modified optical potential for deuterons which had a volume imaginary part instead of a surface imaginary part. The effect of changing the imaginary part into a volume type is a reduction of the contribution to the deuteron scattering from the nuclear interior. This result is consistent with that obtained by use of the Johnson-Soper approach<sup>29)</sup>, and therefore suggests that deuteron breakup is responsible for the required change in the deuteron potential. However, the differences between the Johnson-Soper effective parameters and those in the present analysis suggest a further study of the problem. A

phenomenological investigation will be presented in sect. 5.2.

As shown in Fig. 14, we can obtain a significant improvement for both the analyzing powers and cross sections by introducing this empirical deuteron optical potential. The interference between the one- and (p,d) (d,t) two-step processes is essential to reproduce the anomalies at  $\theta \approx 20^\circ$ . For simplicity and in order to see a general trend of the angular distributions of the analyzing power over a wide mass-number range, we use the same parameter set of the deuteron potential for all nuclei except for  $^{108}\text{Pd}$  which will be discussed later. It is essentially the same potential set in Table 4. Here we made another modification for the spin-orbit force for protons. The depth of the spin-orbit force was reduced from  $V_{\text{LS}}=6.2$  to 4.5 MeV. This modification is not so essential as discussed later in sect. 5.3.

Contributions of various neutron orbits to the two-step processes are explained in Fig. 15. A dominant contribution of the  $d_{5/2}$  orbit accounts for the positive  $A(\theta)$  in forward angles  $\theta < 20^\circ$  for  $^{98}\text{Ru}$  and  $^{104}\text{Pd}$ . A decrease of the contribution of the  $d_{5/2}$  orbit and a relative increase of that of the  $s_{1/2}$  orbit in going from  $^{102}\text{Pd}$  to  $^{108}\text{Pd}$  can explain an appearance of a sharp negative dip for  $^{108}\text{Pd}$ . A redisappearance of it for  $^{126}\text{Te}$  is due to an increase of the contribution of the  $h_{11/2}$  orbit. Large difference in analyzing powers for various orbits appears only in forward angles  $\theta \leq 40^\circ$ , while the each analyzing power focuses almost on the same angular distributions in backward angles  $\theta \geq 40^\circ$ . It should be noticed that the  $j$  dependence of analyzing powers for one-nucleon

transfer reaction<sup>30)</sup> is similarly revealed in the (p,d)(d,t) sequential processes<sup>31)</sup>: a  $d_{5/2}-d_{3/2}$  pair in Fig. 15.

Appearance of a round positive peak in the  $A(\theta)$  at  $\theta \approx 25^\circ$  has been observed only in the case of  $^{108}\text{Pd}$ . This can be reproduced quite well by adding a surface imaginary part to the distorting potential for deuterons, as explained in Fig. 16. This fact implies that deuterons in the intermediate channel break up and/or are absorbed more easily near the nuclear surface of  $^{109}\text{Pd}$  than in the other nuclei. This seems to be correlated with the fact that  $^{110}\text{Pd}$  ( $^{108}\text{Pd}$ ) has a very large deformation parameter<sup>32)</sup> of  $\beta_2=0.25$  (0.24).

In addition to  $A(\theta)$ , the observed  $\sigma(\theta)$  are also well reproduced in their shape as well as in magnitude within a factor of about 2 by including the (p,d)(d,t) processes. The normalization factors are given in Table 6 and will be discussed in sect. 5.7.

As is shown in Fig. 14, the angular distribution of the cross section for the (p,d)(d,t) two-step processes (dashed curves) is very similar in shape to that for the one-step process (dash-dotted curves). Moreover, the cross section of the coherent sum of the two processes (solid curves) has a similar shape of angular distributions to that of the both of the two processes mainly because there occurs a constructive interference between the two processes. Therefore we cannot appreciate the contribution of the (p,d)(d,t) two-step processes to the ground-state (p,t) transitions as far as only the cross-section data are utilized. Indeed strong (p,t)

transitions between  $0^+$  ground states of medium- and heavy-mass nuclei have been considered so far to proceed via a direct one-step transfer of two neutrons in a  $^1S_0$  pair<sup>2)</sup>. According to our data of the analyzing powers  $A(\theta, 0_g^+)$ , however, the previous conclusion mentioned above is wrong. The (p,d) (d,t) two-step process is as strong as the one-step process in the strong ground-state (p,t) transitions in medium- and heavy-mass nuclei. The anomalous analyzing powers due to the interference between the one- and two-step processes prove this fact very clearly.

## Chapter 5 Discussion

### 5.1 Isotope dependence of the analyzing power

The fact that the difference of the contributions of each orbit in the intermediate states of the (p,d) (d,t) process determines the aspect of the angular distributions of  $A(\theta)$  in forward angles  $\theta \leq 20^\circ$  is demonstrated in Fig. 17. The dashed line shows the result of the calculation in which the contributions of both the  $d_{5/2}$  and  $d_{3/2}$  orbits are omitted from the total scattering amplitude. If the component of the  $d_{5/2}$  or  $d_{3/2}$  orbit is added, the  $A(\theta)$  becomes positive or negative at forward angles  $\theta \leq 20^\circ$  according to the respective case. The final result after summing all contributions is indicated by the solid line and reproduces the sign of the measured  $A(\theta)$ . On the contrary, the orbit-dependent behavior of the  $A(\theta)$  cannot be observed in backward angles  $\theta \gtrsim 30^\circ$  where the angular distributions are very similar for each single-particle orbit. It should be noted that no orbit-dependent behavior is observed in the shape of the cross section  $\sigma(\theta)$  as is shown in Fig. 17.

In order to see the systematic aspect of the  $A(\theta)$  around  $\theta \approx 20^\circ$  for all nuclei in the  $N=50-82$  shell, we made an artificial calculation as shown in Fig. 18. Although the corresponding spectroscopic amplitudes for each isotope (Table 3) are employed in the calculation, the scattering amplitude  $\beta$  are all calculated by using the reaction parameters fixed to  $^{98}\text{Ru}$ . This procedure is adequate to investigate the effect of the

nuclear structure involved because it can reduce the effect due to the reaction dynamics. It is clearly seen in Fig. 18 that the positive  $A(\theta)$  observed in  $\theta \leq 20^\circ$  becomes negative in going from Ru to Te and various behaviors of  $A(\theta)$  are observed for each isotope. This general trend is consistent with the experimental results.

## 5.2 Effect of the imaginary part of the deuteron optical potential

It has been pointed out<sup>25,33)</sup> that a volume integral of optical potentials is physically more significant than, for instance, the depth of the potential itself. From this point of view, the following study is carried out in order to investigate the effect of the imaginary part of the distorting potential in the intermediate state.

A simple evaluation by using a volume integral  $I$  of the imaginary potential for deuterons

$$I \equiv \frac{1}{3} R_I^3 W_V + R_I^2 a_I W_S \quad (\text{MeV fm}^3)$$

is made, where the parameters are defined in sect. 4.5. If we change the depths of  $W_V$  and  $W_S$  for the deuteron potential with keeping the volume integral  $I$  constant, a relatively small change in the angular distributions of  $A(\theta)$  is observed in forward angles  $\theta \leq 40^\circ$  as shown in Fig. 19. However, the amplitude of the  $A(\theta)$  around  $\theta \approx 55^\circ$  become larger with increasing the ratio of  $W_V$  to  $W_S$ . Fig. 20 shows the similar results. In this case the combinations of the parameters  $W_V$  and  $W_S$  are taken arbitrarily without conserving the volume integral  $I$ . The second minimum around  $\theta \approx 55^\circ$  in the angular distribution of  $\sigma(\theta)$  is rather sensitive to the volume integral  $I$ . It shifts backward in angle with increasing the value of the volume integral  $I$ . An agreement with the data can be obtained

by adjusting the  $W_V$  and  $W_S$ . But it is difficult to eliminate the negative dip of the  $A(\theta)$  around  $\theta \approx 20^\circ$  by the same adjustment.

### 5.3 Effect of the spin-orbit terms of the optical potentials

In the previous calculations in chapter 4, the optical potentials which do not contain spin-orbit interactions have been used for deuterons and tritons. We first examine the effect of the spin-orbit force for deuterons in this section.

Fig.21 shows the  $A(\theta)$  and  $\sigma(\theta)$  calculated by using the deuteron optical potential determined by the elastic scattering<sup>33)</sup> with a polarized deuteron beam of  $E_d=12$  MeV. Only the optical potential for tritons has no spin-orbit interaction. No modification for the imaginary part of the deuteron potential from the surface type is made. The agreement with the data is improved for the angular distribution of  $A(\theta)$  in backward angles, although a small dip appears around  $\theta \approx 15^\circ$ . It should be noted that successful calculational results are obtained in the Nd case without depending on the choice of the deuteron potential.

Next Fig.22 shows the results in the case where the spin-orbit interaction is switched off. The volume imaginary part is used according to the successful calculational procedures in sect. 4.6. The spin-orbit force of deuterons is therefore considered to be not important for the (p,d) (d,t) process.

The effect of the spin-orbit interaction for the triton potential was investigated by using the potential set 2 in Table 5 (Ref. 34). The effect of the spin-orbit force for tritons on the angular distributions of  $A(\theta)$  appears in forward angles  $\theta < 20^\circ$  as shown in Fig. 23; a small dip appears

around  $\theta \approx 15^\circ$ . However, the agreement with the data does not become worse. Therefore it can be concluded that the spin-orbit forces both for tritons and deuterons have no significant effect on the final results of the calculations.

It is generally observed that the calculated  $A(\theta)$  overestimate the data in amplitude. This fact is strongly correlated with the spin-orbit force for protons. A shallow spin-orbit potential for protons can give rise to a significant overall reduction of  $A(\theta)$  in amplitude as shown in Fig. 24. The depth of the spin-orbit potential is reduced from  $V_{LS} = 6.2$  to 3.1 MeV in this case.

#### 5.4 Finite-range effect

To evaluate the finite-range effect in the (p,t) and (p,d) (d,t) processes, numerical calculations were done in the case of the reaction  $^{144}\text{Nd}(p,t)^{142}\text{Nd}$ . Since the exact-finite-range program to compute the one-step (p,t) transition is not available, only the distance between a proton and a cluster of two neutrons is considered to be finite in the one-step process. For the (p,d) (d,t) process, the full finite-range calculations are made<sup>23)</sup>. However, there remains an uncertainty in the relative intensity between the one-step and two-step transitions. The normalization is made by using the result of the zero-range calculation, so that a rough estimation of the finite-range effect is made in this section.

It is assumed that both the intrinsic wave function  $\phi_d$  for a deuteron and  $\phi_t$  for a triton have the pure s-wave spatial part. The forms of  $\phi_d$  and  $\phi_t$  are assumed to be<sup>17)</sup>

$$\phi_d(r_1) = N_d \frac{e^{-ar_1} - e^{-br_1}}{r_1},$$

$$\phi_t(r_1, r_2) = N_t e^{-\eta^2(2r_2^2 + \frac{3}{2}r_1^2)},$$

with

$$a = 0.233 \text{ fm}^{-1}, \quad b = 1.45 \text{ fm}^{-1},$$

$$\eta^2 = 0.0634 \text{ fm}^{-2},$$

where  $N_d$  and  $N_t$  are spatial normalization constants. For the n-p interaction potential, we take a Gaussian form:

$$V_{np}(r) = -V_0 e^{-(r/\xi)^2}$$

with a range parameter  $\xi=1.49$  fm.

Fig. 25 shows the calculated  $A(\theta)$  which should be compared with the zero-range calculation. A slight difference is observed around  $\theta \approx 20^\circ$  and  $50^\circ$ . The finite-range effect, however, is small.

## 5.5 Effect of the non-orthogonality term

The strength of the non-orthogonality term and its effect on  $A(\theta)$  are investigated in the  $^{142}\text{Nd}$  case. The finite-range method is used to calculate the overlap  $\langle \phi_d | \phi_t \rangle$ , while the zero-range approximation with the same normalization constant given in sect. 4.5 is applied for the first step in the  $(p,d)(d,t)$  process. The intrinsic wave functions in sect. 5.4 are used for  $\phi_d$  and  $\phi_t$ .

The strength of the non-orthogonality term is smaller than that of the interaction term [ $T^{VV}$  in eq. (21)] by a factor of about 10 as shown in Fig. 26. The resultant calculations including the non-orthogonality term show that there is essentially no effect on the  $A(\theta)$ . (Fig. 26)

## 5.6 Effect of inelastic two-step processes

It has been pointed out by many authors that the two-step processes via inelastic excitations are important in  $(p,t)$  transitions leading to the collective states. This reaction mechanism has been clearly confirmed by a recent investigation of the analyzing power for the  $2_1^+$  transitions in  $(p,t)$  reactions<sup>35,36</sup>. Therefore the contributions of inelastic two-step processes via the first  $2^+$  ( $2_1^+$ ) states of the initial and final nuclei should be estimated.

An estimation for these contributions was done in the  $^{104}\text{Pd}(p,t)^{102}\text{Pd}$  reaction. The wave functions of the  $2_1^+$  states are constructed by using the quasiparticle random-phase-approximation (RPA) model<sup>19</sup>. Details of the formalism and relevant spectroscopic amplitudes are given in Ref. 36). For the inelastic scattering process, we employ macroscopic form factors which are obtained as the derivative of the optical potential. The deformation parameters are taken as  $\beta_2=0.2$  for both target and residual nucleus. The relative importance of the  $(p,p')(p',t)$  and  $(p,t')(t',t)$  processes to the one-step process is explained in Fig. 27. The strength of the  $(p,p')(p',t)$  is smaller than that of one-step process by 0.5%, while the  $(p,t')(t',t)$  process is much smaller and negligible. No remarkable change is observed in the analyzing power by including inelastic two-step processes as shown in Fig. 27. The effect of the inelastic two-step processes is minor in comparison with the  $(p,d)(d,t)$  processes which are

as strong as the one-step process.

## 5.7 Absolute values of the cross sections

In the present paper, we calculated the absolute values of the (p,t) cross sections on the basis of the zero-range approximation by using the numerical values for the zero-range normalization constants  $D_0(p,d)$ ,  $D_0(d,t)$  and  $D_0(p,t)$  given by sect. 4.5.

Now we define the ratio  $N$  as  $N \equiv \sigma_{\text{exp}} / \sigma_{\text{th}}$  at the second peak of the angular distributions of the cross section. Here the  $\sigma_{\text{th}}$ 's are the theoretical cross sections mentioned above. In Table 6 are given the ratio  $N$  obtained for five nuclei (see Fig. 14) by the use of the modified optical potential which has been introduced to obtain overall fits with the data.

The ratios obtained are  $N=1 \pm 0.2$  except for the case of  $^{142}\text{Nd}$ . The agreement between the theoretical cross sections and the experimental ones is as good as one would expect in view of the uncertainties in the absolute values of the experimental cross sections (see chapt. 3) and the oversimplification in the optical potentials for deuterons and tritons (see sect. 4.6).

These ratios increase from  $^{98}\text{Ru}_{54}$  to  $^{126}\text{Te}_{74}$  and fall down at  $^{142}\text{Nd}_{82}$ . This fact seems to be related to the model space used for the construction of the nuclear wave functions. The limited model space (only five single-particle orbits) employed for the BCS wave functions is considered to be inadequate for the nuclei near the closed shell. It may be true that the model space is too wide for  $^{98}\text{Ru}$  and too narrow

for  $^{126}\text{Te}$ . The overestimate of the theoretical cross sections for the case of  $^{142}\text{Nd}$  may be due to the simplified assumption of the pure-configuration  $(f_{7/2}^2)$  wave function for the target nucleus  $^{144}\text{Nd}$ .

## Chapter 6 Conclusion

The anomalous analyzing powers for strong  $(p,t)$  ground-state transitions have been observed for the first time by the systematic measurement on fifteen nuclei having neutrons from  $N=54$  to 82. The corresponding cross sections, however, do not show such anomalies. This experimental result demonstrates that the analyzing powers are powerful tools for investigating the reaction mechanism of two-nucleon transfer reactions.

The conventional one-step DWBA cannot explain these anomalies, which only predicts similar angular distributions of the analyzing power for each target nucleus of the fifteen nuclei. The anomalous analyzing powers strongly violate the derivative rule between the cross section and the analyzing power. This fact tells us that other transition processes than the direct one-step process are essential to interpret the anomalies.

The  $(p,d)(d,t)$  two-step processes are then found to be essential for interpreting the experimental result. The anomalies can be accounted for as an interference effect between the  $(p,d)(d,t)$  sequential processes and the direct one-step process. The neutron-number dependence of the anomalous angular distributions of the analyzing powers is determined by the variation of the dominant one-quasiparticle neutron orbits in the intermediate channels in the sequential two-step processes.

The ground-state  $(p,t)$  cross sections for superconducting

nuclei are improved well by including the  $(p,d)$   $(d,t)$  processes which are as strong as the one-step process.

More works should be done for the distorting potential in the intermediate channel in the sequential two-step processes.

## Acknowledgements

I would like to express profound thanks to Prof. K. Yagi for his direction and continuous encouragement, and for many stimulating suggestions and discussions. I would like to thank Dr. Y. Aoki for his direction and discussions, and for his valuable experimental technique. I wish to thank Dr. K.-I. Kubo for the theoretical discussions and suggestions. I wish to acknowledge kind collaboration of Dr. Y. Toba and Messrs. K. Nagano and H. Iida concerning the experimental works and discussions at the Tandem Accelerator Center. I am much indebted to Dr. Y. Tagishi for the polarized-ion source, and to technical staffs of the Tandem Accelerator Center for their assistance.

I would like to thank Prof. J. Sanada, Prof. T. Mikumo and Prof. K. Katori for their warm encouragement throughout this work.

## References

- 1) A. Bohr, B. Mottelson, and D. Pines, Phys. Rev. 110 (1958) 936.
- 2) See, e.g., R. A. Broglia, O. Hansen, and C. Riedel, Adv. Nucl. Phys. 6 (1973) 287, and references therein.
- 3) G. R. Satchler, Nucl. Phys. 55 (1964) 1.
- 4) C. L. Lin and S. Yoshida, Prog. Theor. Phys. 32 (1964) 885.
- 5) N. K. Glendenning, Phys. Rev. 137 (1965) B102.
- 6) See, e. g., E. R. Flynn, R. A. Hardekopf, J. D. Sherman, and J. W. Sunies, Phys. Lett. 61B (1976) 433.
- 7) G. Igo, J. C. S. Chai, R. F. Casten, T. Udagawa, and T. Tamura, Nucl. Phys. A207 (1973) 289.
- 8) J. A. Macdonald, N. A. Jelley, and J. Cerny, Phys. Lett. 47B (1973) 237.
- 9) K. Yagi, S. Kunori, Y. Aoki, K. Nagano, Y. Toba, and K.-I. Kubo, Phys. Rev. Lett. 43 (1979) 1087.
- 10) Y. Tagishi and J. Sanada, Nucl. Instr. 164 (1979) 411.
- 11) J. E. Spencer and H. A. Enge, Nucl. Instr. 49 (1967) 181.
- 12) P. Catillon, J. Sura and A. Tarrats, Phys. Lett. 20 (1968) 602.
- 13) G. G. Ohlsen, J. L. McKibben, G. P. Lawrence, P. W. Keaton, Jr., and D. D. Armstrong, Phys. Rev. Lett. 27 (1971) 599.
- 14) A. D. Bacher, G. R. Plattner, H. E. Conzett, D. J. Clark, H. Clark, H. Grunder, and W. F. Trivol, Phys. Rev. C5 (1972) 1147.
- 15) K.-I. Kubo and H. Amakawa, Phys. Rev. C17 (1978) 1271, and references therein.

- 16) Y. Toba, Y. Aoki, S. Kunori, K. Nagano, and K. Yagi, Phys. Rev. C20 (1979) 1204, and references therein.
- 17) N. Hashimoto and M. Kawai, Prog. theor. Phys. 59 (1978) 1245; N. Hashimoto, *ibid.* 59 (1978) 1562.
- 18) N. Austern, Direct Nuclear Reaction Theories (Wiley-Interscience, 1970).
- 19) M. Baranger, Phys. Rev. 120 (1960) 957.
- 20) S. Yoshida, Nucl. Phys. 38 (1962) 380.
- 21) L. S. Kisslinger and R. A. Sorensen, Rev. Mod. Phys. 35 (1963) 853.
- 22) S. Yoshida, Nucl. Phys. 33 (1962) 685.
- 23) M. Toyama and M. Igarashi, private communication.
- 24) F. D. Becchetti, Jr. and G. W. Greenlees, Phys. Rev. 182 (1969) 1190.
- 25) S. A. Hjorth, E. K. Lin, and A. Johnson, Nucl. Phys. A116 (1968) 1.
- 26) E. R. Flynn, D. D. Armstrong, J. G. Berry, and A. G. Blair, Phys. Rev. 182 (1969) 1113.
- 27) B. F. Bayman and K. Kallio, Phys. Rev. 156 (1967) 121.
- 28) A. Bohr and B. Mottelson, Nuclear Structure Vol. 1 (Benjamin, 1969) p.238.
- 29) R. C. Johnson and P. J. R. Soper, Phys. Rev. C1 (1970) 976.
- 30) T. Yule and W. Haeberli, Phys. Rev. Lett. 19 (1967) 756.
- 31) K.-I. Kubo, to be published.
- 32) P. H. Stelson and L. Grodzin, Nucl. Data, Sect. A1, (1965) 21.
- 33) J. M. Lohr and W. Haeberli, Nucl. Phys. A232 (1974) 381.

- 34) R. A. Hardekopf, L. R. Veaser, and P. W. Keaton, Phys. Rev. Lett. 35 (1975) 1623.
- 35) K. Yagi, S. Kunori, Y. Aoki, Y. Higashi, J. Sanada, and Y. Tagishi, Phys. Rev. Lett. 40 (1978) 161.
- 36) K. Yagi, S. Kunori, Y. Aoki, K. Nagano, Y. Tagishi, and Y. Toba, in Proceedings of the International Symposium on Nuclear Direct Reaction Mechanism, (Fukuoka, 1978) p.137.
- 37) K.-I. Kubo, private communication.
- 38) R. C. Johnson, Nucl. Phys. 35 (1962) 654.
- 39) N. B. Gove and A. H. Wapstra, Nucl. Data Tables 11 (1972) 127.

Table 1 Experimental information on fifteen targets for  
(p,t) reactions.

Target	Thickness (mg/cm <sup>2</sup> )	Form	Enrichment (%)	Energy resolution (keV)
<sup>100</sup> Ru	2.1	RuO <sub>2</sub> <sup>a)</sup>	97.24	130
<sup>102</sup> Ru	1.8	Ru <sup>a)</sup>	99.35	50
<sup>104</sup> Ru	1.3	Ru <sup>a)</sup>	99.35	50
<sup>104</sup> Pd	2.0	Pd <sup>b)</sup>	95.25	60
<sup>106</sup> Pd	2.4	Pd <sup>b)</sup>	96.66	60
<sup>108</sup> Pd	2.0	Pd <sup>b)</sup>	98.11	50
<sup>110</sup> Pd	2.9	Pd <sup>b)</sup>	97.73	50
<sup>112</sup> Cd	4.0	Cd <sup>b)</sup>	97.8	100
<sup>114</sup> Cd	4.4	Cd <sup>b)</sup>	99.0	120
<sup>116</sup> Cd	0.8	Cd <sup>a)</sup>	96.85	20
<sup>118</sup> Sn	1.1	SnO <sub>2</sub> <sup>a)</sup>	95.75	40
<sup>122</sup> Te	1.0	Te <sup>a)</sup>	94.71	20
<sup>128</sup> Te	1.8	Te <sup>a)</sup>	99.19	60
<sup>130</sup> Te	1.5	Te <sup>a)</sup>	97.49	60
<sup>144</sup> Nd	1.2	Nd <sub>2</sub> O <sub>3</sub> <sup>a)</sup>	97.51	30

(a) On an aluminum backing.

(b) Self-supporting metallic film.

Table 2 Q-values for ground-state (p,t) reactions.<sup>a)</sup>

Reaction	Q-value(MeV)
$^{100}\text{Ru}(p,t)^{98}\text{Ru}$	-8.660
$^{102}\text{Ru}(p,t)^{100}\text{Ru}$	-7.539
$^{104}\text{Ru}(p,t)^{102}\text{Ru}$	-6.655
$^{104}\text{Pd}(p,t)^{102}\text{Pd}$	-9.145
$^{106}\text{Pd}(p,t)^{104}\text{Pd}$	-8.152
$^{108}\text{Pd}(p,t)^{106}\text{Pd}$	-7.285
$^{110}\text{Pd}(p,t)^{108}\text{Pd}$	-6.475
$^{112}\text{Cd}(p,t)^{110}\text{Cd}$	-7.892
$^{114}\text{Cd}(p,t)^{112}\text{Cd}$	-7.099
$^{116}\text{Cd}(p,t)^{114}\text{Cd}$	-6.362
$^{118}\text{Sn}(p,t)^{116}\text{Sn}$	-7.788
$^{122}\text{Te}(p,t)^{120}\text{Te}$	-8.562
$^{128}\text{Te}(p,t)^{126}\text{Te}$	-6.585
$^{130}\text{Te}(p,t)^{128}\text{Te}$	-6.018
$^{144}\text{Nd}(p,t)^{142}\text{Nd}$	-5.461

(a) Ref. 39).

Table 3 Single particle energies  $\epsilon_j^a$ , and the calculated chemical potential  $\lambda$  and gap energy  $\Delta$ . The  $A_{pt}(0jj)$  and  $A_{pdt}(j)^b$  are the spectroscopic amplitudes for one-step and two-step (p,d) (d,t) processes, respectively.

	$^{100}\text{Ru}$	$^{98}\text{Ru}$	(nlj)	$\epsilon_j$ (MeV)	$A_{pt}(0jj)$	$A_{pdt}(j)$
$\lambda$ (MeV)	0.368	-0.072	$1d_{5/2}$	-0.075	1.018	1.439
$\Delta$ (MeV)	1.062	0.922	$2s_{1/2}$	1.382	0.378	0.534
			$0g_{7/2}$	1.786	0.615	0.870
			$0h_{11/2}$	2.561	0.540	0.764
			$1d_{3/2}$	3.087	0.259	0.366

	$^{102}\text{Ru}$	$^{100}\text{Ru}$	(nlj)	$\epsilon_j$ (MeV)	$A_{pt}(0jj)$	$A_{pdt}(j)$
$\lambda$ (MeV)	0.772	0.364	$1d_{5/2}$	-0.066	0.859	1.215
$\Delta$ (MeV)	1.215	1.071	$2s_{1/2}$	1.372	0.485	0.685
			$0g_{7/2}$	1.769	0.810	1.146
			$0h_{11/2}$	2.555	0.703	0.995
			$1d_{3/2}$	3.055	0.336	0.476

a) Calculated values for target by using the formula in Ref. 21).

b)  $A_{pdt}(j) \equiv A_{pd}(j) \times A_{dt}(j)$ ; see sect. 4.5.

Table 3 (continued)

	$^{104}\text{Ru}$	$^{102}\text{Ru}$	(nlj)	$\epsilon_j$ (MeV)	$A_{pt}(0jj)$	$A_{pdt}(j)$
$\lambda$ (MeV)	1.108	0.763	$1d_{5/2}$	-0.057	0.742	1.049
$\Delta$ (MeV)	1.334	1.221	$2s_{1/2}$	1.364	0.541	0.765
			$0g_{7/2}$	1.753	0.959	1.357
			$0h_{11/2}$	2.548	0.854	1.207
			$1d_{3/2}$	3.023	0.411	0.581
	$^{104}\text{Pd}$	$^{102}\text{Pd}$	(nlj)	$\epsilon_j$ (MeV)	$A_{pt}(0jj)$	$A_{pdt}(j)$
$\lambda$ (MeV)	0.668	0.292	$1d_{5/2}$	-0.057	0.887	1.255
$\Delta$ (MeV)	1.208	1.082	$2s_{1/2}$	1.364	0.462	0.653
			$0g_{7/2}$	1.473	0.880	1.244
			$0h_{11/2}$	2.548	0.673	0.951
			$1d_{3/2}$	3.023	0.326	0.461
	$^{106}\text{Pd}$	$^{104}\text{Pd}$	(nlj)	$\epsilon_j$ (MeV)	$A_{pt}(0jj)$	$A_{pdt}(j)$
$\lambda$ (MeV)	0.993	0.659	$1d_{5/2}$	-0.049	0.777	1.099
$\Delta$ (MeV)	1.306	1.213	$2s_{1/2}$	1.355	0.524	0.741
			$0g_{7/2}$	1.457	1.015	1.435
			$0h_{11/2}$	2.542	0.806	1.140
			$1d_{3/2}$	2.992	0.392	0.554

Table 3 (continued)

	$^{108}\text{Pd}$	$^{106}\text{Pd}$	(nlj)	$\epsilon_j$ (MeV)	$A_{\text{pt}}(0jj)$	$A_{\text{pdt}}(j)$
$\lambda$ (MeV)	1.288	0.982	$1d_{5/2}$	-0.042	0.699	0.989
$\Delta$ (MeV)	1.364	1.310	$2s_{1/2}$	1.347	0.551	0.779
			$0g_{7/2}$	1.442	1.087	1.537
			$0h_{11/2}$	2.536	0.927	1.311
			$1d_{3/2}$	2.962	0.454	0.642
	$^{110}\text{Pd}$	$^{108}\text{Pd}$	(nlj)	$\epsilon_j$ (MeV)	$A_{\text{pt}}(0jj)$	$A_{\text{pdt}}(j)$
$\lambda$ (MeV)	1.566	1.277	$1d_{5/2}$	-0.034	0.636	0.900
$\Delta$ (MeV)	1.389	1.367	$2s_{1/2}$	1.338	0.551	0.779
			$0g_{7/2}$	1.427	1.104	1.561
			$0h_{11/2}$	2.530	1.039	1.470
			$1d_{3/2}$	2.933	0.514	0.727
	$^{112}\text{Cd}$	$^{110}\text{Cd}$	(nlj)	$\epsilon_j$ (MeV)	$A_{\text{pt}}(0jj)$	$A_{\text{pdt}}(j)$
$\lambda$ (MeV)	1.451	1.153	$1d_{5/2}$	-0.027	1.451	0.932
$\Delta$ (MeV)	1.324	1.315	$0g_{7/2}$	1.133	1.102	1.559
			$2s_{1/2}$	1.330	0.556	0.786
			$0h_{11/2}$	2.524	0.978	1.383
			$1d_{3/2}$	2.905	0.484	0.685

Table 3 (continued)

	$^{114}\text{Cd}$	$^{112}\text{Cd}$	(nlj)	$\epsilon_j$ (MeV)	$A_{pt}(0jj)$	$A_{pdt}(j)$
$\lambda$ (MeV)	1.733	1.441	$1d_{5/2}$	-0.020	0.592	0.837
$\Delta$ (MeV)	1.316	1.326	$0g_{7/2}$	1.119	1.043	1.475
			$2s_{1/2}$	1.322	0.544	0.769
			$0h_{11/2}$	2.518	1.092	1.544
			$1d_{3/2}$	2.878	0.546	0.772
	$^{116}\text{Cd}$	$^{114}\text{Cd}$	(nlj)	$\epsilon_j$ (MeV)	$A_{pt}(0jj)$	$A_{pdt}(j)$
$\lambda$ (MeV)	2.006	1.723	$1d_{5/2}$	-0.013	0.530	0.750
$\Delta$ (MeV)	1.293	1.317	$0g_{7/2}$	1.106	0.951	1.345
			$2s_{1/2}$	1.315	0.509	0.720
			$0h_{11/2}$	2.512	1.201	1.699
			$1d_{3/2}$	2.851	0.611	0.864
	$^{118}\text{Sn}$	$^{116}\text{Sn}$	(nlj)	$\epsilon_j$ (MeV)	$A_{pt}(0jj)$	$A_{pdt}(J)$
$\lambda$ (MeV)	1.938	1.631	$1d_{5/2}$	-0.006	0.528	0.747
$\Delta$ (MeV)	1.214	1.233	$0g_{7/2}$	0.813	0.866	1.225
			$2s_{1/2}$	1.307	0.522	0.738
			$0h_{11/2}$	2.506	1.168	1.652
			$1d_{3/2}$	2.825	0.590	0.834

Table 3 (continued)

	$^{122}\text{Te}$	$^{120}\text{Te}$	(nlj)	$\epsilon_j$ (MeV)	$A_{pt}(0jj)$	$A_{pdt}(j)$
$\lambda$ (MeV)	2.173	1.878	$1d_{5/2}$	0.006	0.453	0.640
$\Delta$ (MeV)	1.126	1.134	$0g_{7/2}$	0.508	0.648	0.916
			$2s_{1/2}$	1.293	0.468	0.661
			$0h_{11/2}$	2.494	1.268	1.793
			$1d_{3/2}$	2.775	0.654	0.925
	$^{128}\text{Te}$	$^{126}\text{Te}$	(nlj)	$\epsilon_j$ (MeV)	$A_{pt}(0jj)$	$A_{pdt}(j)$
$\lambda$ (MeV)	2.857	2.640	$1d_{5/2}$	0.023	0.321	0.453
$\Delta$ (MeV)	0.939	1.037	$0g_{7/2}$	0.473	0.435	0.615
			$2s_{1/2}$	1.272	0.307	0.435
			$0h_{11/2}$	2.477	1.320	1.867
			$1d_{3/2}$	2.705	0.785	1.110
	$^{130}\text{Te}$	$^{128}\text{Te}$	(nlj)	$\epsilon_j$ (MeV)	$A_{pt}(0jj)$	$A_{pdt}(j)$
$\lambda$ (MeV)	3.051	2.848	$1d_{5/2}$	0.0287	0.275	0.389
$\Delta$ (MeV)	0.798	0.941	$0g_{7/2}$	0.462	0.369	0.522
			$2s_{1/2}$	1.266	0.259	0.367
			$0h_{11/2}$	2.471	1.223	1.730
			$1d_{3/2}$	2.683	0.766	1.084

Table 4 Optical-potential parameters for the first analysis in chapter 4 and bound state potential parameters for neutrons.

	p	d	t	n
		(SET 1)	(SET 1)	
$V_R$	$46.96+0.4Z/A^{1/3}$ $+24.0\xi^a)$	$(94.6+0.4Z/A^{1/3})$ $\times[1-3\exp(-r_R A^{1/3})]$	166.7	f)
$r_R$	1.17	1.15	1.16	1.27
$a_R$	0.75	0.81	0.752	0.67
$W_V$	2.14	0	$37.5-127.4\xi$	
$W_S$	$6.3+12.0\xi$	$12.28+341.5\sqrt{B(E2)^c)/A}$	0	
$r_I$	1.32	1.34	1.498	
$a_I$	$0.51+0.7\xi$	0.68	0.817	
$V_{LS}$	6.2	0	0	$9.05-5.85\xi$
$r_{LS}$	1.01			1.27
$a_{LS}$	0.75			0.67
$r_C$	1.25	1.15	1.25	
ref.	b)	d)	e)	g)

a)  $\xi \equiv (N-Z)/A$     b) Ref. 24.

c)  $B(E2; 0^+ \rightarrow 2^+)$  in  $10^3 \text{ fm}^4$  for target nucleus in (p,t) reactions was taken from Ref. 32.

d) Ref. 25.    e) Ref. 26.

f) Adjusted to give the experimental binding energy.

g) Ref. 28.

Table 5 Optical-potential parameters for the second analysis in chapter 4 and those used in chapter 5.

	Deuterons		Tritons	
	(SET 2)	(SET 3)	(SET 2)	(SET 3)
$V_R$	$91.13+2.20Z/A^{1/3}$	98.0	152.5	176.0
$r_R$	1.05	1.15	1.20	1.14
$a_R$	0.80	0.81	0.65	0.72
$w_V$	0	18.0	13.7	18.0
$w_S$	$218A^{-2/3}$	0	0	0
$r_I$	1.43	1.34	1.60	1.61
$a_I$	$0.50+0.013A^{2/3}$	0.68	0.98	0.82
$V_{LS}$	3.5	0	6.0	0
$r_{LS}$	0.75		1.15	
$a_{LS}$	0.5		0.84	
$r_C$	1.3	1.15	1.30	1.14
ref.	a)	b)	c)	d)

a) Ref. 33.

b) Modified set from SET 1; see sect. 4.6.

c) Ref. 34.

d) Ref. 17.

Table 6 Ratios N of experimental to theoretical cross sections for five nuclei in Fig. 14.

	$^{98}_{\text{Ru}}$	$^{102}_{\text{Ru}}$	$^{108}_{\text{Pd}}$	$^{126}_{\text{Te}}$	$^{142}_{\text{Nd}}$
N	0.8	0.8	1.2	1.3	0.5

## Figure captions

- Fig. 1. Layout of the beam preparation system.
- Fig. 2. Illustration of the double Faraday cup.
- Fig. 3. Block diagram of the circuits for data accumulation.
- Fig. 4. Typical vertical spread of tritons on the focal plane of ESP-90 magnetic spectrograph.
- Fig. 5. Momentum spectra of tritons for both spin-up and spin-down. Each residual nucleus is indicated. In the present paper, the notation of each isotope is given by the residual nucleus in the (p,t) reaction.
- Fig. 6. Angular distributions of cross sections and analyzing powers for  $^{98,102}\text{Ru}$  and  $^{102,108}\text{Pd}$ . The lines are to guide the eye.
- Fig. 7. Angular distributions of analyzing powers for (p,t) ground-state transitions of  $E_p=22.0$  MeV. The lines are to guide the eye.
- Fig. 8. Angular distributions of cross sections for (p,t) ground-state transitions at  $E_p=22.0$  MeV. The lines are to guide the eye.
- Fig. 9. Summary for angular distributions of analyzing powers. The hatched area covers all the data points of analyzing powers. The  $A_0$  in the angular correction factor is taken as  $A_0=128$ .
- Fig. 10. Comparison of typical experimental cross sections and analyzing powers with the theoretical ones calculated in terms of the one-step DWBA (solid lines). The

normalization of the cross section to the data is made arbitrarily.

Fig. 11. Comparison between measured angular distributions of analyzing powers and the calculations in terms of one- and two-step DWBA. For the optical potential parameters, the set 1 for deuterons and the set 1 for tritons are used. The solid curves represent the calculated analyzing powers. The dot-dashed curves correspond to the one-step process only.

Fig. 12. Calculated cross sections with the same optical potential parameters as those in Fig. 11 (solid lines). The data are arbitrarily normalized to the theoretical curves.

Fig. 13. Relative strengths of the one- and two-step processes. The solid curves represent the calculated cross sections with the same optical potential sets as those in Fig. 11. The dot-dashed curves and the dashed curves represent the theoretical cross sections corresponding, respectively, to the one-step process only and the two-step process only. No normalization to the data is made.

Fig. 14. Experimental and calculated analyzing powers  $A(\theta)$  and cross sections  $\sigma(\theta)$ . The optical potential set 3 for deuterons and the set 3 for tritons are used. The depth of the spin-orbit force for protons is reduced from  $V_{LS}=6.2$  to 4.5 MeV. Dot-dashed (dashed) curves are the one-step (two-step) DWBA calculations

and solid curves are the coherent sum of the two processes. The measured cross sections are arbitrarily normalized to the theoretical curves.

Fig. 15. Contributions of each orbit to the analyzing powers and cross sections in the two-step processes. Solid curves are the coherent sum of the each process. Optical potential parameters are the same as those in Fig. 14.

Fig. 16. Effect of the imaginary part of the deuteron optical potential on the calculated analyzing powers for  $^{108}\text{Pd}$ . Potential parameters are the same as those in Fig. 14. The  $W_S$  is taken as  $W_S=12.5$  MeV in the indication of  $W_V+W_S$ .

Fig. 17. Shell effect of the (p,d) (d,t) two-step process on the analyzing powers [(a), (b)] and cross sections [(c)] for  $^{126}\text{Te}$ . Solid lines in (a) and (c) represent the calculations corresponding to the coherent sum of the one- and two-step processes and those in (b) corresponding to the two-step processes only. In (a), (b) and (c), the dot-dashed (dotted) curves represent the calculations without the contribution of  $d_{5/2}$  ( $d_{3/2}$ ) and the dashed curves without both  $d_{5/2}$  and  $d_{3/2}$  in (p,d) (d,t) two-step processes. Optical potential parameters are the same as those in Fig. 14.

Fig. 18. General trend of the angular distributions of the calculated analyzing powers for the nuclei in the N=50-82 shell.

Fig. 19. Effect of the imaginary part of the deuteron optical potential on the angular distributions of the analyzing powers for  $^{116}\text{Sn}$ . The potential set 3 for deuterons and the potential set 3 for tritons are used. The depth of the spin-orbit force for protons is not modified. The curves represent the calculated analyzing powers corresponding, respectively, to  $W_S=16.3$  and  $W_V=0$  (dashed lines),  $W_S=11.7$  and  $W_V=1.6$  (solid lines),  $W_S=6.7$  and  $W_V=3.1$  (dot-dashed lines) in the unit of MeV. The potential set 1 is used for tritons.

Fig. 20. Effect of the imaginary part of the deuteron optical potential on the angular distributions of the analyzing powers and the cross sections for  $^{116}\text{Sn}$ . The potential set 1 with the modified imaginary part is used for deuterons. The curves represent the calculations corresponding, respectively, to  $W_S=0$  and  $W_V=25.1$  (solid lines),  $W_S=16.3$  and  $W_V=0$  (dashed lines),  $W_S=8.4$  and  $W_V=8.4$  (dot-dashed lines) in the unit of MeV. The potential set 1 is used for tritons.

Fig. 21. Calculated analyzing powers and cross sections for  $^{142}\text{Nd}$  with the potential set 2 for deuterons and the potential set 1 for tritons. Dot-dashed (dashed) curves are the one-step (two-step)DWBA calculations and solid curves are the coherent sum of the two processes.

Fig. 22. Effect of the spin-orbit force for deuterons on the

calculated analyzing powers. The potential parameters are the same as those in Fig. 21 except for the imaginary part of the deuteron potential which has  $W_V$  instead of  $W_S$ . The coherent sum of one- and two-step processes is represented in (a) and the two-step process in (b).

Fig. 23. Effect of the spin-orbit force for tritons on the calculated analyzing powers. Solid lines (dashed lines) in (a) are the calculations with (without) the spin-orbit interaction for one- and two-step processes. Solid lines (dashed lines) in (b) are the calculations for one-step processes only with (without) the spin-orbit interaction. Dashed lines (dot-dashed lines) in (b) are the calculations for two-step processes only with (without) the spin-orbit interaction. The set 2 for tritons and the set 1 for deuterons are used for the optical potential parameters.

Fig. 24. Effect of the spin-orbit force for protons on the calculated analyzing powers for one- and two-step (p,d) (d,t) processes. The set 3 for deuterons and the set 3 for tritons are used for the optical potential parameters.

Fig. 25. Finite-range calculations for analyzing powers compared to zero-range calculations. The set 3 is used for the deuteron optical potential and the set 3 for the triton optical potential.

Fig. 26. Effect of the non-orthogonality term on the analyzing

powers [(a),(b)] and the cross sections [(c)]. Curves in (b) are the two-step calculations only. Solid lines (dashed lines) in both (a) and (b) are the calculations including (excluding) the non-orthogonality term. Curves in (c) are the cross sections corresponding, respectively, to the non-orthogonality term only ( $T^{\text{no}}$ ) (dashed lines), the interaction term only ( $T^{\text{vv}}$ ) (dot-dashed lines) and the coherent sum of the two terms ( $T^{\text{vv}}+T^{\text{no}}$ ). The optical potential parameters are the same as those in Fig. 25.

Fig. 27. Effect of the inelastic two-step processes on the analyzing powers (left side) and the cross sections (right side). The potential set 2 is used in triton channels. The cross sections for each process represent the relative strengths.

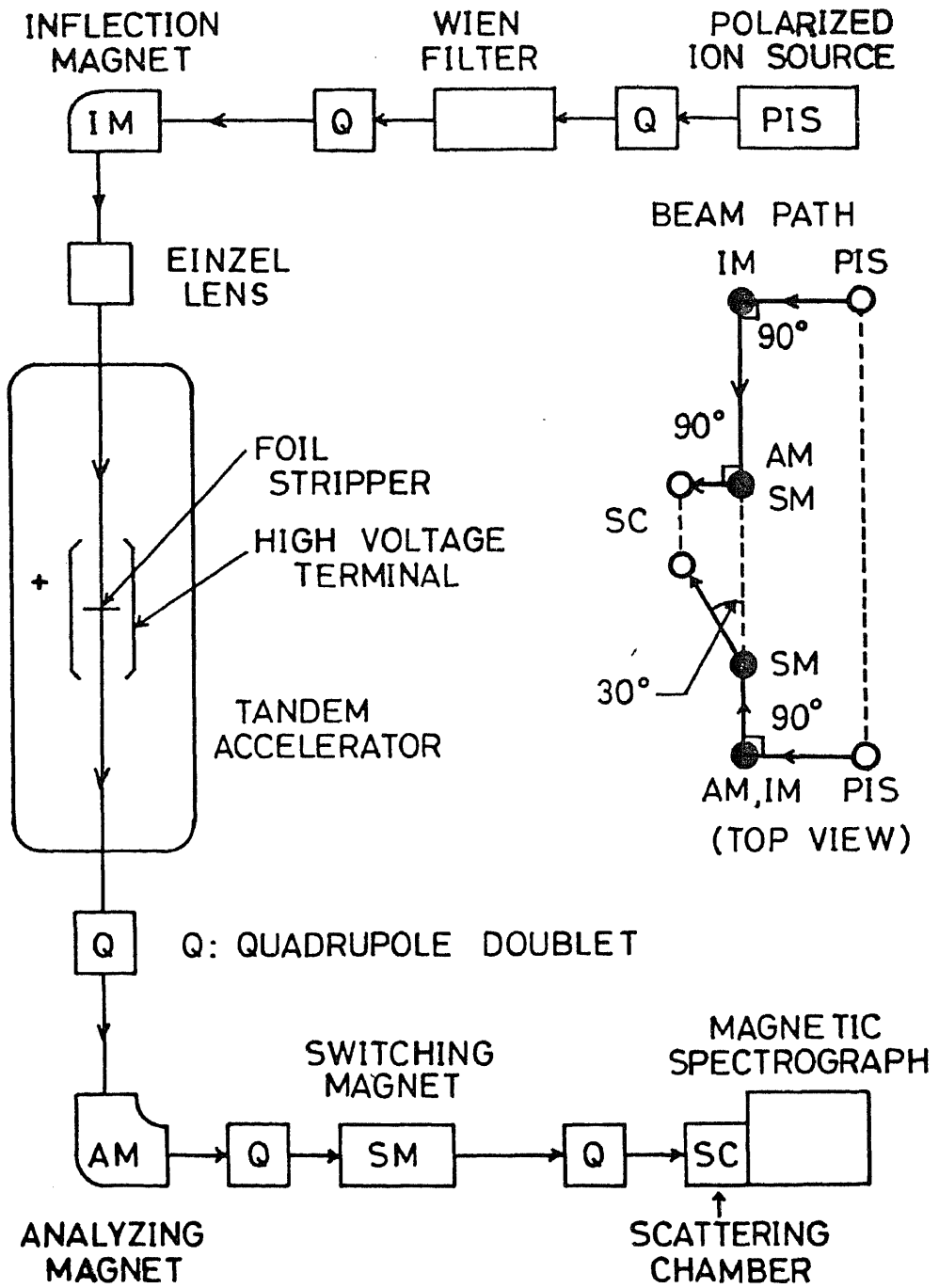


Fig. 1

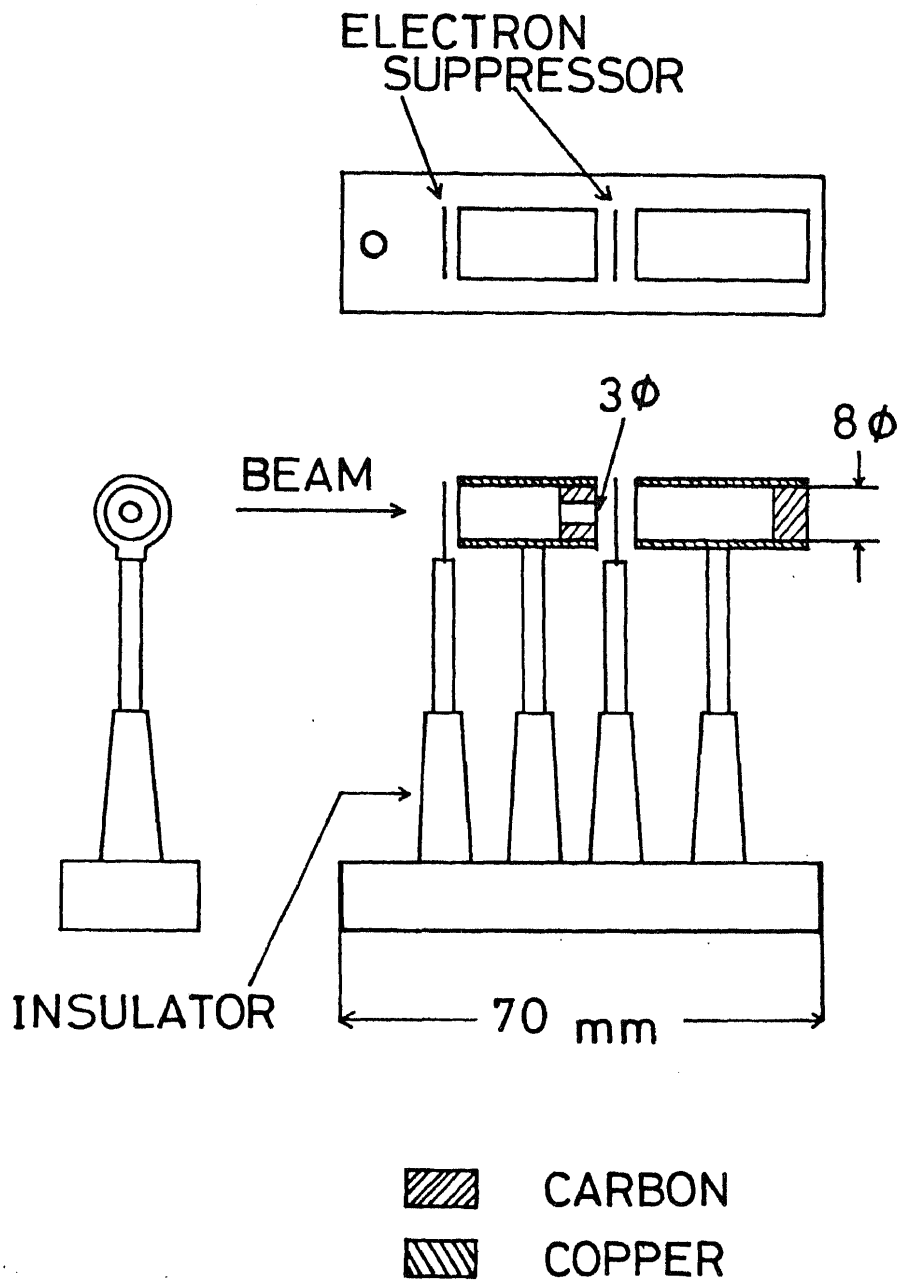


Fig. 2

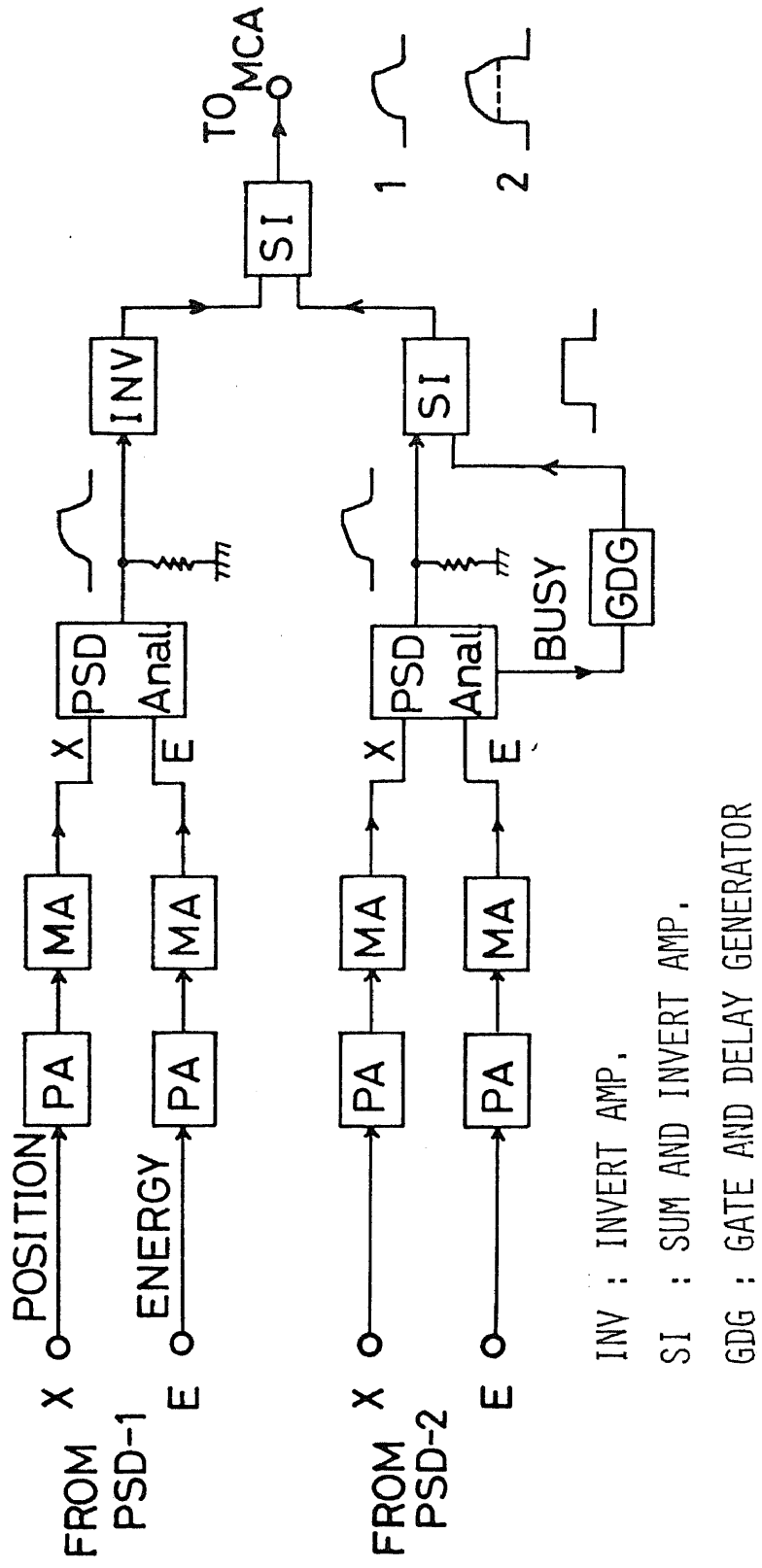


Fig. 3

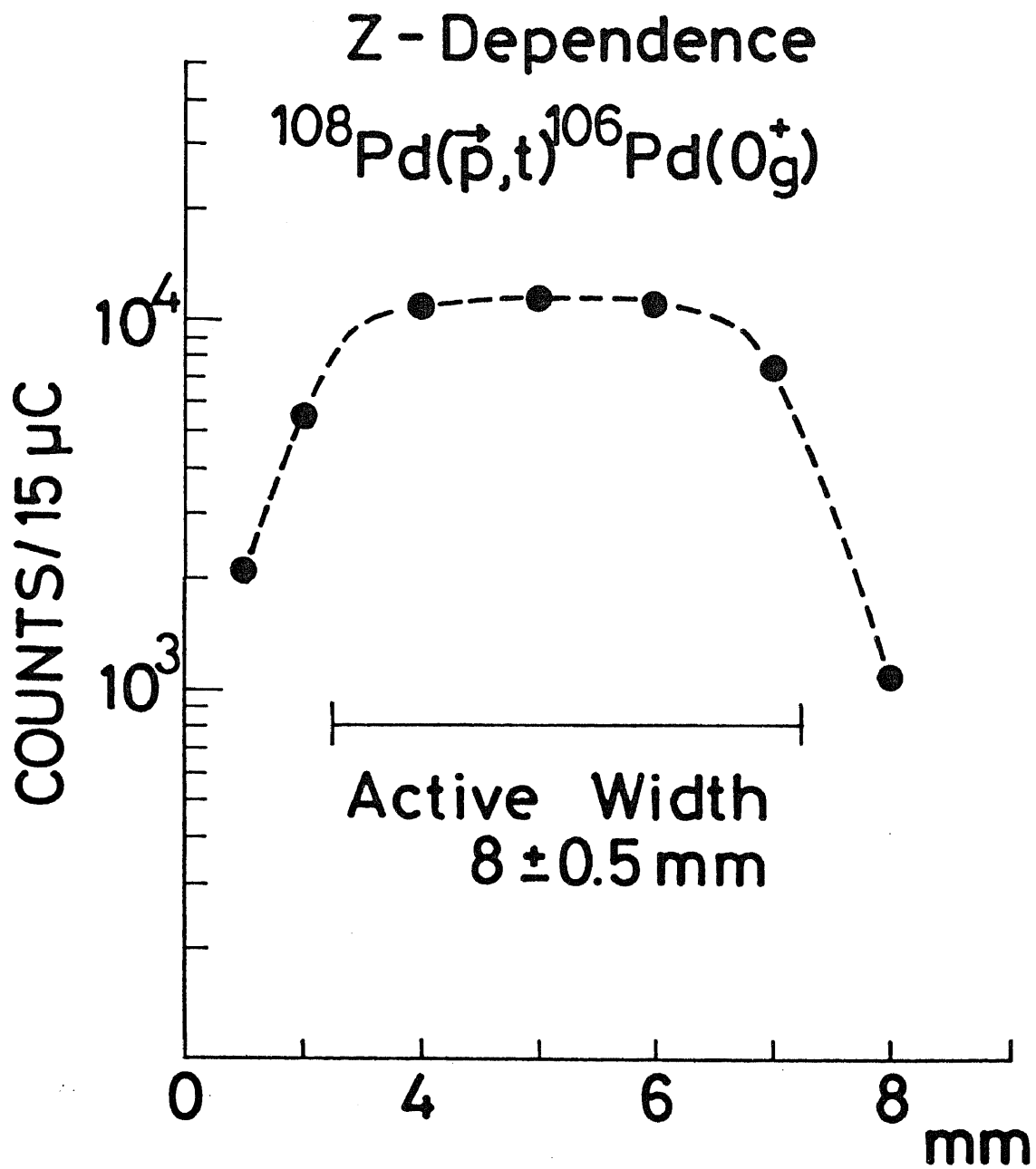


Fig. 4

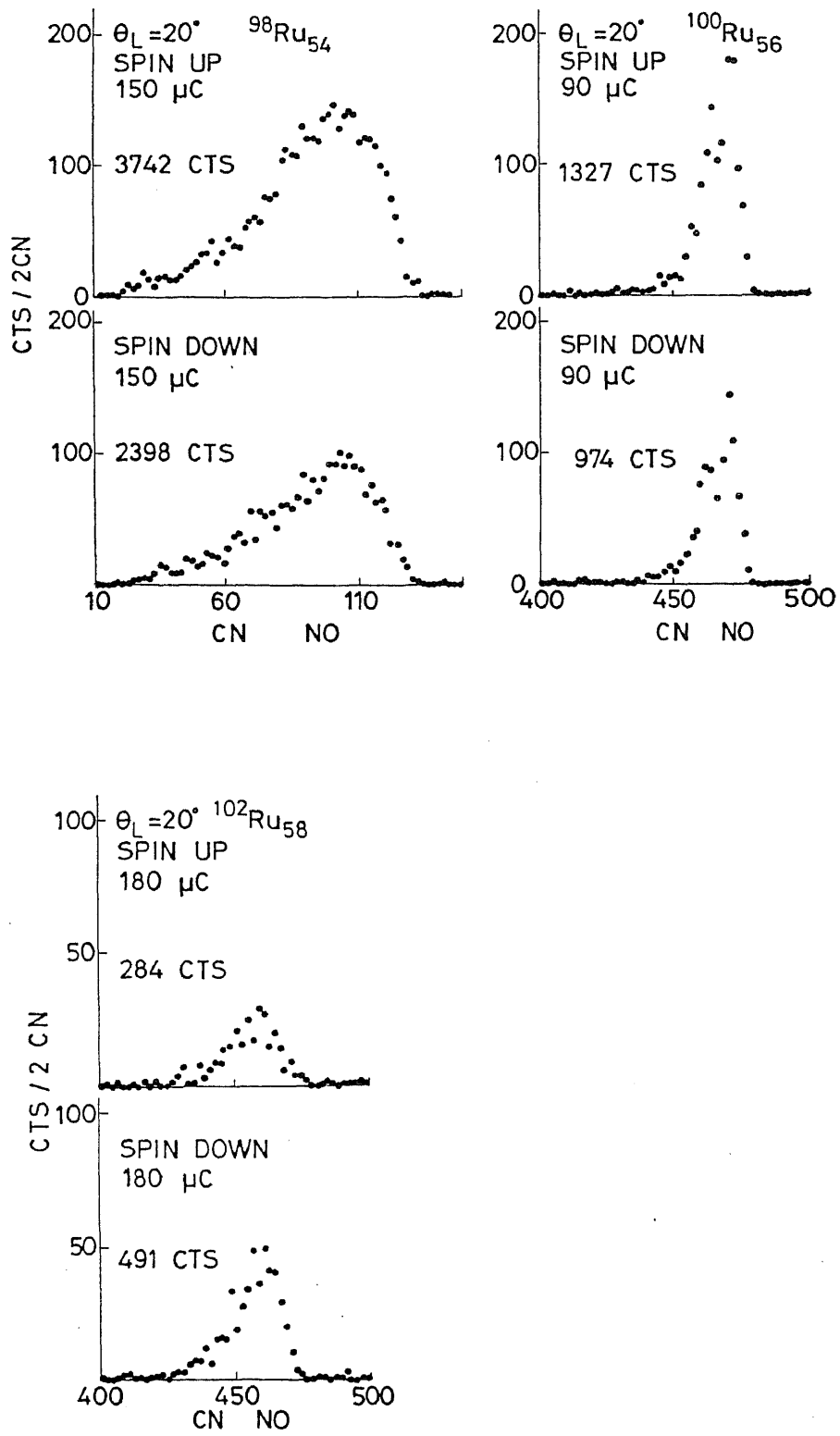


Fig. 5 - 1

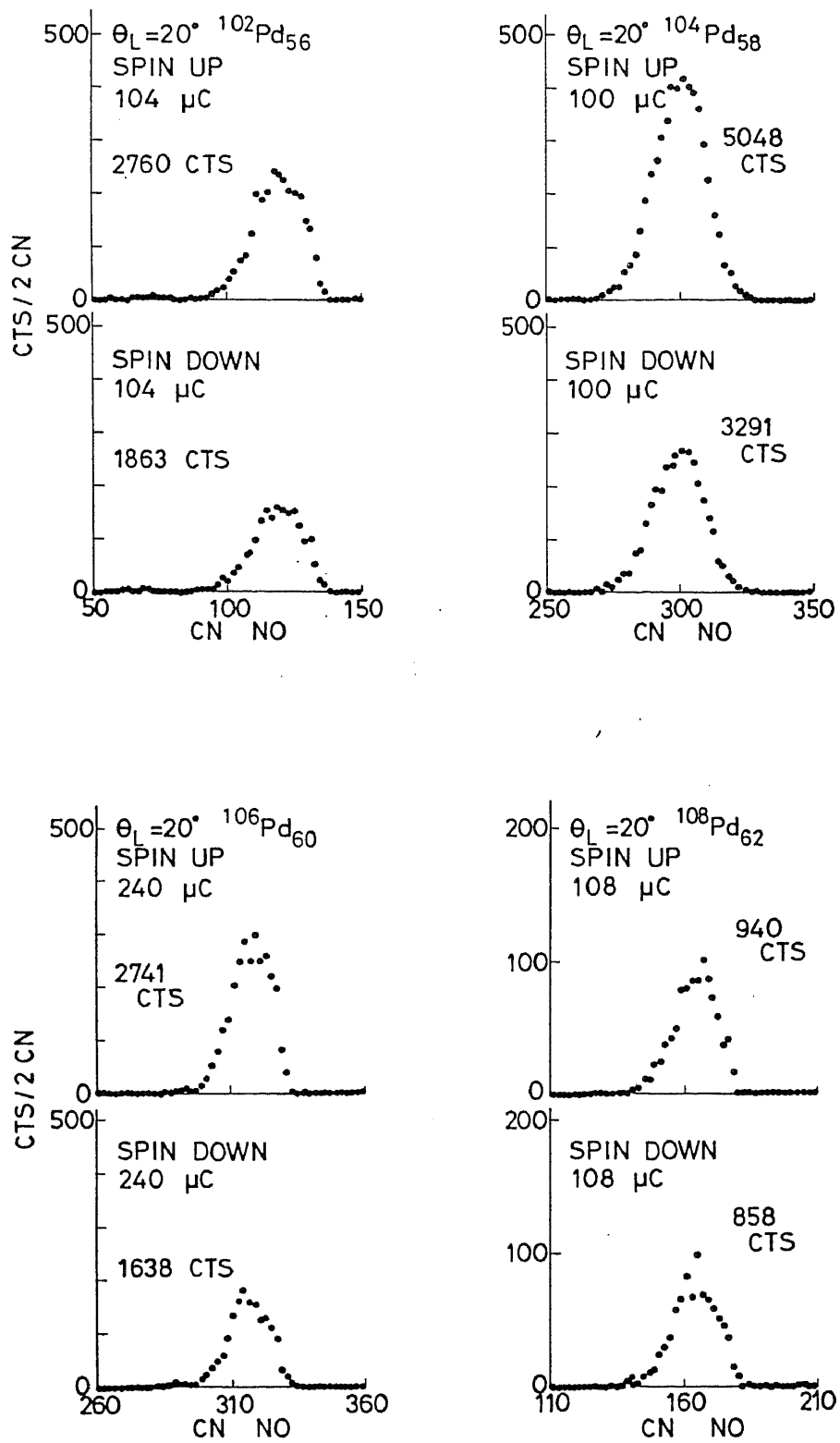


Fig. 5 - 2

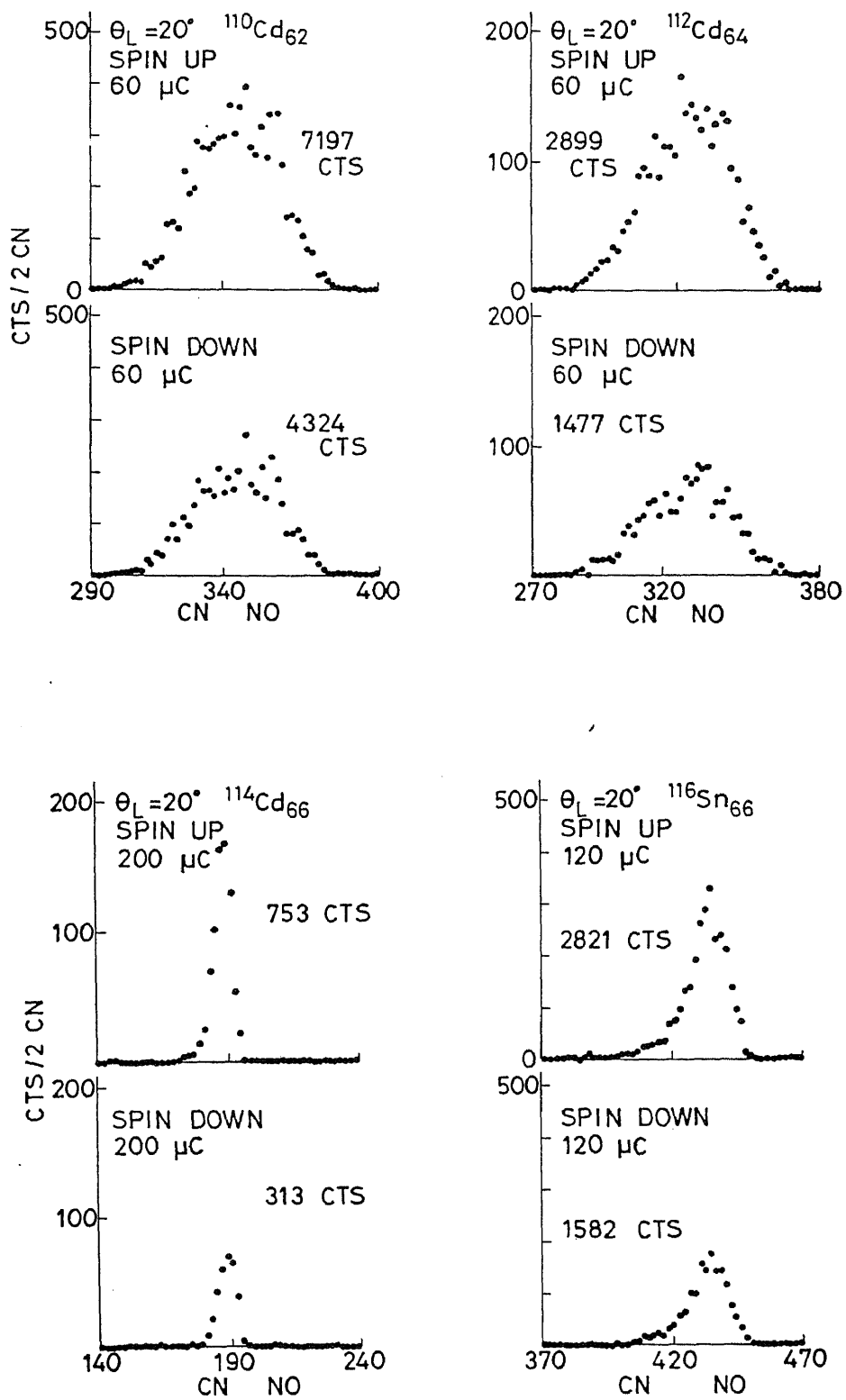


Fig. 5 - 3

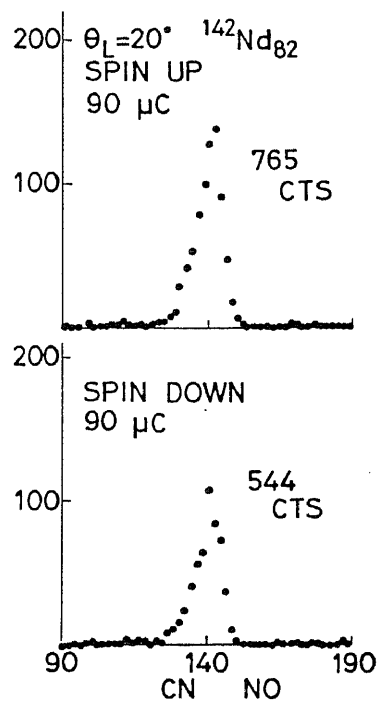
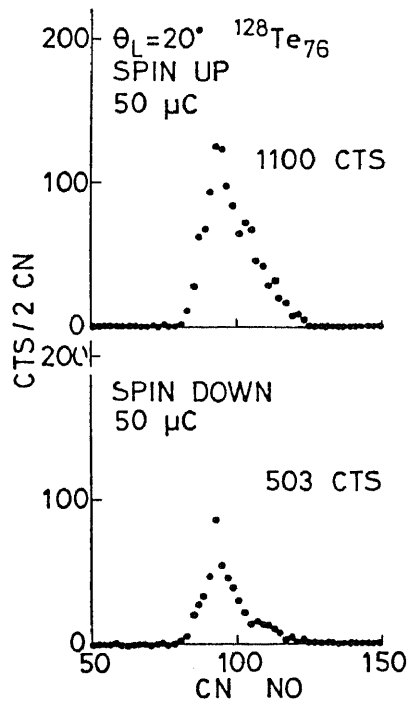
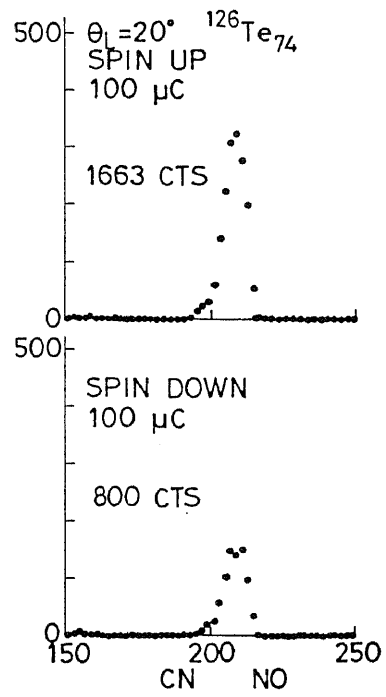
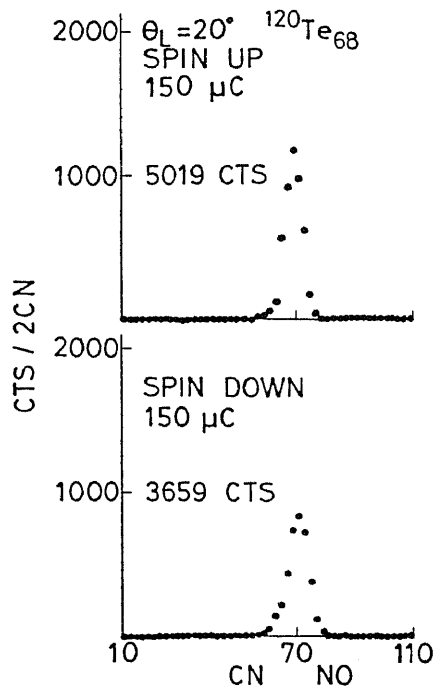


Fig. 5 - 4

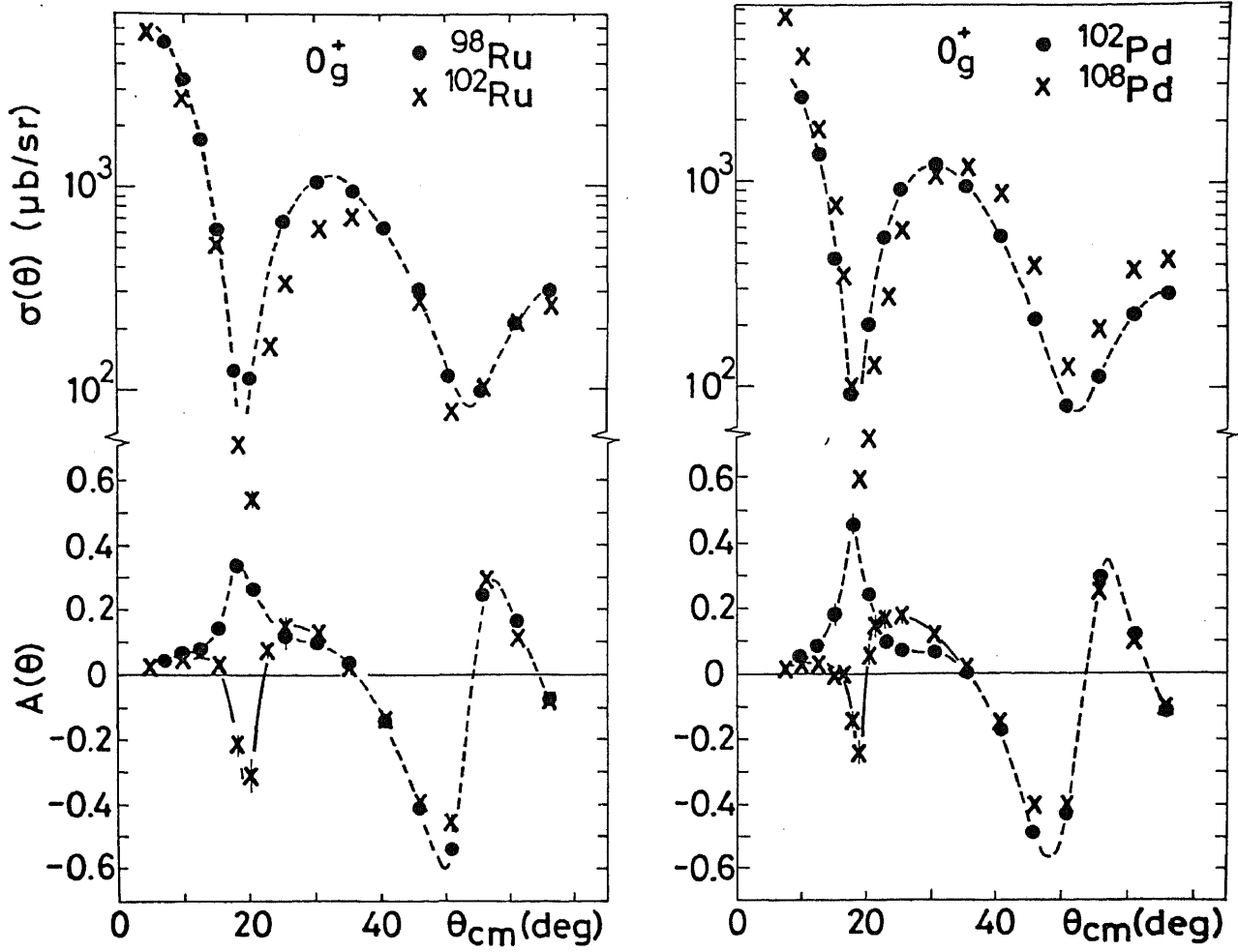


Fig. 6

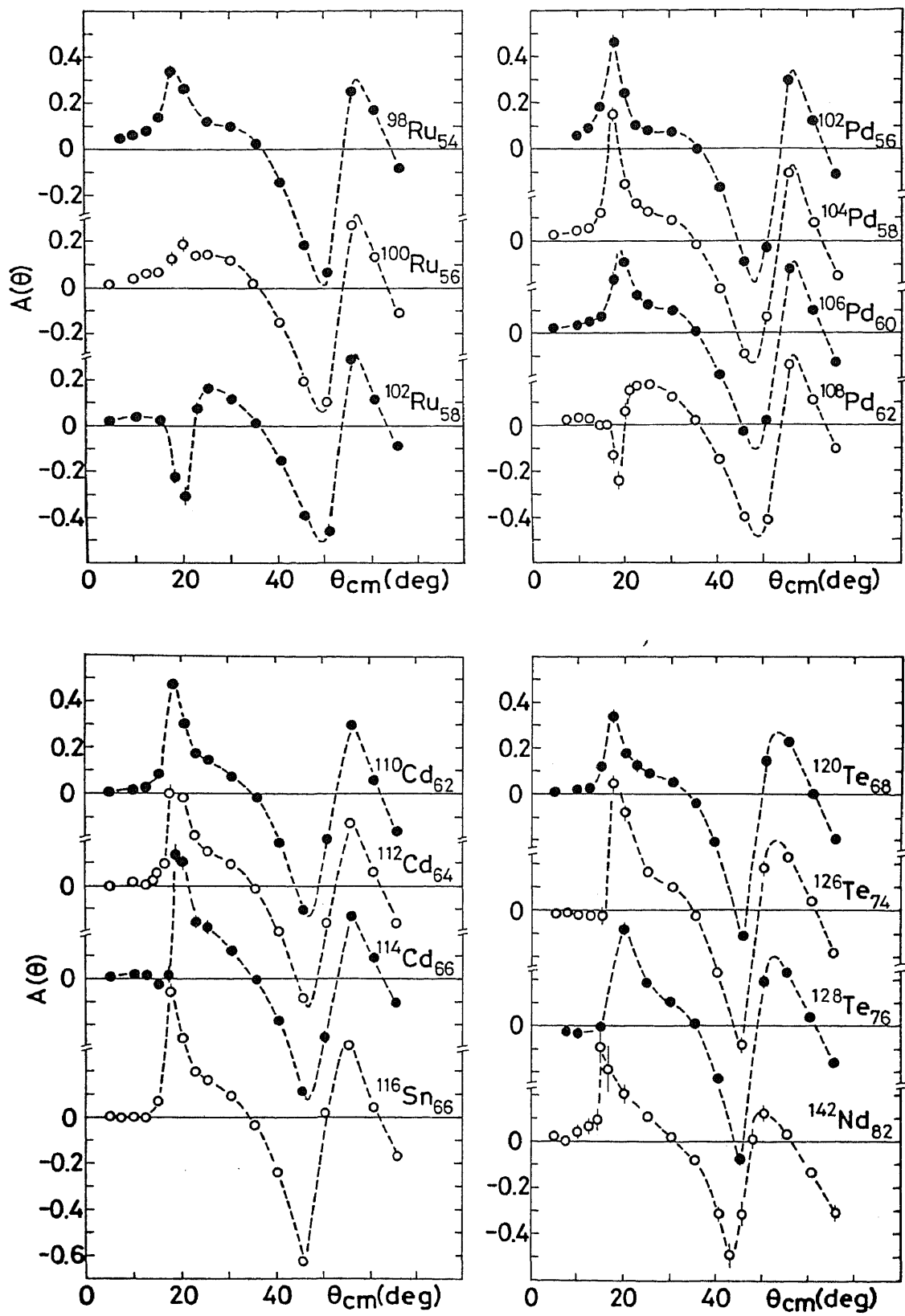


Fig. 7

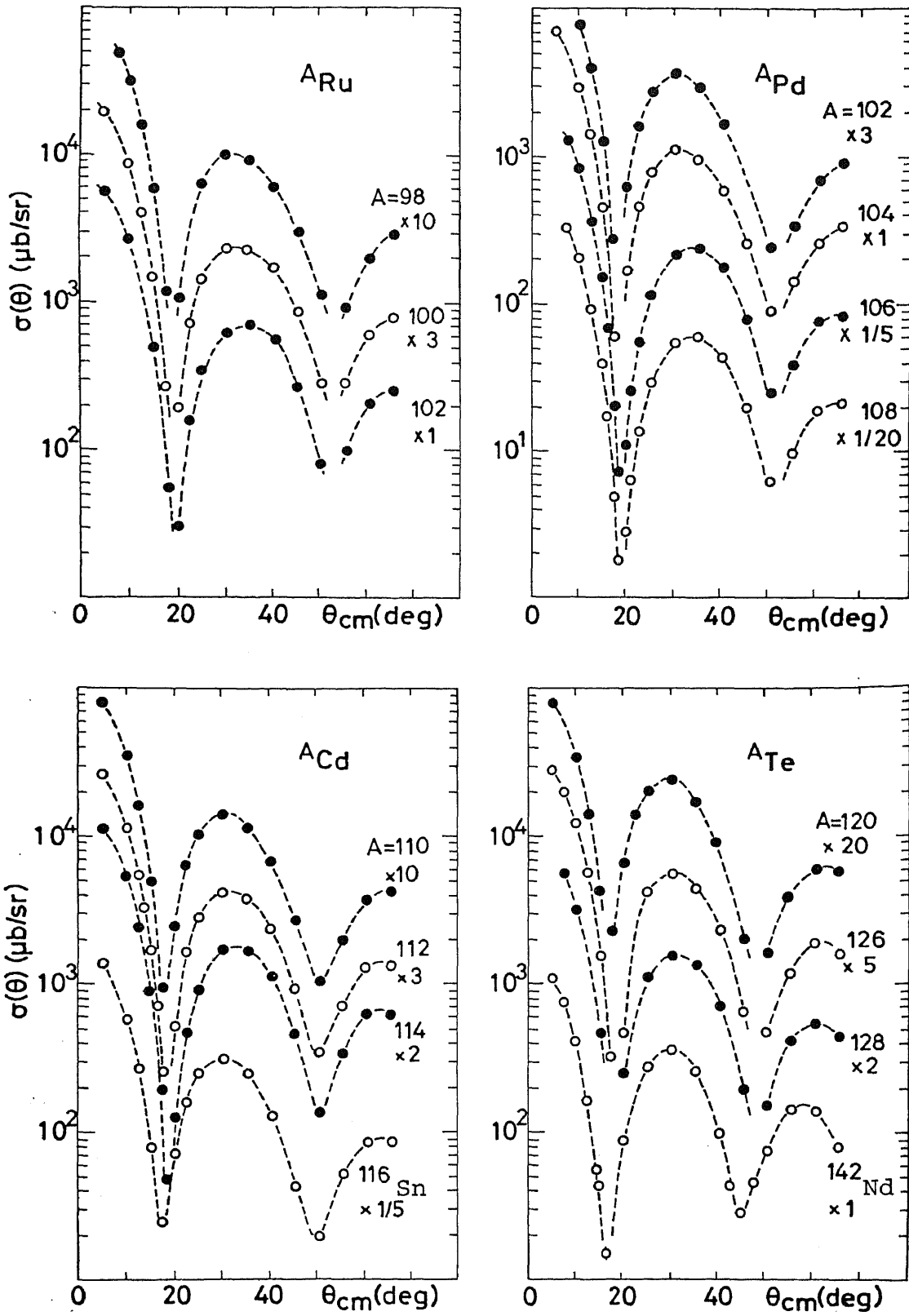


Fig. 8

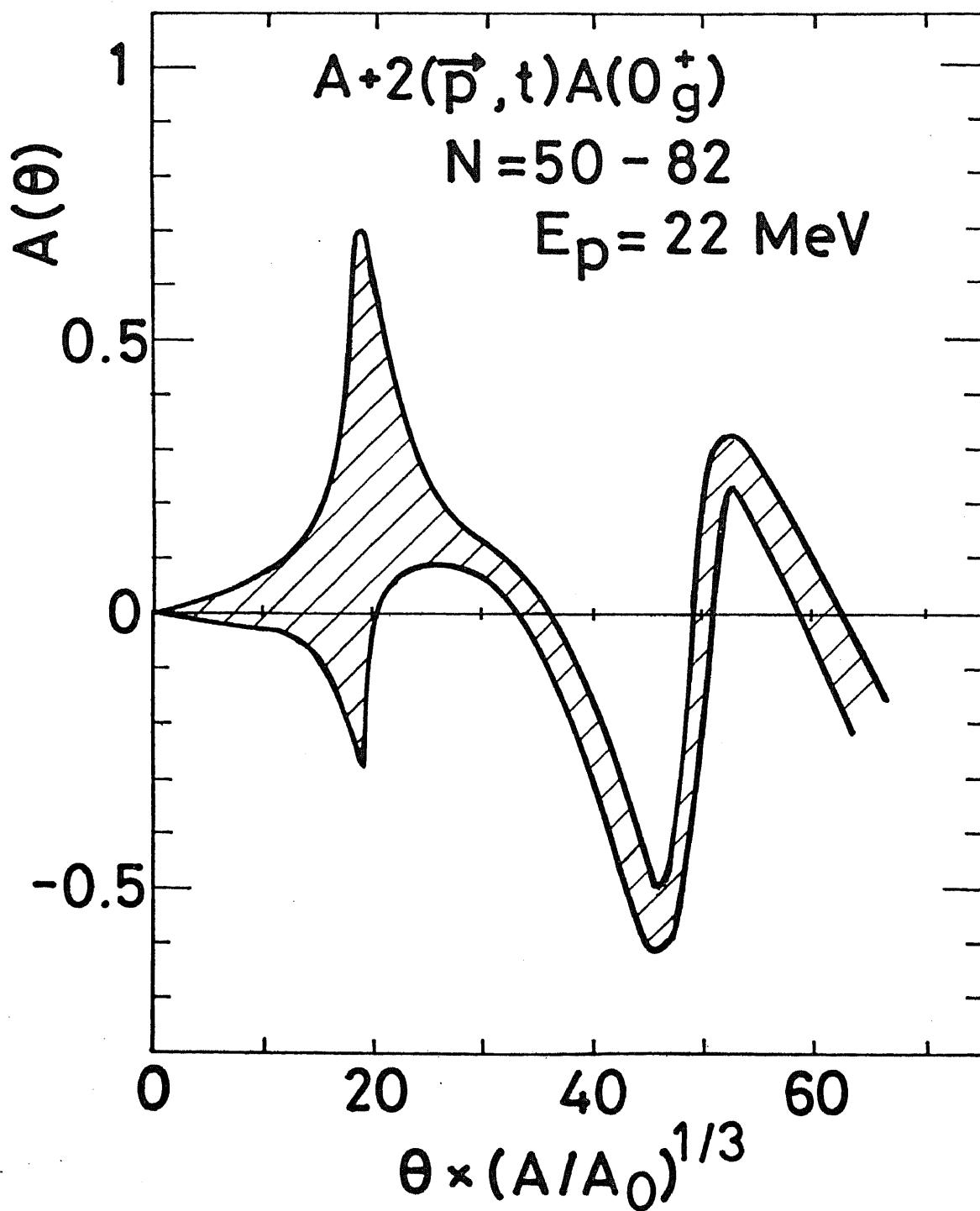


Fig. 9

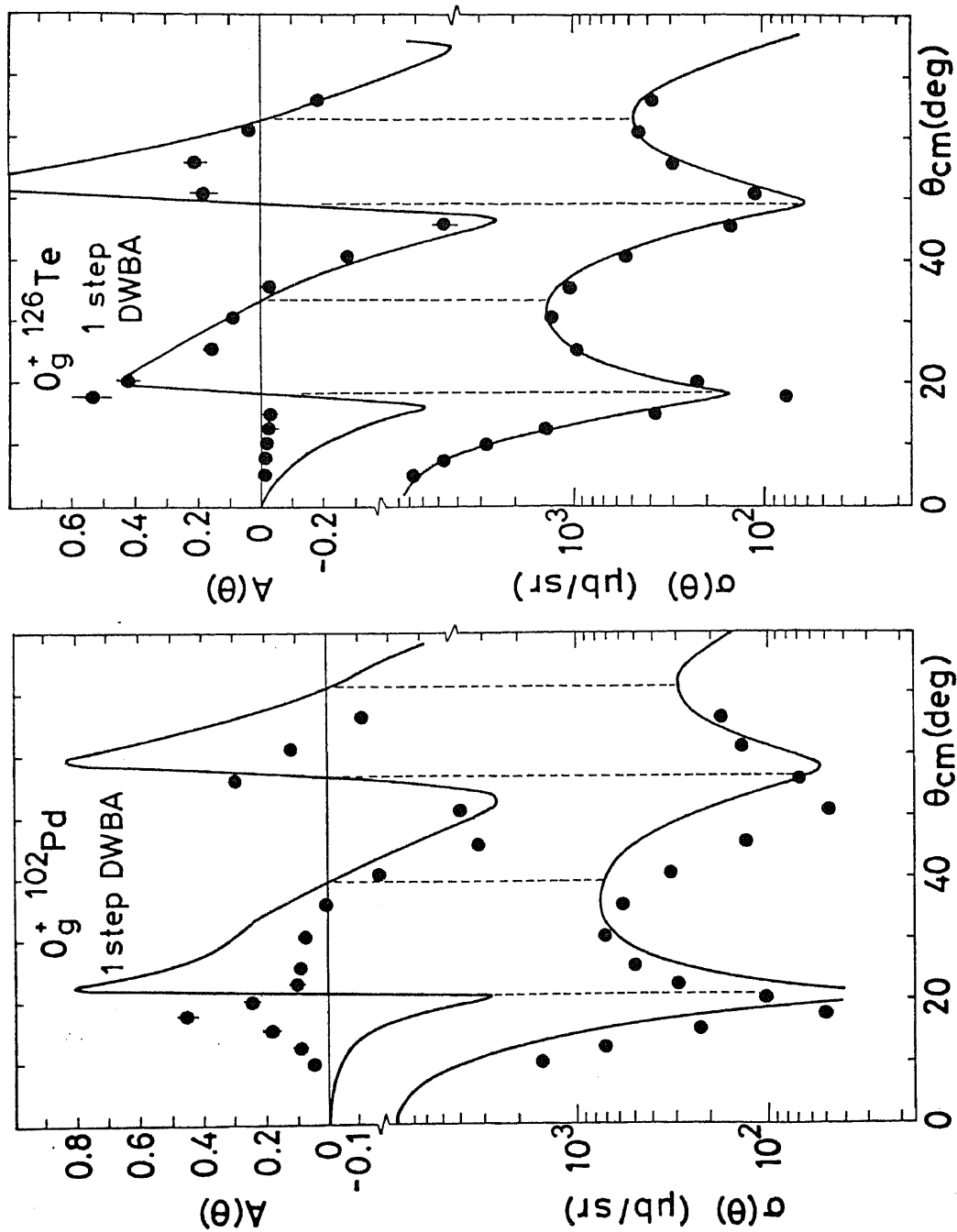


Fig. 10

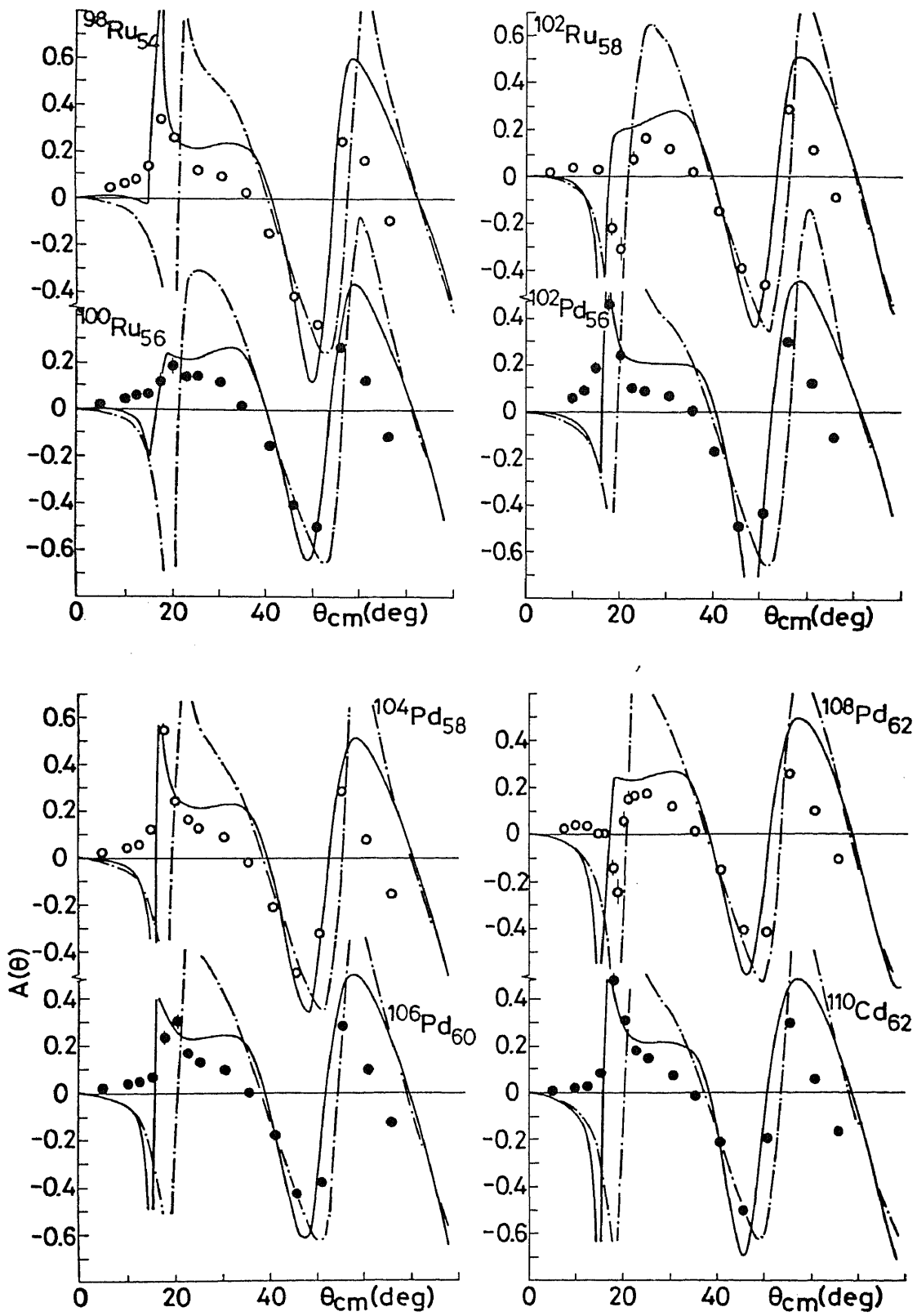


Fig. 11 - 1

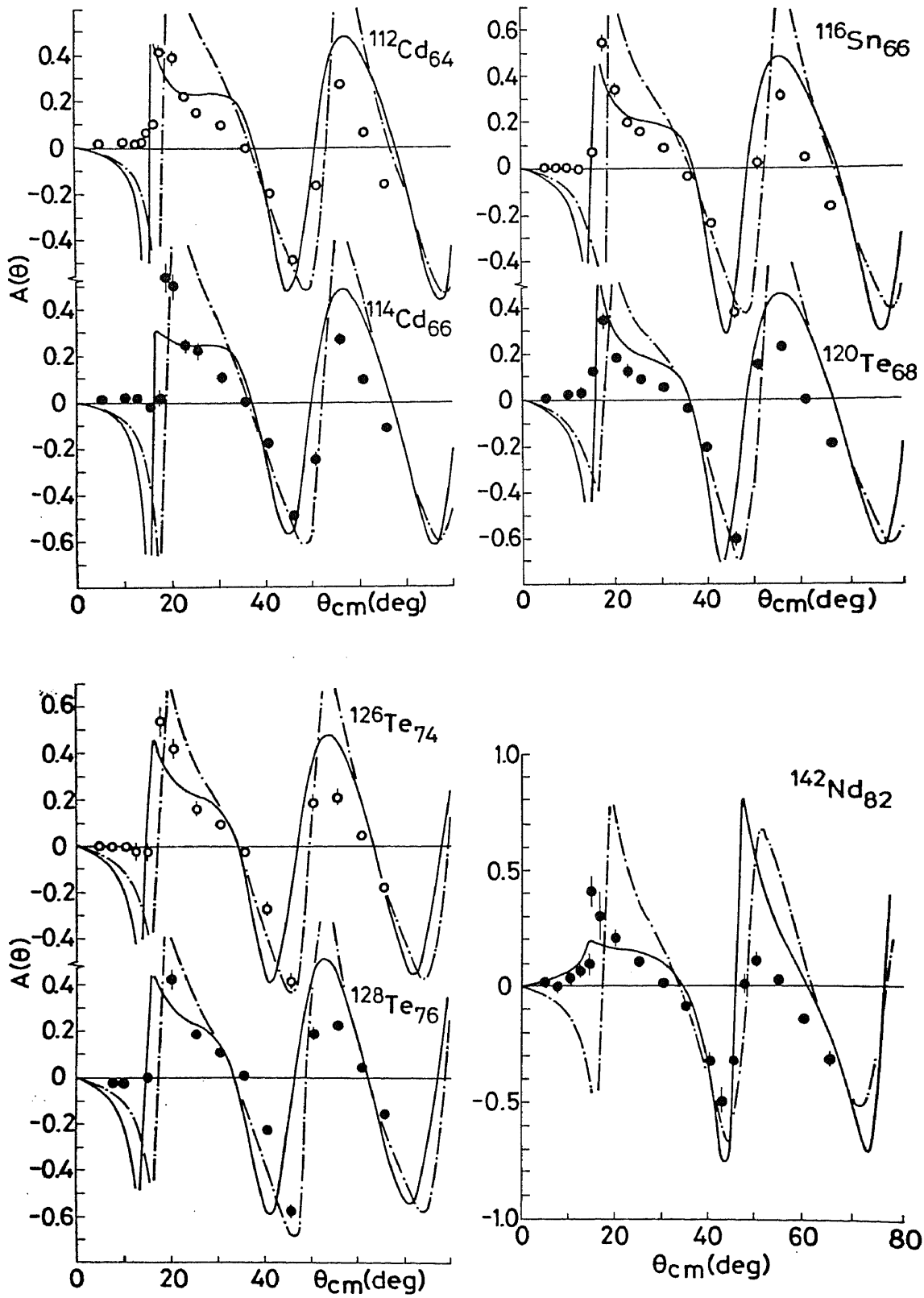


Fig. 11 - 2

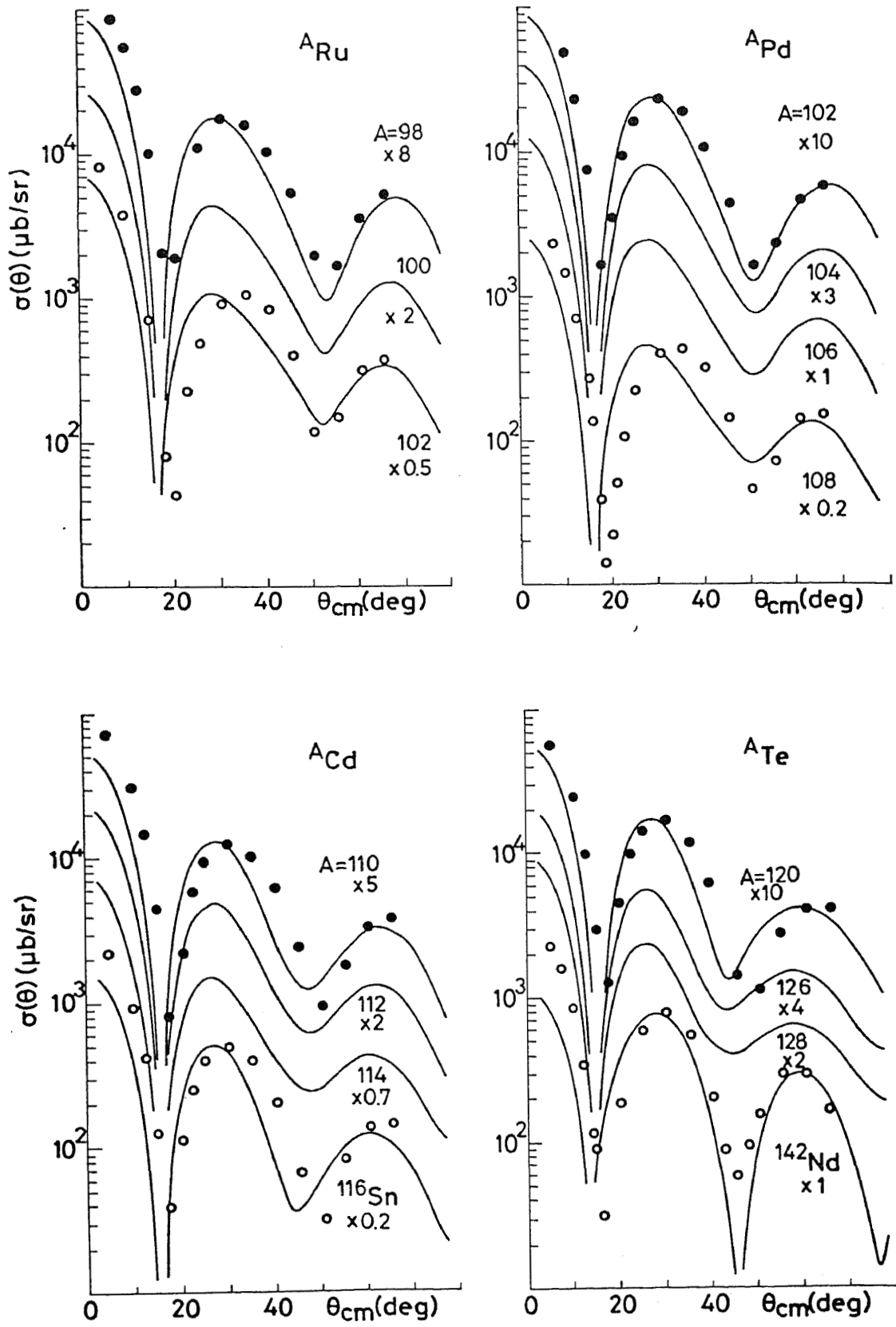


Fig. 12

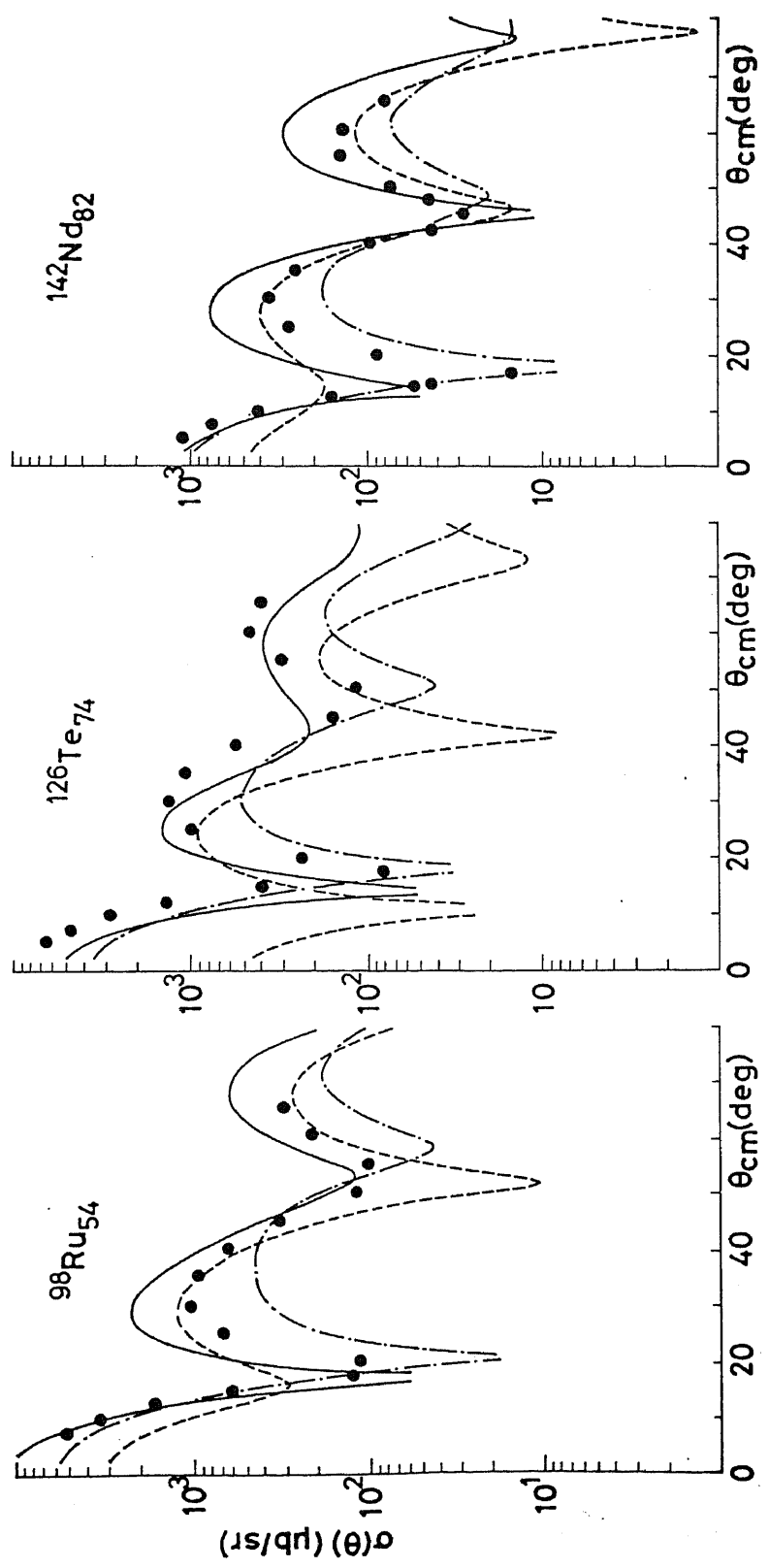


Fig. 13

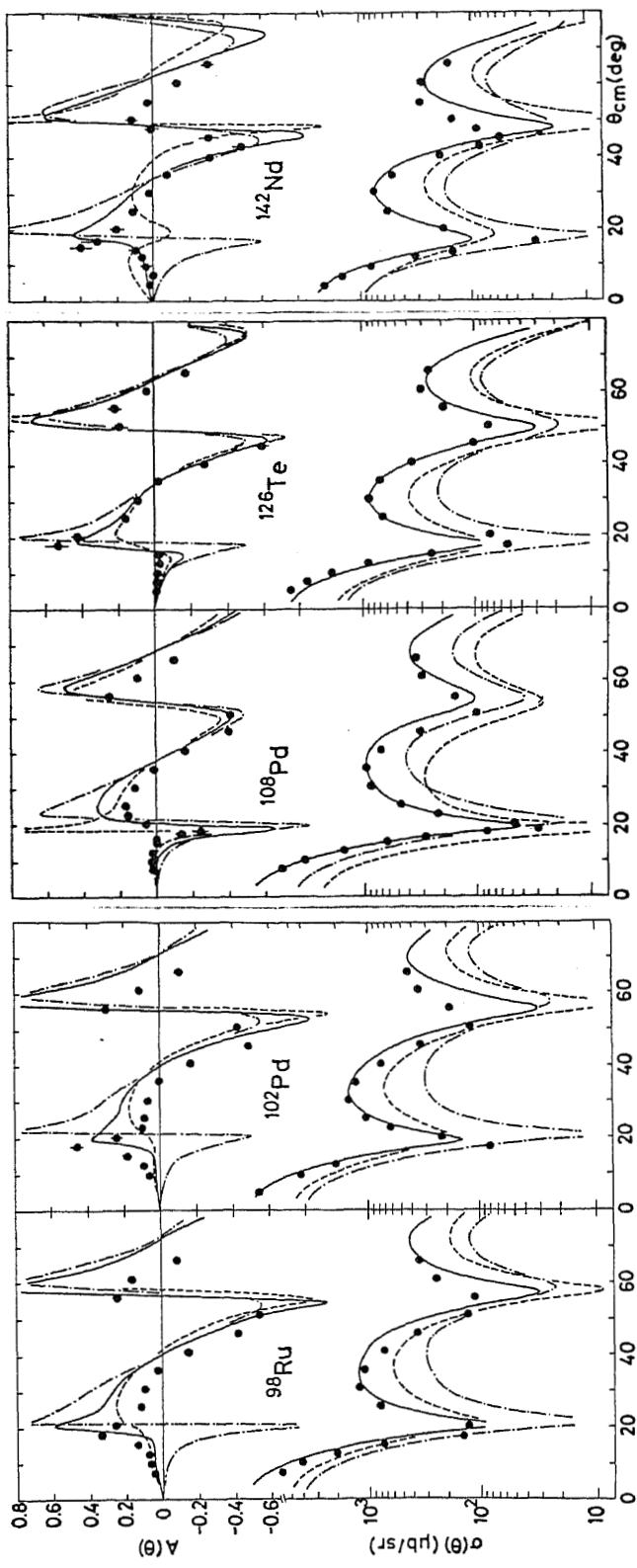


Fig. 14

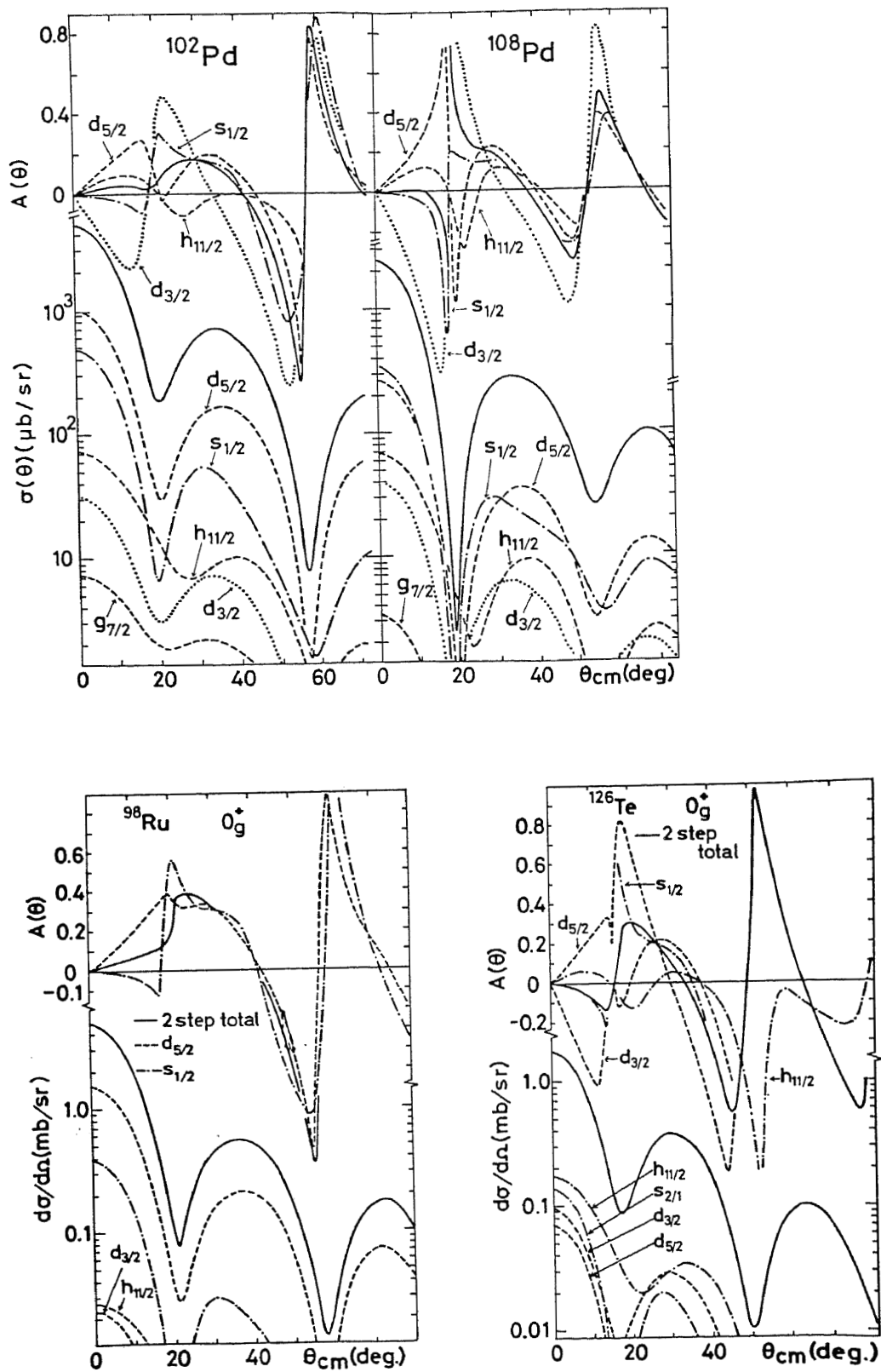


Fig. 15

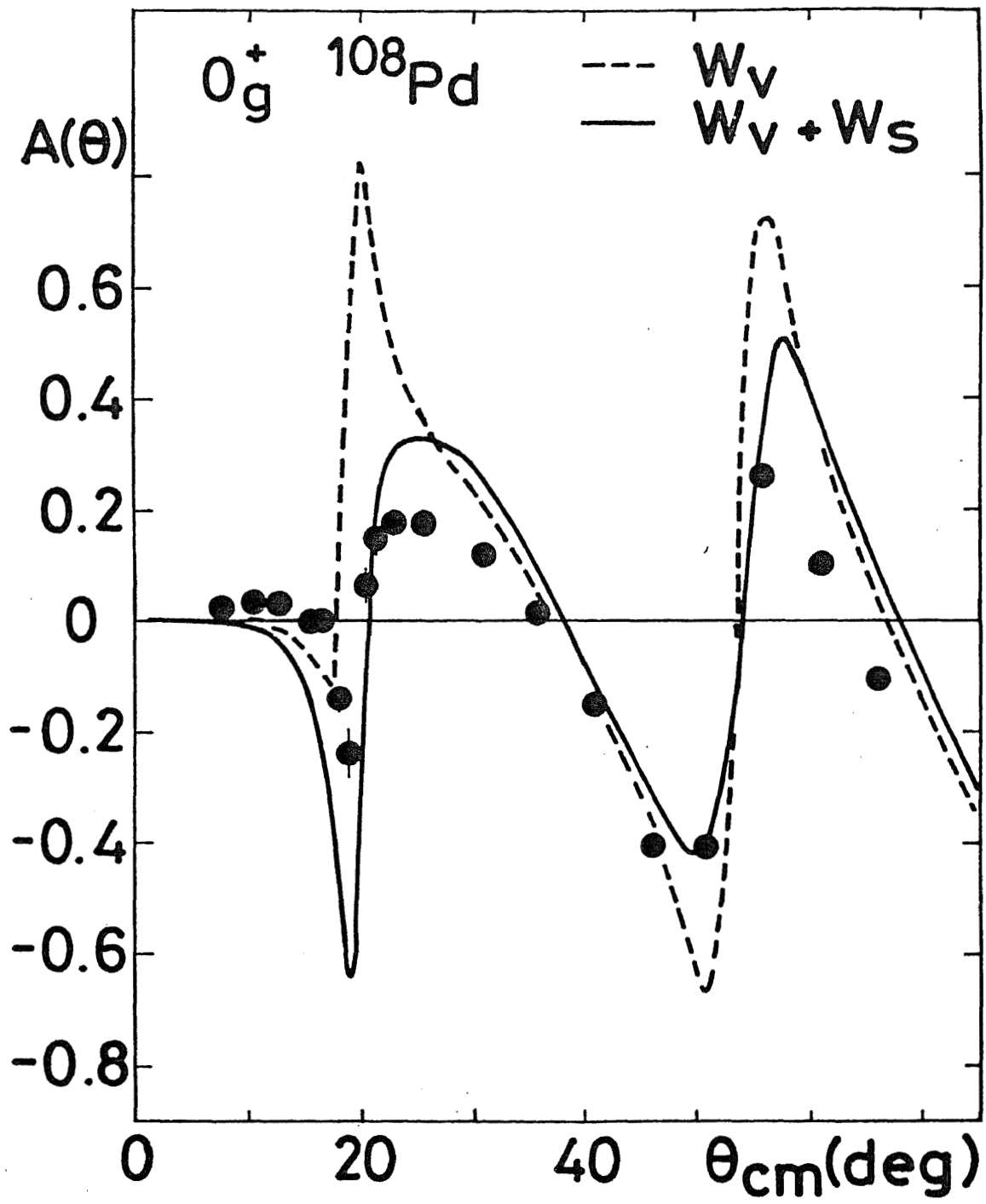


Fig. 16

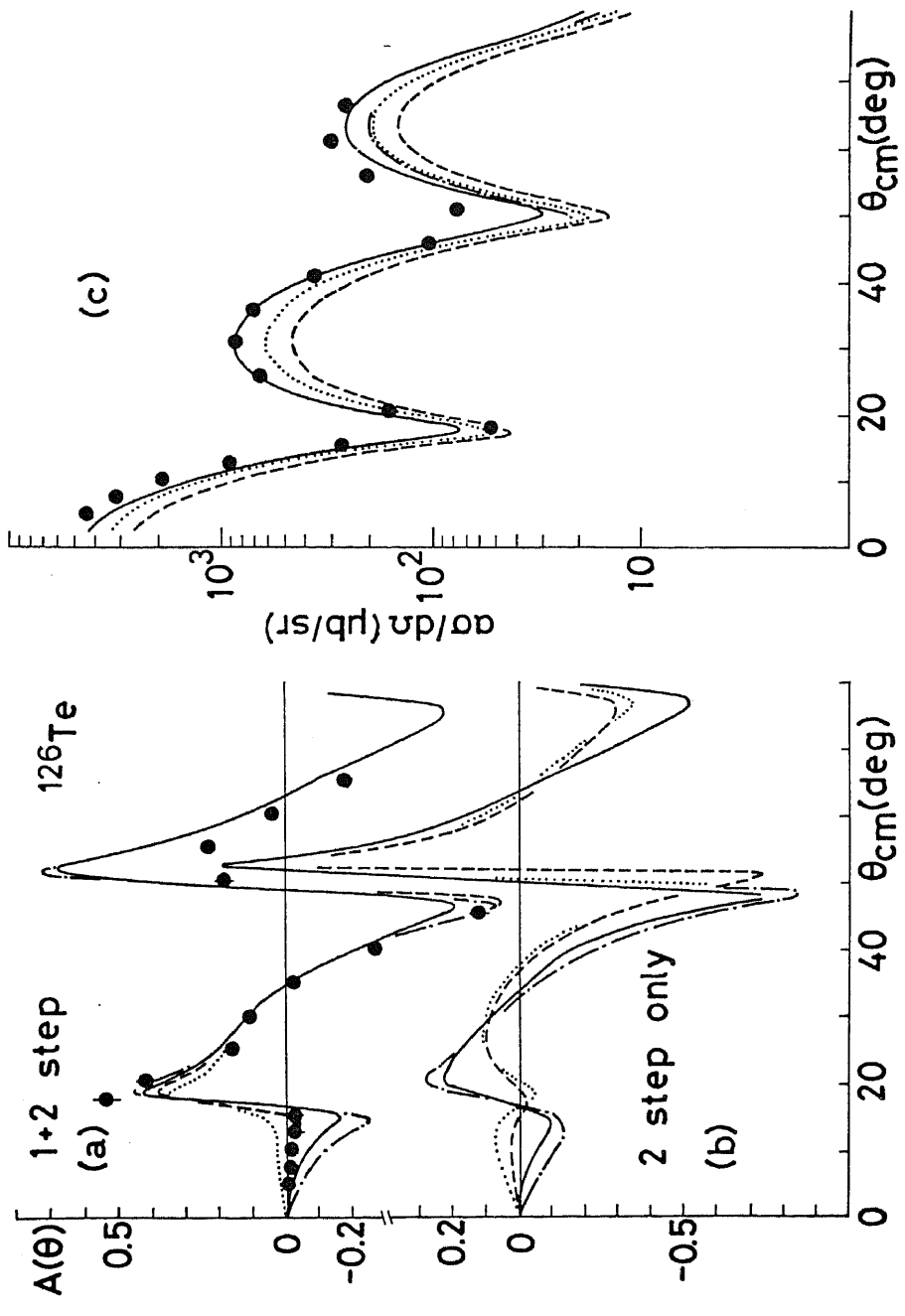


Fig. 17

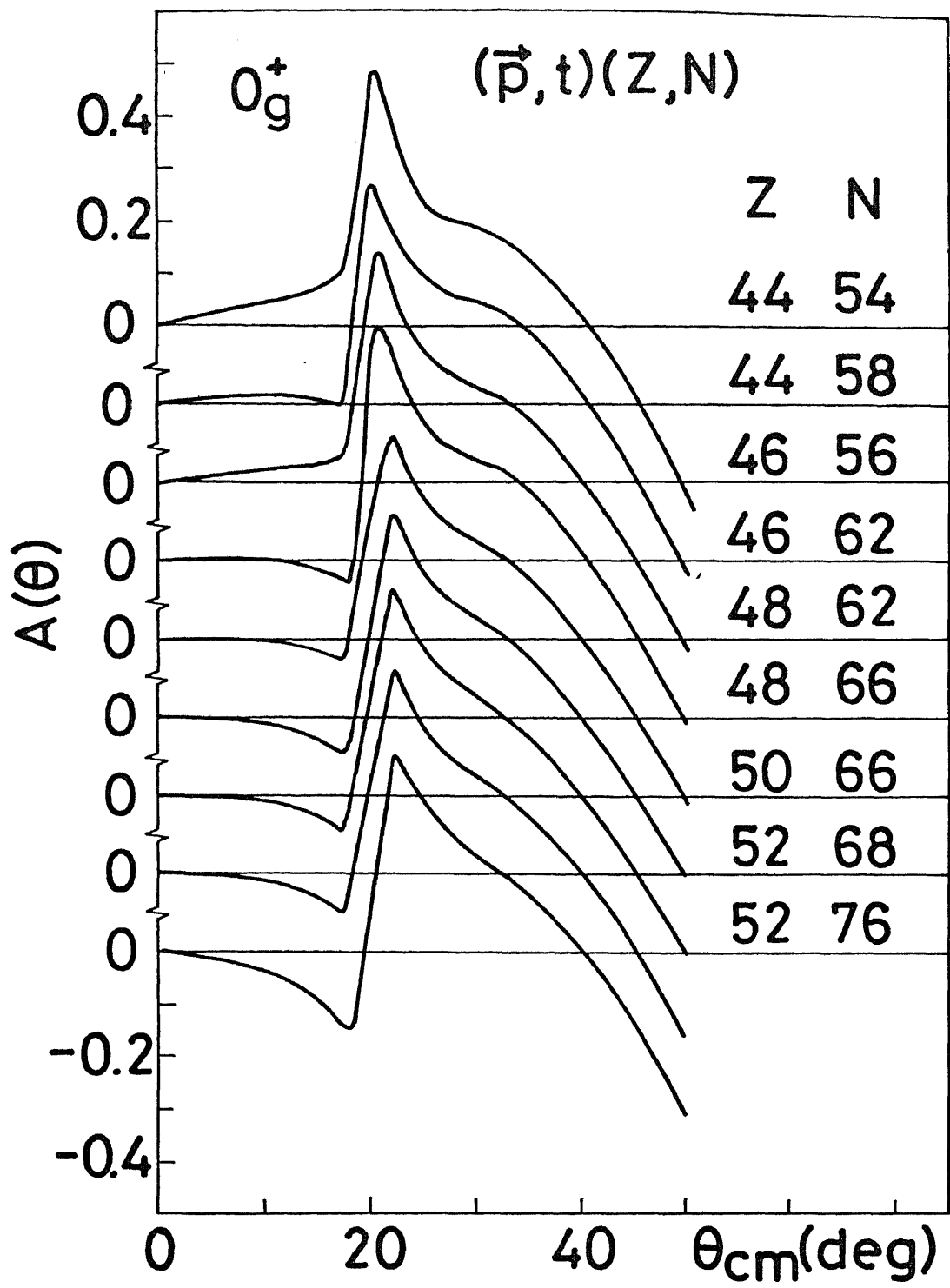


Fig. 18

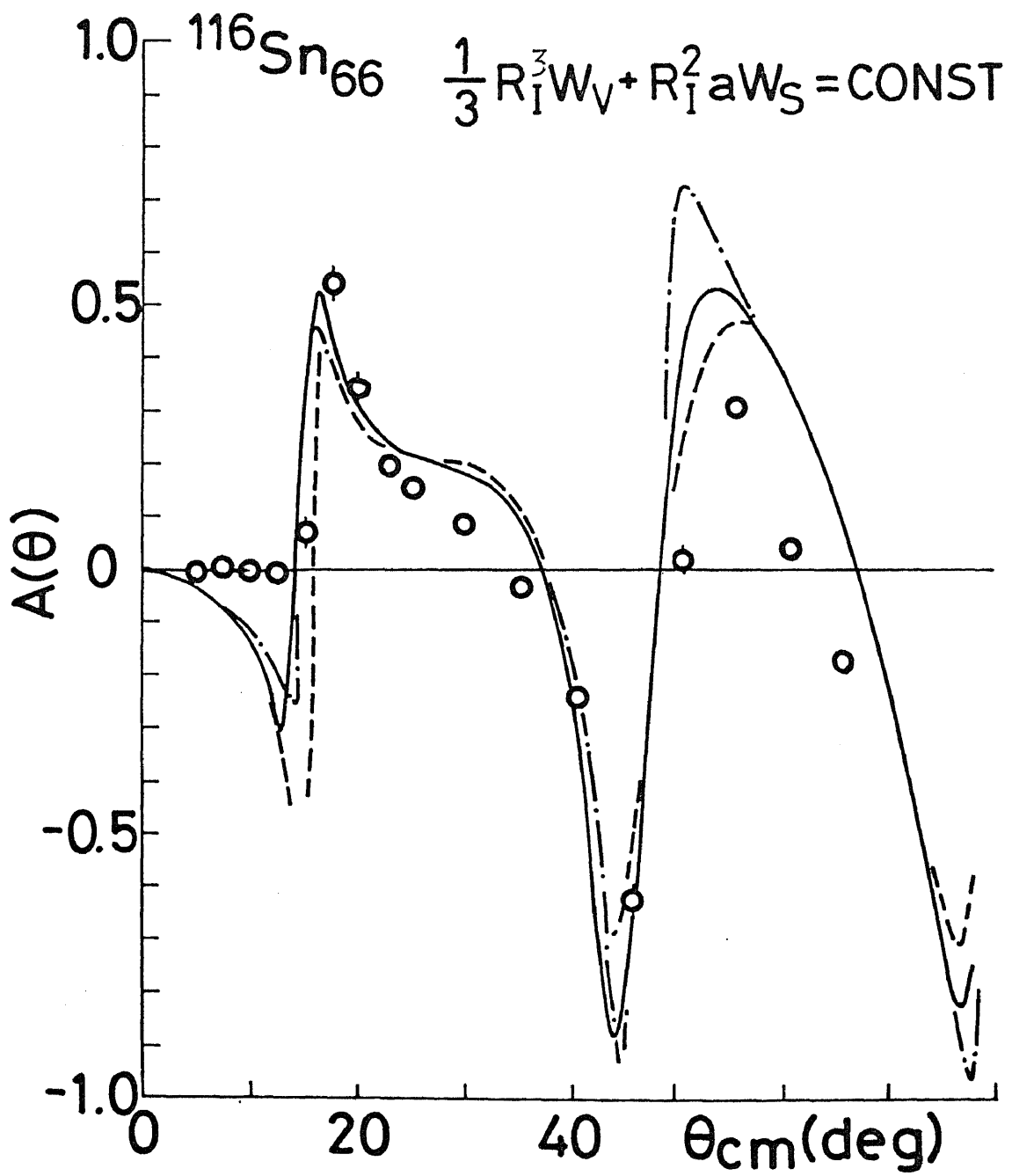


Fig. 19

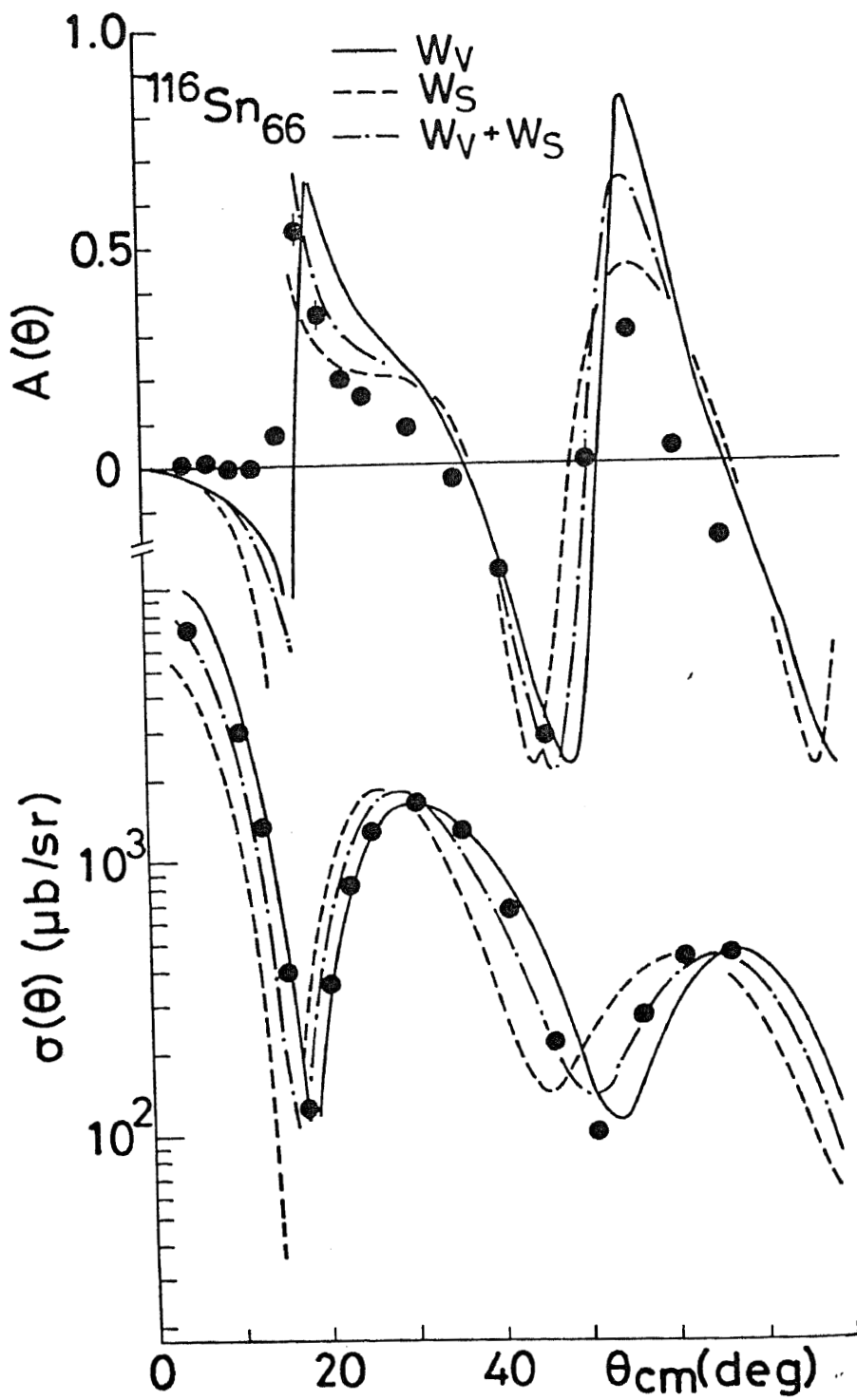


Fig. 20

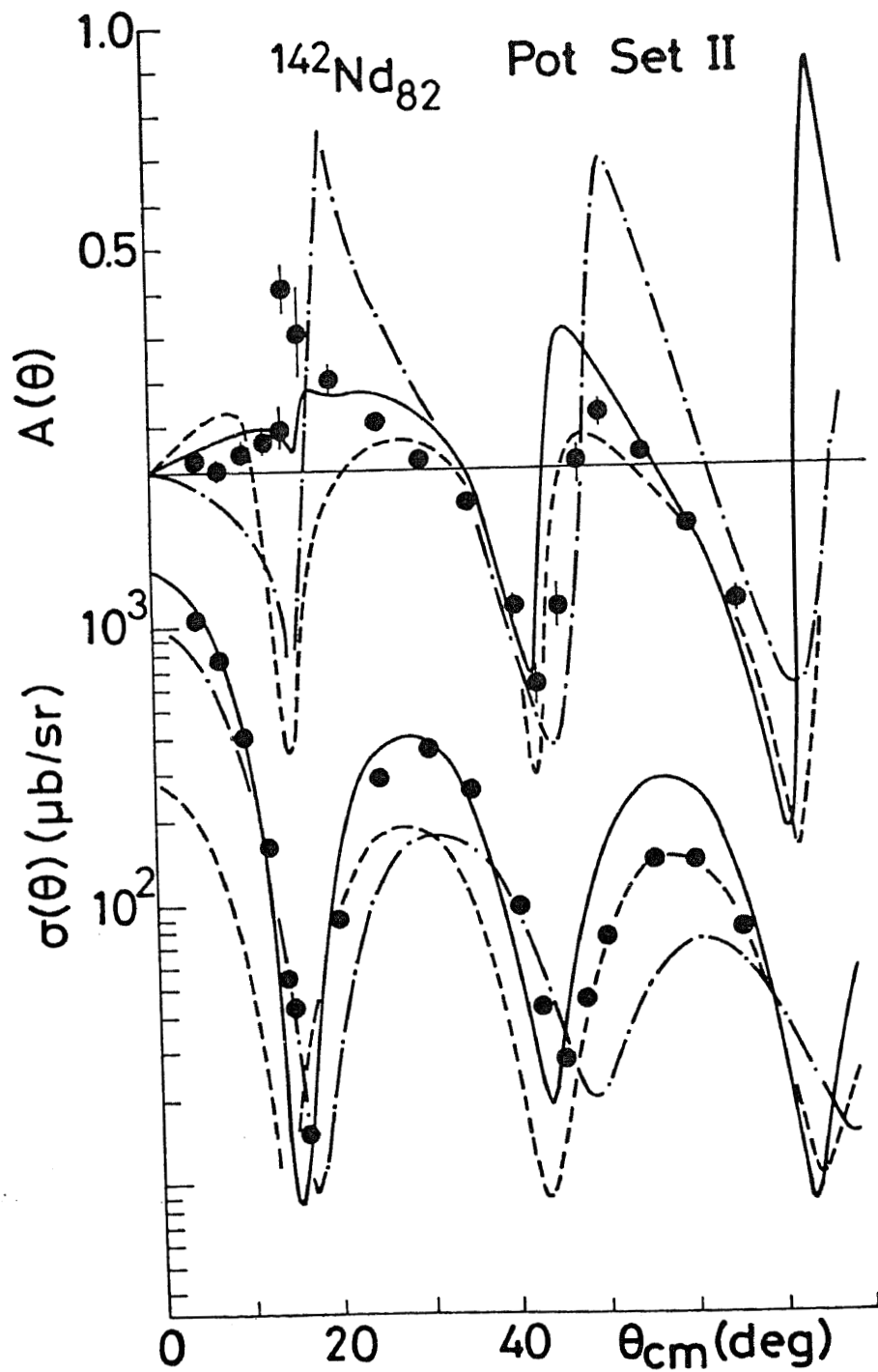


Fig. 21

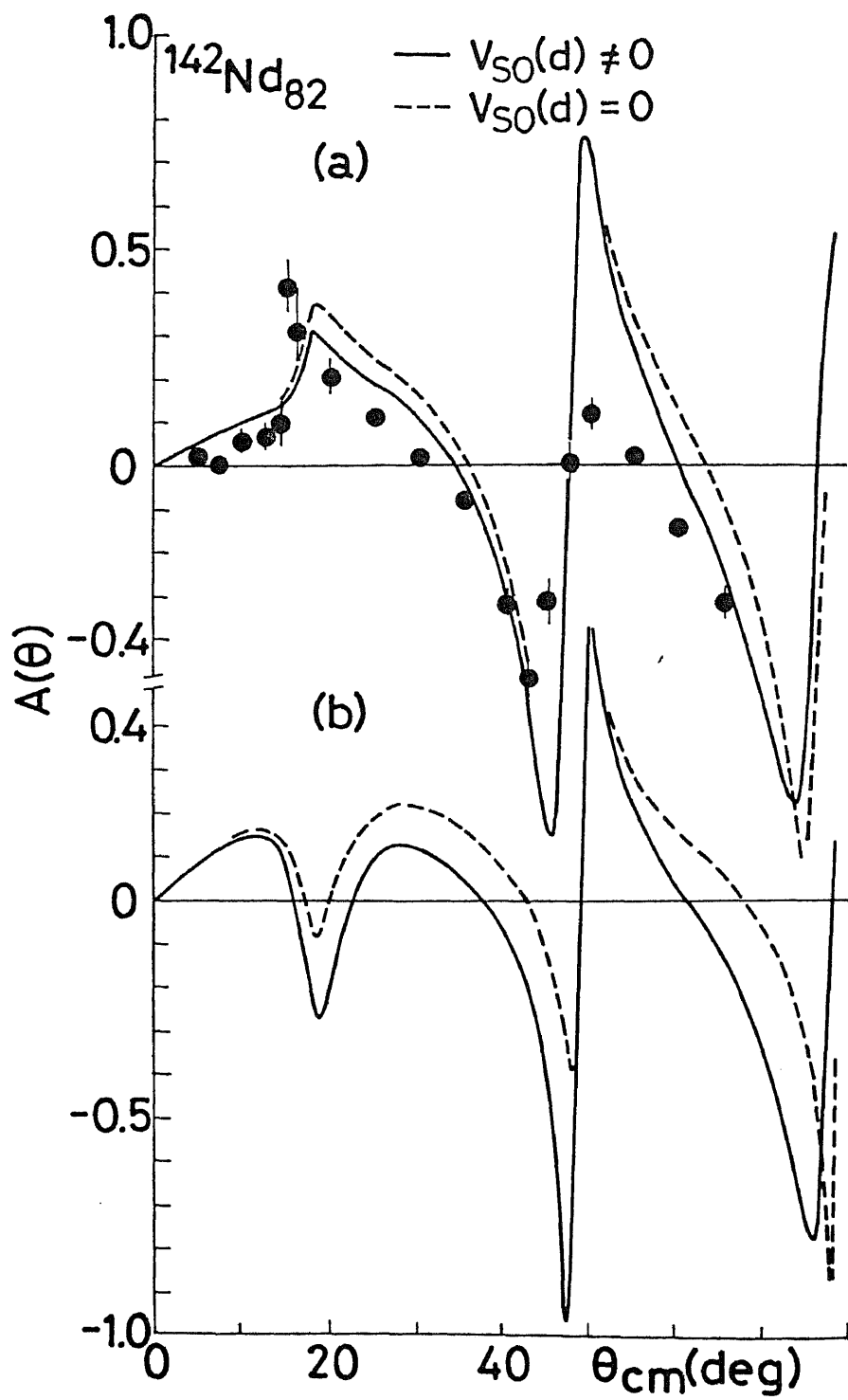


Fig. 22

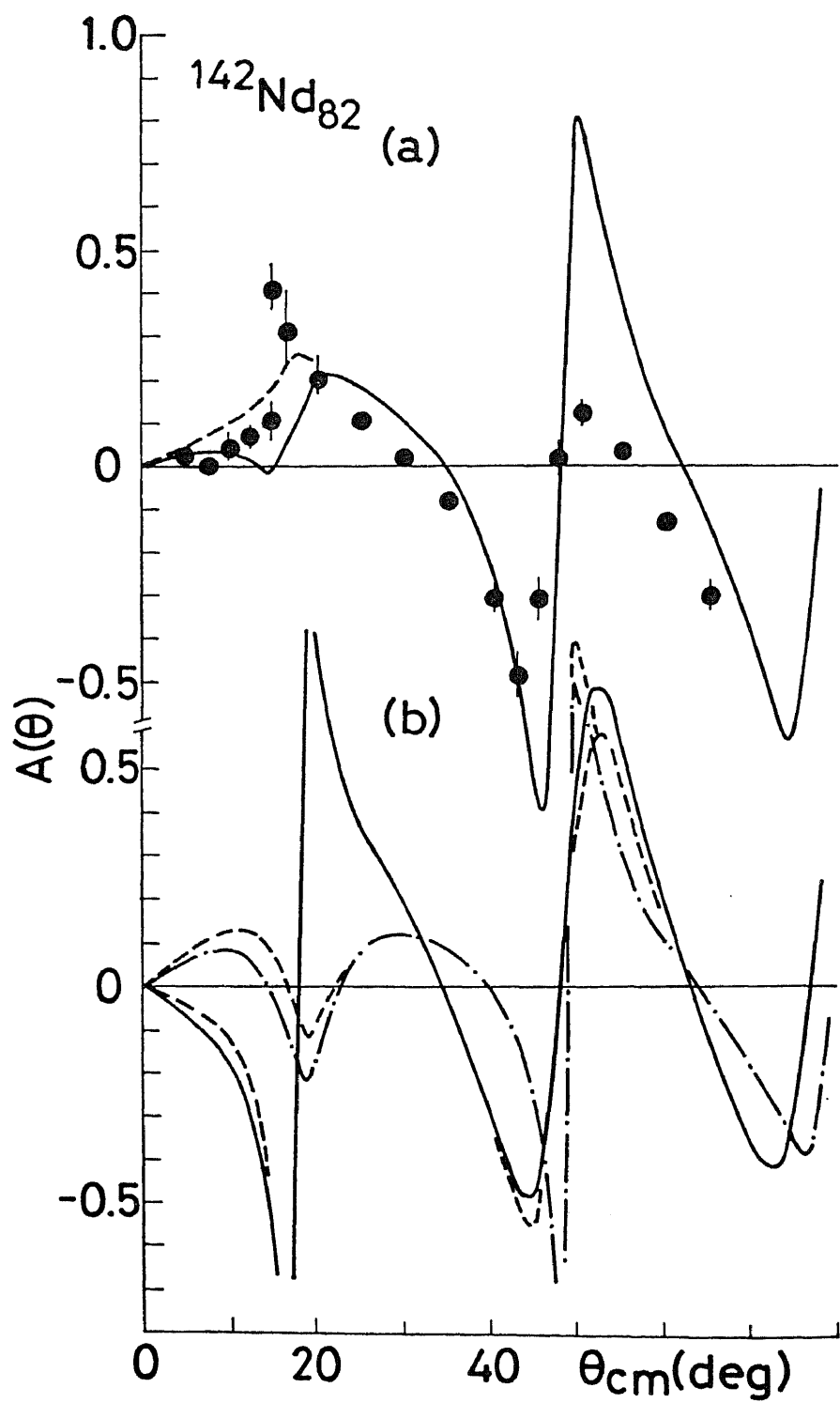


Fig. 23

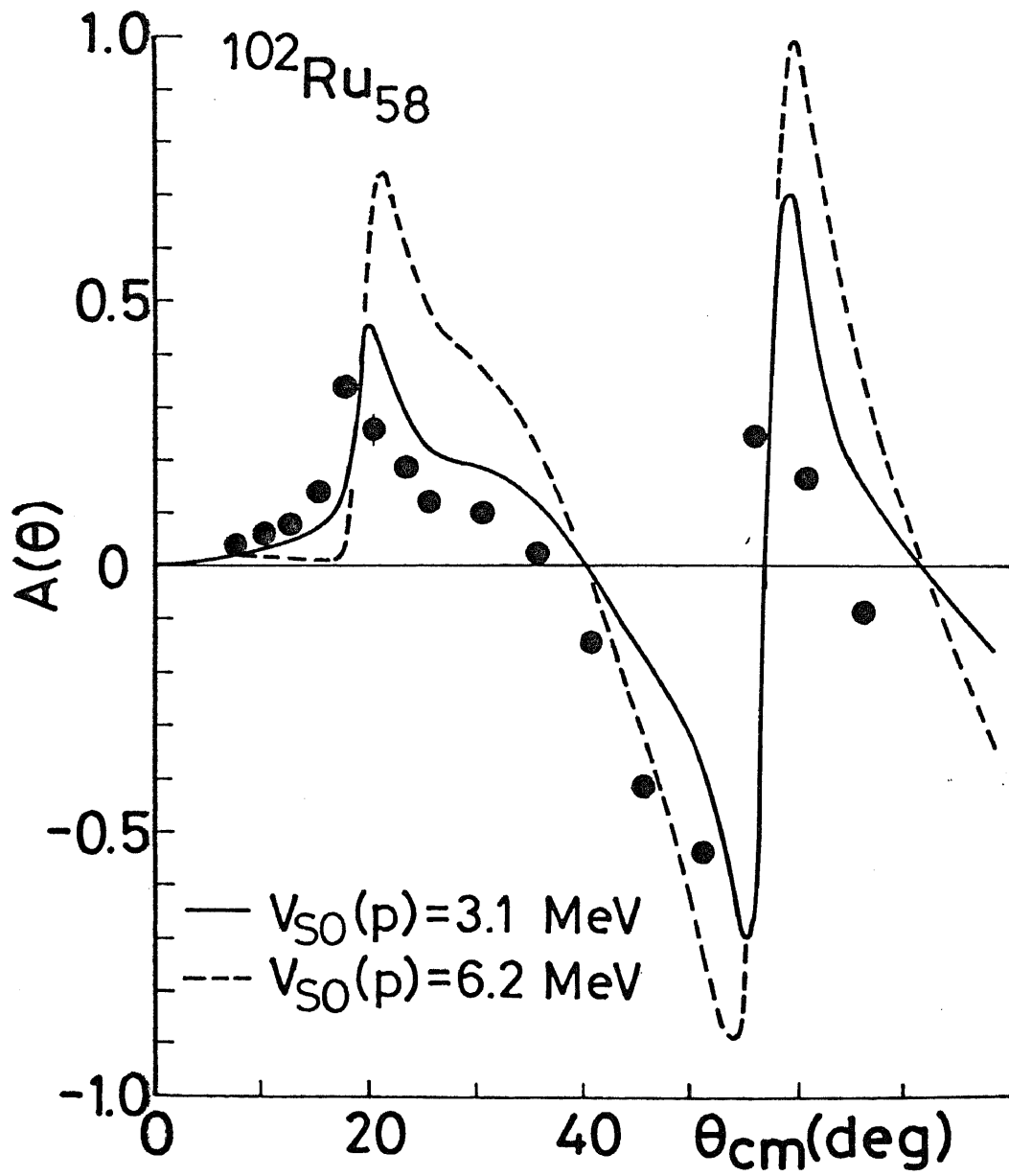


Fig. 24

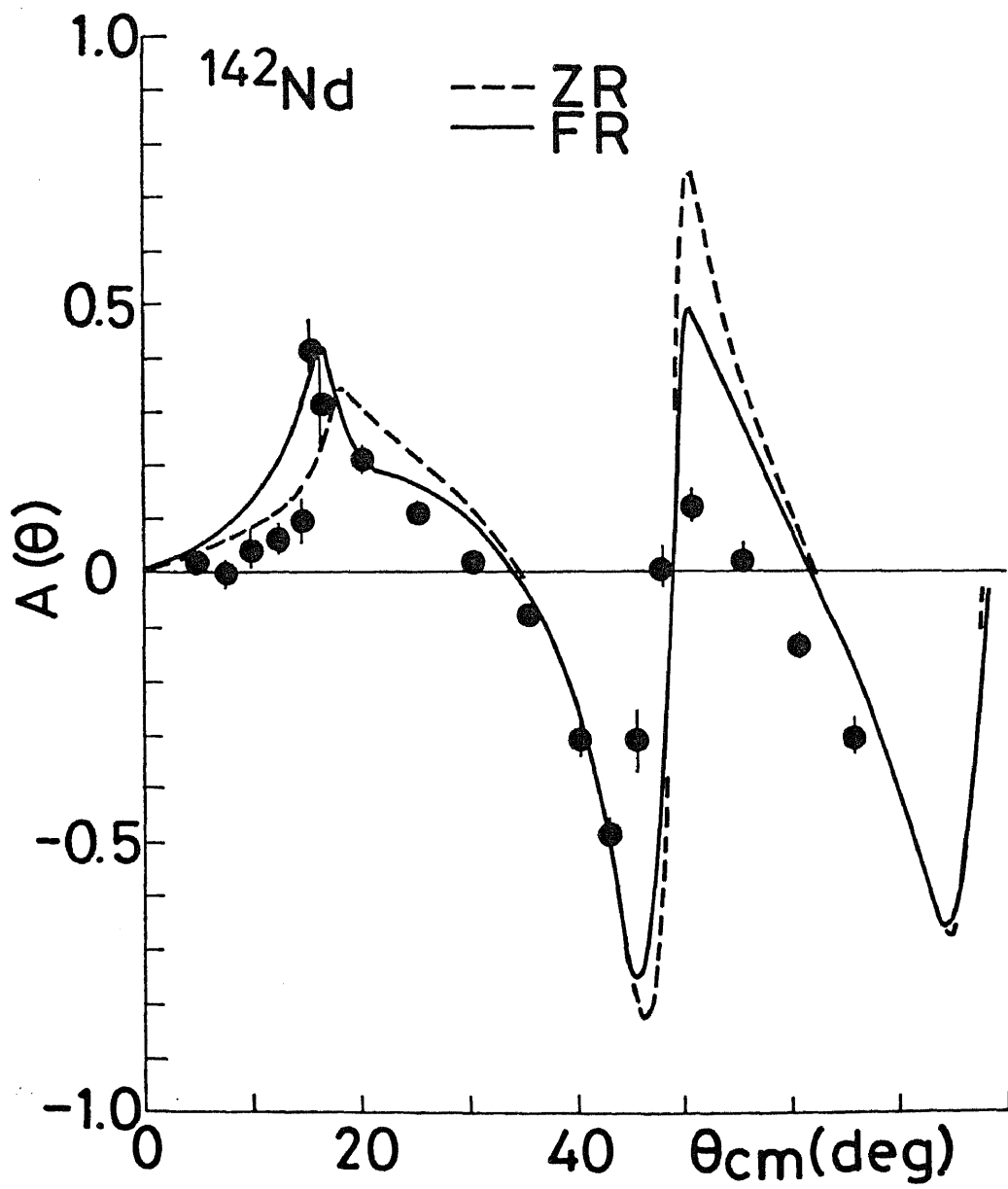


Fig. 25

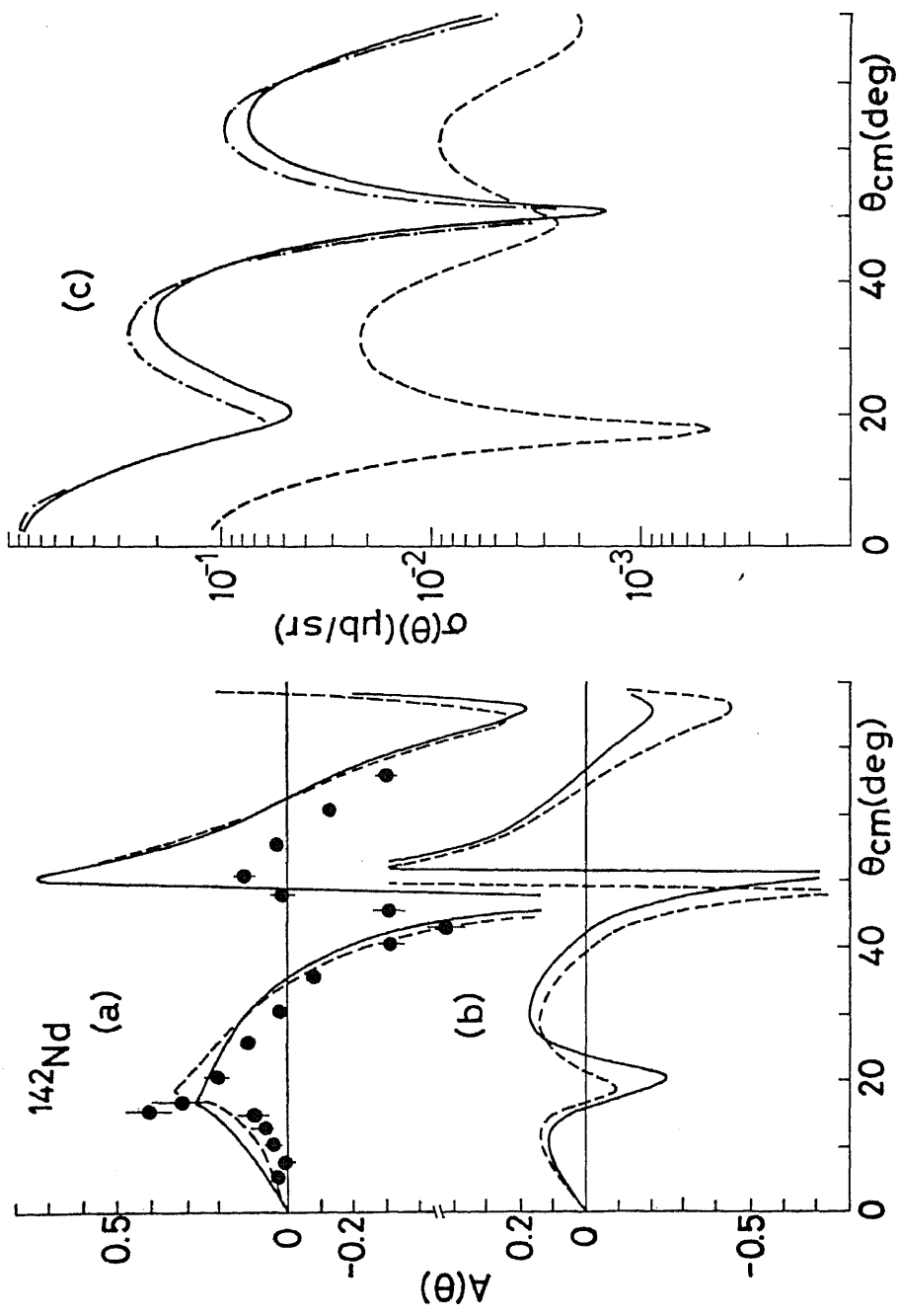


Fig. 26

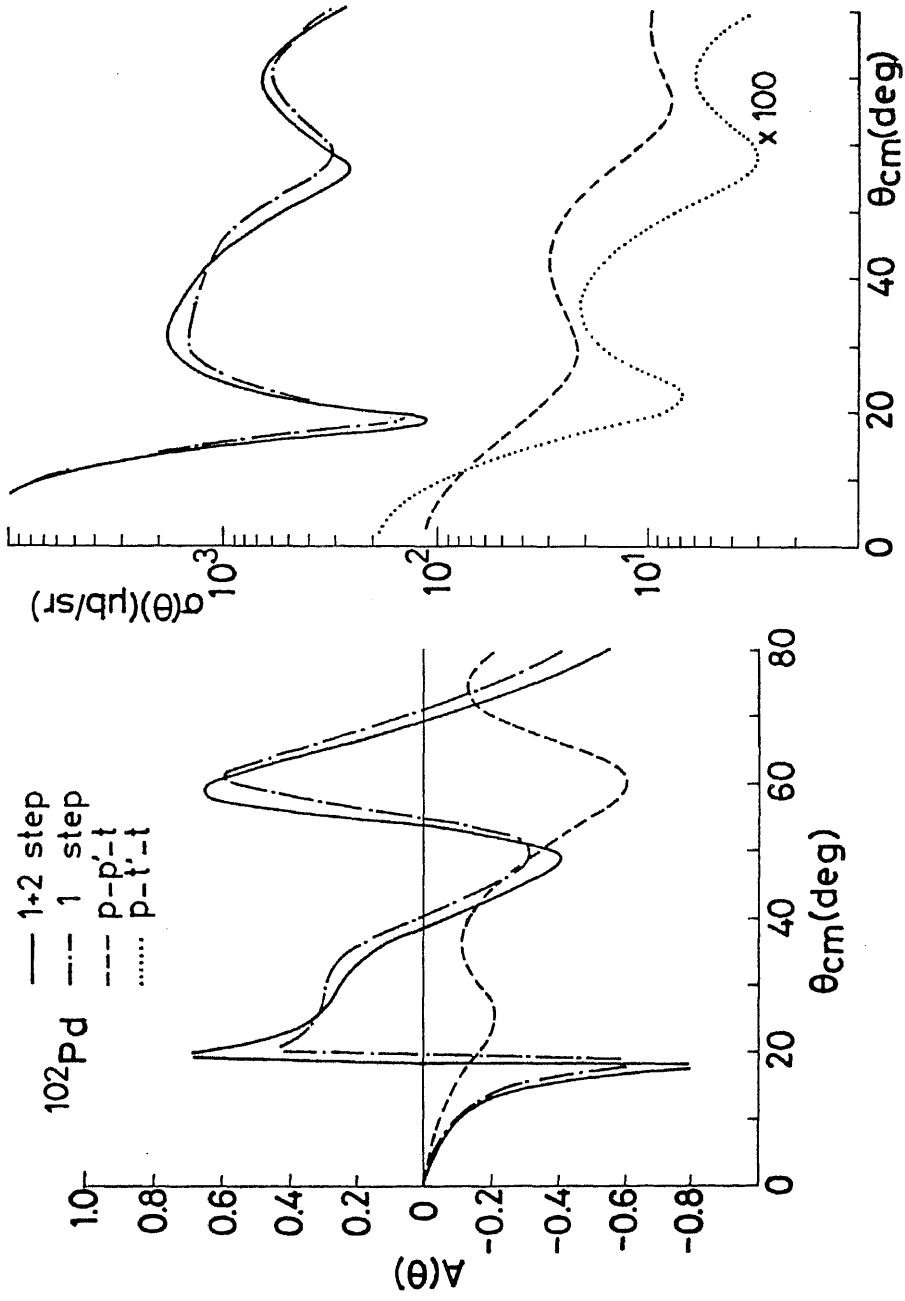


Fig. 27

Appendix 1 Expression for the  $A(\theta)$  in terms of the reduced amplitude B

We first define two right-handed coordinate systems; the system  $S_1$  and the system  $S_2$ . In the system  $S_1$ , the z-axis is perpendicular to the reaction plane and the y-axis is parallel to the direction of an incident beam. The system  $S_2$  is the same as that defined by the Madison convention in which z-axis is taken to be parallel to the direction of the incident beam and the y-axis is perpendicular to the reaction plane. The calculation of the reduced amplitude is usually made in the system  $S_2$ , because the polar angle in the system  $S_2$  equals the scattering angle. The reduced amplitudes B described in each system are connected by the equation<sup>3)</sup>

$$B_j^{m'_f \sigma'_f \sigma'_i}(S_1) = \sum_{m_f \sigma_f \sigma_i} B_j^{m_f \sigma_f \sigma_i}(S_2) D_{\mu \mu'}^{j*}(R_{12}) D_{\sigma_f \sigma'_f}^{S_f*}(R_{12}) D_{\sigma_i \sigma'_i}^{S_i}(R_{12}), \quad (\text{A1.1})$$

where the  $D_{\mu \mu'}^j(R_{12})$  are the rotation matrices and  $R_{12}$  means the Euler angles of the rotation necessary to take the system  $S_1$  into coincidence with the system  $S_2$ . In this case,  $R_{12} = (\pi/2, \pi/2, \pi/2)$  and  $\mu = m_f + \sigma_f - \sigma_i$  and  $\mu' = m'_f + \sigma'_f - \sigma'_i$ .

As shown in eq. (33), the differential cross section for the spin substates  $m'_f, \sigma'_f, \sigma'_i$  are proportional to the value  $|B_j^{m'_f \sigma'_f \sigma'_i}|^2$ . In the case of an incident particle with spin 1/2, we can easily express the analyzing power in the system  $S_1$  on the basis of the physical meaning of eq. (38),

$$\begin{aligned}
A(\theta) &= \frac{\sum_{j m_f' \sigma_f'} \left[ |B_j^{m_f' \sigma_f' \frac{1}{2}}(s_1)|^2 - |B_j^{m_f' \sigma_f' -\frac{1}{2}}(s_1)|^2 \right]}{\sum_{j m_f' \sigma_f' \sigma_i'} |B_j^{m_f' \sigma_f' \sigma_i'}(s_1)|^2} \\
&= \frac{\sum_{j m_f' \sigma_f' \sigma_i'} \sigma_i' B_j^{m_f' \sigma_f' \sigma_i'}(s_1) B_j^{m_f' \sigma_f' \sigma_i'}(s_1)^*}{s_i \sum_{j m_f' \sigma_f' \sigma_i'} |B_j^{m_f' \sigma_f' \sigma_i'}(s_1)|^2} \quad (A1.2)
\end{aligned}$$

In order to use the reduced amplitude described in the system  $S_2$ , it is necessary to transform the above expression from the system  $S_1$  to the system  $S_2$ . By inserting eq. (A1.1) into eq. (A1.2), the numerator of eq. (A2.2) is written as

$$\begin{aligned}
&\sum_{j m_f' \sigma_f' \sigma_i'} \sigma_i' B_j^{m_f' \sigma_f' \sigma_i'}(s_1) B_j^{m_f' \sigma_f' \sigma_i'}(s_1)^* \\
&= \sqrt{s_i(s_i+1)} \sum_{j m_f' \sigma_f' \sigma_i'} \langle S_i, 1 \sigma_i' | S_i, \sigma_i \rangle \sum_{\substack{m_f \sigma_f \sigma_i \\ m_f'' \sigma_f'' \sigma_i''}} B_j^{m_f \sigma_f \sigma_i}(s_2) B_j^{m_f'' \sigma_f'' \sigma_i''}(s_2)^* \\
&\quad \times D_{\mu \mu'}^{j*}(R_{12}) D_{\mu'' \mu'''}^j(R_{12}) D_{\sigma_f \sigma_f'}^{S_f*}(R_{12}) D_{\sigma_f'' \sigma_f'''}^{S_f}(R_{12}) D_{\sigma_i \sigma_i'}^{S_i}(R_{12}) D_{\sigma_i'' \sigma_i'''}^{S_i}(R_{12})
\end{aligned} \quad (A1.3)$$

Generally, the rotation matrices satisfy the equation

$$\sum_{m'} D_{m m'}^{S*}(R_{12}) D_{m'' m'}^S(R_{12}) = \delta_{m m''}$$

and

$$\begin{aligned}
& D_{mm'}^{S*}(R_{12}) D_{m''m'}^S(R_{12}) \\
& = (-1)^{m-m'} \sum_k \langle SS-mm'' | kq \rangle \langle SS-m'm' | k0 \rangle D_{q0}^k(R_{12}) . \quad (A1.4)
\end{aligned}$$

Then, applying these relations to the rotation matrices, the eq. (A1.3) can be rewritten as

$$\begin{aligned}
& \sum_{j m_f' \sigma_f' \sigma_i'} \sigma_i' B_j^{m_f' \sigma_f' \sigma_i'}(S_1) B_j^{m_f' \sigma_f' \sigma_i'}(S_1)^* \\
& = \sqrt{S_i(S_i+1)} \sum_{j m_f \sigma_f \sigma_i} \sum_q D_{q0}^1 (-1)^q \langle S_i 1 \sigma_i - q | S_i \sigma_i - q \rangle \\
& \quad \times B_j^{m_f \sigma_f \sigma_i}(S_2) B_j^{m_f \sigma_f \sigma_i}(S_1)^* . \quad (A1.5)
\end{aligned}$$

Summing over  $q$ , we can obtain the following results;

$$\begin{aligned}
& \sum_{j m_f' \sigma_f' \sigma_i'} \sigma_i' B_j^{m_f' \sigma_f' \sigma_i'}(S_1) B_j^{m_f' \sigma_f' \sigma_i'}(S_1)^* \\
& = - \sum_{j m_f \sigma_f \sigma_i} \sqrt{(S_i - \sigma_i)(S_i + \sigma_i + 1)} \text{Im} \left[ B_j^{m_f \sigma_f \sigma_i}(S_2) B_j^{m_f-1, \sigma_f, \sigma_i+1}(S_2)^* \right] , \quad (A1.6)
\end{aligned}$$

where the notation  $\text{Im}$  means "taking the imaginary parts".

The denominator of eq. (A1.2) has the same expression after the transformation. Then the analyzing power is expressed in the system  $S_2$  as the function of the scattering angle  $\theta$ :

$$A(\theta) = - \frac{\sum_{j m_f \sigma_f \sigma_i} \sqrt{(S_i - \sigma_i)(S_i + \sigma_i + 1)} \text{Im} \left[ B_j^{m_f \sigma_f \sigma_i}(\theta) B_j^{m_f-1, \sigma_f, \sigma_i+1}(\theta)^* \right]}{S_i \sum_{j m_f \sigma_f \sigma_i} |B_j^{m_f \sigma_f \sigma_i}(\theta)|^2} . \quad (A1.7)$$

Appendix 2 Derivative relation between the  $A(\theta)$  and  $\sigma(\theta)$

The one-step DWBA leads to the derivative relation between the  $A(\theta)$  and  $\sigma(\theta)$  in the ground state  $0_g^+(p,t)0_g^+$  transition. This relation does not depend on whether the zero-range or the finite-range approximation is employed. In this appendix, we follow the procedure given by K. I. Kubo<sup>37)</sup> using the zero-range approximation.

The reduced amplitude  $\beta$  described in the system  $S_2$  (see Appendix 1) generally satisfies the following relation<sup>3)</sup>:

$$\beta_{l s j}^{m_f \sigma_f \sigma_i}(\theta) = (-1)^{m_f + j' + l + s_f - s_i} \beta_{l s j}^{-m_f - \sigma_f - \sigma_i}(\theta) . \quad (\text{A2.1})$$

In the  $(p,t)$  transition between  $0_g^+$  ground states, we have  $l=s=j=0$  and  $s_i=s_f$ . Then the eq. (A2.1) becomes

$$\beta^{m_f \sigma_f \sigma_i}(\theta) = (-1)^{m_f} \beta^{-m_f - \sigma_f - \sigma_i}(\theta) . \quad (\text{A2.2})$$

Here we drop the  $l, s, j$  because they are unique. By using the above relation, the differential cross section in eq. (33) can be written as

$$\sigma(\theta) = K ( |B^{0 \frac{1}{2} \frac{1}{2}}(\theta)|^2 + |B^{1 \frac{1}{2} - \frac{1}{2}}(\theta)|^2 ) , \quad (\text{A2.3})$$

where

$$K \equiv \frac{\mu_i \mu_f}{(2\pi \hbar^2)^2} \cdot \frac{k_f}{k_i} \cdot \frac{2J_f + 1}{2J_i + 1} . \quad (\text{A2.4})$$

From eq. (41), the analyzing power is written as

$$A(\theta) = \frac{2 \operatorname{Im} [ B^{\circ \frac{1}{2} \frac{1}{2}}(\theta) B^{|\frac{1}{2} - \frac{1}{2}|*}(\theta) ]}{|B^{\circ \frac{1}{2} \frac{1}{2}}(\theta)|^2 + |B^{|\frac{1}{2} - \frac{1}{2}|}(\theta)|^2} \quad (\text{A2.5})$$

The explicit form of the reduced amplitude is given by<sup>3)</sup>

$$B_j^{m_f \sigma_f \sigma_i}(\theta) = \sum_{\ell s} A_{\ell s}^{J_f J_i} \sum_{L_f J_f}^{L_i - L_f - \ell} i^{L_i - L_f - \ell} \left[ \frac{(L_f - m_f)!}{(L_f + m_f)!} \right]^{1/2} \begin{pmatrix} j & \ell & s \\ J_i & L_i & S_i \\ J_f & L_f & S_f \end{pmatrix} P_{L_f}^{m_f}(\theta) I_{L_f J_f, L_i J_i}^{\ell s j} \\ \times \hat{L}_f^2 \hat{\ell} \hat{s} \hat{L}_i \hat{J}_f \langle J_f j \sigma_f - m_f, m_f - \sigma_f + \sigma_i | J_i \sigma_i \rangle \\ \times \langle L_i S_i 0 \sigma_i | J_i \sigma_i \rangle \langle L_f S_f - m_f \sigma_f | J_f \sigma_f - m_f \rangle \langle L_f \ell 0 0 | L_i 0 \rangle, \quad (\text{A2.6})$$

where  $L_i$  ( $L_f$ ) and  $J_i$  ( $J_f$ ) are the orbital and the total angular momentum of the initial (final) partial wave, respectively, and  $\hat{x}$  stands for  $(2x+1)^{1/2}$ . When  $l=s=j=0$ , we have  $L_i=L_f=L$  and  $J_i=J_f=J$  because of the property of the vector coupling. In this case, the radial integral  $I_{L_f J_f, L_i J_i}^{\ell s j}$  is reduced to the form of

$$I_{LJ} = \frac{2\pi^{1/2}}{k_i k_f} \cdot \frac{B}{A} \int f_{LJ} \left( \frac{A}{B} r \right) F_0(r) f_{LJ}(r) dr, \quad (\text{A2.7})$$

where  $A$  and  $B$  are the masses of target and residual nucleus, respectively, and  $f_{LJ}$  is the partial wave of the distorted wave. The  $F_0(r)$  is the radial part of the form factor.

We consider the spin-orbit force as a perturbation and assume that it affects only phase shifts of the partial wave:

$$f_{LJ} \approx \hat{f}_L e^{iC_L \langle \vec{L} \cdot \vec{\sigma} \rangle}, \quad (\text{A2.8})$$

where

$$\langle \vec{L} \cdot \vec{\sigma} \rangle = L \quad \text{for } J = L + \frac{1}{2}$$

$$\text{or } -(L+1) \quad \text{for } J = L - \frac{1}{2}.$$

The  $\hat{f}_L$  is a partial wave in the case of no spin-orbit coupling and independent of  $J$ . The  $C_L$  is a small parameter related to the strength of the spin-orbit force. By inserting eq. (A2.8) into eq. (A2.7), we obtain

$$I_{LJ} = e^{i\bar{C}_L \langle \vec{L} \cdot \vec{\sigma} \rangle} \hat{I}_L, \quad (\text{A2.9})$$

where  $\hat{I}_L$  is the radial integral in terms of  $\hat{f}_L$ , and  $\bar{C}_L$  is a sum of two  $C_L$ 's for the incident and exit channel.

From eq. (A2.6), we have

$$B^{o \frac{1}{2} \frac{1}{2}}(\theta) = \frac{A_0}{2\sqrt{2}} \sum_{LJ} (2J+1) I_{LJ} P_L(\theta), \quad (\text{A2.10})$$

and

$$B^{i \frac{1}{2} \frac{1}{2}}(\theta) = \frac{A_0}{\sqrt{2}} \sum_{LJ} (-1)^{J-L-\frac{1}{2}} I_{LJ} P_L^i(\theta), \quad (\text{A2.11})$$

where  $A_0$  denotes the spectroscopic amplitude. By inserting

eq. (A2.9) into eqs. (A2.10) and (A2.11), and applying a Taylor expansion for exponent in eq. (A2.9), we obtain the following results in the first-order approximation for  $\bar{C}_L$ ;

$$B^{0\frac{1}{2}\frac{1}{2}}(\theta) = \frac{A_0}{\sqrt{2}} \sum_L (2L+1) \hat{I}_L P_L(\theta) \quad , \quad (\text{A2.12})$$

and

$$B^{1\frac{1}{2}-\frac{1}{2}}(\theta) = \frac{i}{\sqrt{2}} A_0 \sum_L \bar{C}_L (2L+1) \hat{I}_L P_L'(\theta) \quad . \quad (\text{A2.13})$$

If we assume that the  $\bar{C}_L$  is effective only for a few L, we can take it outside the summation over L and replace it by an average quantity  $\bar{C}$ . This procedure is similar to that by R. C. Johnson<sup>38)</sup>. Then we have the following relation by comparing eq. (A2.12) with (A2.13):

$$\frac{d}{d\theta} B^{0\frac{1}{2}\frac{1}{2}}(\theta) = \frac{i}{\bar{C}} B^{1\frac{1}{2}-\frac{1}{2}}(\theta) \quad , \quad (\text{A2.14})$$

because we have the relation

$$\frac{d}{d\theta} P_L(\theta) = -P_L'(\theta) \quad . \quad (\text{A2.15})$$

In the expression for the cross section (A2.3), the first term of the right-hand side is dominant because the second term is proportional to  $C^2$  from eq. (A2.13) and can be neglected in our first-order approximation. Then we have

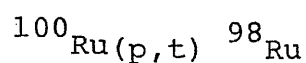
$$\sigma(\theta) \approx K |B^{o\frac{1}{2}\frac{1}{2}}(\theta)|^2 . \quad (\text{A2.16})$$

By inserting eqs. (A2.14) and (A2.16) to eq. (A2.5), we obtain the final result:

$$A(\theta) = \bar{C} \frac{d}{d\theta} \sigma(\theta) / \sigma(\theta) . \quad (\text{A2.17})$$

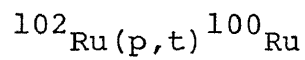
Appendix 3

A3.1. Experimental results of differential cross sections  $\sigma(\theta)$  and analyzing powers  $A(\theta)$  in the center of mass system for (p,t) ground-state transitions. Statistical errors are indicated by  $\delta\sigma/\sigma$  and  $\delta A$ .



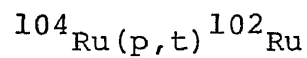
$\theta_{\text{lab}}$ (deg)	$\theta_{\text{cm}}$ (deg)	$\sigma(\theta)$ ( $\mu\text{b}/\text{sr}$ )	$\delta\sigma/\sigma$ (%)	$A(\theta)$ ( $\times 100$ )	$\delta A$ ( $\times 100$ )
7.5	7.7	5044	0.2	4.8	0.2
10.0	10.2	3224	0.2	6.4	0.3
12.5	12.8	1613	0.3	8.1	0.4
15.0	15.3	590	0.5	14.0	0.6
17.5	17.9	119	1.2	33.8	1.4
20.0	20.5	108	1.3	26.2	1.5
25.0	25.6	653	0.5	11.8	0.6
30.0	30.7	1004	0.4	9.8	0.5
35.0	35.8	902	0.4	2.3	0.5
40.0	40.8	602	0.4	-14.7	0.5
45.0	45.9	306	0.5	-41.7	0.6
50.0	51.0	111	0.9	-53.9	0.9
55.0	56.1	94	1.0	24.8	1.1
60.0	61.1	201	0.7	16.6	0.8
65.0	66.2	290	0.6	- 8.7	0.7

A3.2. Experimental results of differential cross sections  $\sigma(\theta)$  and analyzing powers  $A(\theta)$  in the center of mass system for (p,t) ground-state transitions. Statistical errors are indicated by  $\delta\sigma/\sigma$  and  $\delta A$ .



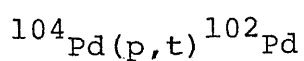
$\theta_{\text{lab}}$ (deg)	$\theta_{\text{cm}}$ (deg)	$\sigma(\theta)$ ( $\mu\text{b}/\text{sr}$ )	$\delta\sigma/\sigma$ (%)	$A(\theta)$ ( $\times 100$ )	$\delta A$ ( $\times 100$ )
5.0	5.1	6548	0.2	1.7	0.3
10.0	10.2	2923	0.3	4.4	0.4
12.5	12.8	1374	0.4	6.1	0.5
15.0	15.3	499	0.8	6.8	0.9
17.5	17.9	89	1.5	12.7	1.9
20.0	20.4	65	2.1	18.9	2.5
22.5	23.0	241	0.9	14.2	1.1
25.0	25.5	477	0.8	14.2	1.1
30.0	30.6	769	0.5	11.8	0.6
35.0	35.7	769	0.5	1.4	0.6
40.0	40.8	570	0.4	-15.3	0.5
45.0	45.9	291	0.6	-40.4	0.7
50.0	50.9	95	1.1	-49.7	1.2
55.0	56.0	96	0.9	27.0	1.1
60.0	61.1	206	0.6	12.8	0.8
65.0	66.1	265	0.6	-11.4	0.7

A3.3. Experimental results of differential cross sections  $\sigma(\theta)$  and analyzing powers  $A(\theta)$  in the center of mass system for (p,t) ground-state transitions. Statistical errors are indicated by  $\delta\sigma/\sigma$  and  $\delta A$ .



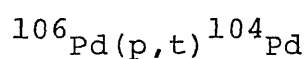
$\theta_{\text{lab}}$ (deg)	$\theta_{\text{cm}}$ (deg)	$\sigma(\theta)$ ( $\mu\text{b}/\text{sr}$ )	$\delta\sigma/\sigma$ (%)	$A(\theta)$ ( $\times 100$ )	$\delta A$ ( $\times 100$ )
5.0	5.1	5669	0.3	2.0	0.3
10.0	10.2	2614	0.4	4.3	0.5
15.0	15.3	499	0.9	2.9	1.0
18.0	18.4	54	2.7	-21.7	3.1
20.0	20.4	30	3.6	-30.6	4.0
22.5	23.0	156	1.6	7.6	1.8
25.0	25.5	331	1.1	16.2	1.2
30.0	30.6	614	0.8	11.8	0.9
35.0	35.7	705	0.6	1.5	0.7
40.0	40.8	563	0.6	-14.8	0.8
45.0	45.8	269	0.7	-38.7	0.9
50.0	50.9	80	1.3	-45.9	1.5
55.0	56.0	99	1.1	28.9	1.3
60.0	61.0	211	0.7	11.7	0.9
65.0	66.1	253	0.7	- 9.0	0.8

A3.4. Experimental results of differential cross sections  $\sigma(\theta)$  and analyzing powers  $A(\theta)$  in the center of mass system for (p,t) ground-state transitions. Statistical errors are indicated by  $\delta\sigma/\sigma$  and  $\delta A$ .



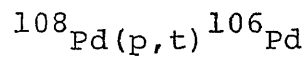
$\theta_{\text{lab}}$ (deg)	$\theta_{\text{cm}}$ (deg)	$\sigma(\theta)$ ( $\mu\text{b}/\text{sr}$ )	$\delta\sigma/\sigma$ (%)	$A(\theta)$ ( $\times 100$ )	$\delta A$ ( $\times 100$ )
10.0	10.2	2625	0.3	5.4	0.3
12.5	12.8	1324	1.3	8.6	1.6
15.0	15.3	422	1.4	18.1	1.7
17.5	17.9	93	2.1	46.1	2.3
20.0	20.4	201	1.5	24.4	1.8
22.5	23.0	540	1.3	9.9	1.5
25.0	25.5	920	1.4	7.6	1.7
30.0	30.6	1207	0.4	7.0	0.5
35.0	35.7	967	0.4	0.2	0.5
40.0	40.8	547	0.6	-16.9	0.7
45.0	45.9	219	0.7	-49.2	0.7
50.0	51.0	81	1.1	-43.3	1.2
55.0	56.0	114	0.9	29.9	1.0
60.0	61.1	231	0.7	12.2	0.7
65.0	66.2	297	0.6	-11.0	0.7

A3.5. Experimental results of differential cross sections  $\sigma(\theta)$  and analyzing powers  $A(\theta)$  in the center of mass system for (p,t) ground-state transitions. Statistical errors are indicated by  $\delta\sigma/\sigma$  and  $\delta A$ .



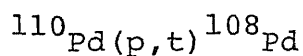
$\theta_{\text{lab}}$ (deg)	$\theta_{\text{cm}}$ (deg)	$\sigma(\theta)$ ( $\mu\text{b}/\text{sr}$ )	$\delta\sigma/\sigma$ (%)	$A(\theta)$ ( $\times 100$ )	$\delta A$ ( $\times 100$ )
5.0	5.1	6924	0.2	2.3	0.2
10.0	10.2	2967	0.3	4.4	0.3
12.5	12.8	1439	0.7	5.5	0.9
15.0	15.3	446	0.7	12.0	0.8
17.5	17.9	60	1.8	54.5	1.9
20.0	20.4	166	1.1	24.4	1.2
22.5	23.0	465	1.3	16.2	1.5
25.0	25.5	784	0.5	13.2	0.6
30.0	30.6	1111	0.3	8.9	0.3
35.0	35.7	950	0.5	- 1.5	0.5
40.0	40.8	580	0.5	-20.6	0.6
45.0	45.9	255	0.6	-49.0	0.7
50.0	50.9	90	1.1	-33.2	1.2
55.0	56.0	142	0.8	28.9	1.0
60.0	61.0	277	0.5	7.6	0.6
65.0	66.1	330	0.5	-15.1	0.6

A3.6. Experimental results of differential cross sections  $\sigma(\theta)$  and analyzing powers  $A(\theta)$  in the center of mass system for (p,t) ground-state transitions. Statistical errors are indicated by  $\delta\sigma/\sigma$  and  $\delta A$ .



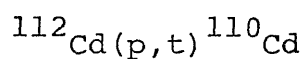
$\theta_{\text{lab}}$ (deg)	$\theta_{\text{cm}}$ (deg)	$\sigma(\theta)$ ( $\mu\text{b}/\text{sr}$ )	$\delta\sigma/\sigma$ (%)	$A(\theta)$ ( $\times 100$ )	$\delta A$ ( $\times 100$ )
5.0	5.1	8246	0.2	2.1	0.3
10.0	10.2	3704	0.3	3.7	0.4
12.5	12.8	1799	0.7	5.1	0.8
15.0	15.3	563	1.0	6.8	1.1
17.5	17.8	62	2.1	23.8	2.4
20.0	20.4	89	1.5	30.6	1.8
22.5	22.9	394	1.0	17.0	1.2
25.0	25.5	688	0.5	12.6	0.6
30.0	30.6	1119	0.4	9.9	0.5
35.0	35.7	1096	0.4	0.2	0.5
40.0	40.7	758	0.4	-18.0	0.5
45.0	45.8	351	0.6	-43.0	0.7
50.0	50.9	113	1.1	-38.0	1.3
55.0	55.9	171	0.8	27.8	1.0
60.0	61.0	345	0.5	9.8	0.6
65.0	66.0	401	0.5	-12.6	0.6

A3.7. Experimental results of differential cross sections  $\sigma(\theta)$  and analyzing powers  $A(\theta)$  in the center of mass system for (p,t) ground-state transitions. Statistical errors are indicated by  $\delta\sigma/\sigma$  and  $\delta A$ .



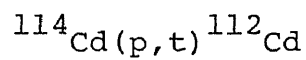
$\theta_{\text{lab}}$ (deg)	$\theta_{\text{cm}}$ (deg)	$\sigma(\theta)$ ( $\mu\text{b}/\text{sr}$ )	$\delta\sigma/\sigma$ (%)	$A(\theta)$ ( $\times 100$ )	$\delta A$ ( $\times 100$ )
7.5	7.6	6567	0.2	2.3	0.3
10.0	10.2	4119	0.3	3.2	0.3
12.5	12.7	1843	0.9	3.0	1.1
15.0	15.3	780	0.7	- 0.3	0.8
16.0	16.3	348	1.3	0.1	1.6
17.5	17.8	99	1.8	-13.9	2.1
18.5	18.8	36	2.9	-23.9	3.5
20.0	20.4	57	2.4	5.8	2.9
21.0	21.4	129	1.6	14.9	1.9
22.5	22.9	277	1.1	16.8	1.3
25.0	25.5	582	1.0	17.6	1.2
30.0	30.6	1082	0.4	12.4	0.4
35.0	35.6	1192	0.4	1.3	0.5
40.0	40.7	877	0.4	-15.4	0.5
45.0	45.8	391	0.6	-40.6	0.7
50.0	50.8	122	1.1	-41.4	1.2
55.0	55.9	192	0.9	26.0	1.0
60.0	61.0	376	0.6	10.1	0.7
65.0	66.0	415	0.6	-10.6	0.7

A3.8. Experimental results of differential cross sections  $\sigma(\theta)$  and analyzing powers  $A(\theta)$  in the center of mass system for (p,t) ground-state transitions. Statistical errors are indicated by  $\delta\sigma/\sigma$  and  $\delta A$ .



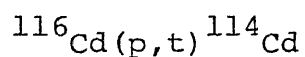
$\theta_{\text{lab}}$ (deg)	$\theta_{\text{cm}}$ (deg)	$\sigma(\theta)$ ( $\mu\text{b}/\text{sr}$ )	$\delta\sigma/\sigma$ (%)	$A(\theta)$ ( $\times 100$ )	$\delta A$ ( $\times 100$ )
5.0	5.1	8196	0.1	0.9	0.2
10.0	10.2	3543	0.3	1.8	0.4
12.5	12.7	1644	0.5	2.8	0.6
15.0	15.3	501	0.9	8.8	1.1
17.5	17.8	94	1.5	47.9	1.7
20.0	20.4	247	0.9	30.5	1.1
22.5	22.9	641	0.8	17.8	1.0
25.0	25.5	1034	0.5	14.6	0.6
30.0	30.6	1405	0.4	7.5	0.5
35.0	35.7	1152	0.4	-1.5	0.5
40.0	40.7	679	0.4	-21.5	0.5
45.0	45.8	268	0.6	-50.5	0.7
50.0	50.9	103	1.0	-19.6	1.2
55.0	55.9	198	0.6	29.9	0.5
60.0	61.0	373	0.4	6.0	0.5
65.0	66.0	418	0.4	-16.6	0.5

A3.9. Experimental results of differential cross sections  $\sigma(\theta)$  and analyzing powers  $A(\theta)$  in the center of mass system for (p,t) ground-state transitions. Statistical errors are indicated by  $\delta\sigma/\sigma$  and  $\delta A$ .



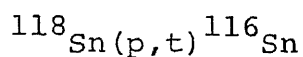
$\theta_{\text{lab}}$ (deg)	$\theta_{\text{cm}}$ (deg)	$\sigma(\theta)$ ( $\mu\text{b}/\text{sr}$ )	$\delta\sigma/\sigma$ (%)	$A(\theta)$ ( $\times 100$ )	$\delta A$ ( $\times 100$ )
5.0	5.1	8683	0.2	1.1	0.2
10.0	10.2	3872	0.3	1.8	0.4
12.5	12.7	1862	0.5	0.9	0.5
13.8	14.0	1117	0.6	2.2	0.7
15.0	15.3	573	0.8	5.9	1.0
16.3	16.6	240	1.3	9.9	1.5
17.5	17.8	85	1.7	41.1	1.9
20.0	20.4	171	1.5	38.7	1.7
22.5	22.9	551	0.8	22.2	1.0
25.0	25.5	959	0.6	15.3	0.7
30.0	30.5	1414	0.4	10.3	0.4
35.0	35.6	1263	0.4	- 0.8	0.4
40.0	40.7	800	0.4	-19.6	0.5
45.0	45.8	311	0.6	-48.8	0.7
50.0	50.8	114	1.1	-16.5	1.2
55.0	55.9	234	0.8	26.8	0.9
60.0	60.9	430	0.6	6.1	0.7
65.0	66.0	446	0.5	-16.0	0.6

A3.10. Experimental results of differential cross sections  $\sigma(\theta)$  and analyzing powers  $A(\theta)$  in the center of mass system for (p,t) ground-state transitions. Statistical errors are indicated by  $\delta\sigma/\sigma$  and  $\delta A$ .



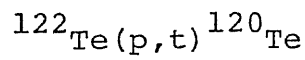
$\theta_{\text{lab}}$ (deg)	$\theta_{\text{cm}}$ (deg)	$\sigma(\theta)$ ( $\mu\text{b}/\text{sr}$ )	$\delta\sigma/\sigma$ (%)	$A(\theta)$ ( $\times 100$ )	$\delta A$ ( $\times 100$ )
5.0	5.1	5726	0.9	1.1	1.1
10.0	10.2	2739	0.5	1.6	0.5
12.5	12.7	1244	1.4	1.5	1.6
15.0	15.3	453	1.2	- 2.5	1.3
17.0	17.3	98	2.4	2.1	2.9
18.5	18.8	24	3.5	54.3	3.8
20.0	20.4	63	3.1	50.3	3.4
22.5	22.9	247	2.2	24.7	2.6
25.0	25.4	469	2.2	22.4	2.6
30.0	30.5	859	0.6	12.1	0.7
35.0	35.6	864	0.6	- 0.7	0.7
40.0	40.7	576	0.7	-18.4	0.8
45.0	45.7	230	1.7	-49.0	1.7
50.0	50.8	77	2.0	-25.4	2.3
55.0	55.9	169	1.4	27.1	1.5
60.0	60.9	311	1.0	9.1	1.1
65.0	65.9	315	1.0	-11.6	1.1

A3.11 Experimental results of differential cross sections  $\sigma(\theta)$  and analyzing powers  $A(\theta)$  in the center of mass system for (p,t) ground-state transitions. Statistical errors are indicated by  $\delta\sigma/\sigma$  and  $\delta A$ .



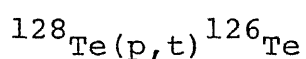
$\theta_{\text{lab}}$ (deg)	$\theta_{\text{cm}}$ (deg)	$\sigma(\theta)$ ( $\mu\text{b}/\text{sr}$ )	$\delta\sigma/\sigma$ (%)	$A(\theta)$ ( $\times 100$ )	$\delta A$ ( $\times 100$ )
5.0	5.1	6877	0.2	0.5	0.3
7.5	7.6			- 0.1	0.5
10.0	10.2	2903	0.4	- 0.5	0.5
12.5	12.7	1338	0.8	- 0.3	1.0
15.0	15.3	396	1.4	7.3	1.7
17.5	17.8	124	2.1	54.8	2.3
20.0	20.4	357	1.5	34.4	1.8
22.5	22.9	797	1.0	20.0	1.2
25.0	25.5	1249	0.7	16.3	0.8
30.0	30.5	1563	0.6	9.0	0.7
35.0	35.6	1235	0.7	- 3.6	0.8
40.0	40.7	639	0.9	-24.0	1.1
45.0	45.8	212	1.4	-62.5	1.5
50.0	50.8	98	2.1	1.8	2.5
55.0	55.9	260	1.3	31.0	1.5
60.0	61.0	423	1.0	4.0	1.2
65.0	66.0	428	1.0	-17.0	1.2

A3.12. Experimental results of differential cross sections  $\sigma(\theta)$  and analyzing powers  $A(\theta)$  in the center of mass system for (p,t) ground-state transitions. Statistical errors are indicated by  $\delta\sigma/\sigma$  and  $\delta A$ .



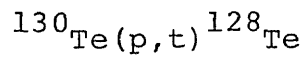
$\theta_{\text{lab}}$ (deg)	$\theta_{\text{cm}}$ (deg)	$\sigma(\theta)$ ( $\mu\text{b}/\text{sr}$ )	$\delta\sigma/\sigma$ (%)	$A(\theta)$ ( $\times 100$ )	$\delta A$ ( $\times 100$ )
5.0	5.1	4089	1.0	0.6	1.2
10.0	10.2	1769	0.5	2.2	0.5
12.5	12.7	713	1.7	3.1	2.1
15.0	15.3	238	1.3	12.5	1.5
17.5	17.8	115	2.2	34.2	2.5
20.0	20.4	330	1.1	18.1	1.2
22.5	22.9	721	1.7	12.7	2.1
25.0	25.5	1018	1.5	9.0	1.8
30.0	30.5	1216	0.6	5.4	0.7
35.0	35.6	855	0.5	-3.5	0.6
39.0	39.7	454	0.6	-20.6	0.8
45.0	45.8	101	1.4	-60.8	1.4
50.0	50.8	83	1.5	14.9	1.7
55.0	55.9	198	1.0	22.8	1.1
60.0	60.9	300	0.8	0.5	1.0
65.0	66.0	292	0.8	-19.5	1.0

A3.13. Experimental results of differential cross sections  $\sigma(\theta)$  and analyzing powers  $A(\theta)$  in the center of mass system for (p,t) ground-state transitions. Statistical errors are indicated by  $\delta\sigma/\sigma$  and  $\delta A$ .



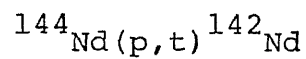
$\theta_{\text{lab}}$ (deg)	$\theta_{\text{cm}}$ (deg)	$\sigma(\theta)$ ( $\mu\text{b}/\text{sr}$ )	$\delta\sigma/\sigma$ (%)	$A(\theta)$ ( $\times 100$ )	$\delta A$ ( $\times 100$ )
5.0	5.1	5619	0.4	- 1.2	0.4
7.5	7.6	4017	0.5	- 0.9	0.5
10.0	10.2	2413	0.6	- 1.5	0.7
12.5	12.7	1136	1.9	- 2.5	2.2
15.0	15.3	317	2.5	- 2.5	3.0
17.5	17.8	66	3.4	54.3	3.7
20.0	20.3	193	2.0	42.4	2.3
25.0	25.4	849	1.2	16.4	1.5
30.0	30.5	1114	0.6	10.3	0.7
35.0	35.6	903	0.8	- 2.3	1.0
40.0	40.6	464	1.1	-26.9	1.4
45.0	45.7	129	2.1	-58.7	2.3
50.0	50.7	96	2.5	18.7	2.9
55.0	55.8	248	0.9	23.2	1.0
60.0	60.8	383	0.7	4.2	0.8
65.0	65.9	326	0.8	-18.1	0.9

A3.14. Experimental results of differential cross sections  $\sigma(\theta)$  and analyzing powers  $A(\theta)$  in the center of mass system for (p,t) ground-state transitions. Statistical errors are indicated by  $\delta\sigma/\sigma$  and  $\delta A$ .



$\theta_{\text{lab}}$ (deg)	$\theta_{\text{cm}}$ (deg)	$\sigma(\theta)$ ( $\mu\text{b}/\text{sr}$ )	$\delta\sigma/\sigma$ (%)	$A(\theta)$ ( $\times 100$ )	$\delta A$ ( $\times 100$ )
7.5	7.6	2852	0.5	- 2.6	0.6
10.0	10.2	1643	0.7	-, 2.8	0.8
15.0	15.2	239	1.8	- 0.3	2.1
20.0	20.3	125	2.5	42.4	2.6
25.0	25.4	546	1.0	18.8	1.1
30.0	30.5	792	0.8	10.9	0.9
35.0	35.5	673	0.8	0.9	0.9
40.0	40.6	351	1.1	-22.7	1.2
45.0	45.6	98	1.6	-57.6	1.6
50.0	50.7	77	1.8	19.1	2.1
55.0	55.8	217	1.0	23.0	1.1
60.0	60.8	271	0.9	4.3	1.0
65.0	65.8	223	0.9	-15.6	1.1

A3.15. Experimental results of differential cross sections  $\sigma(\theta)$  and analyzing powers  $A(\theta)$  in the center of mass system for (p,t) ground-state transitions. Statistical errors are indicated by  $\delta\sigma/\sigma$  and  $\delta A$ .



$\theta_{\text{lab}}$ (deg)	$\theta_{\text{cm}}$ (deg)	$\sigma(\theta)$ ( $\mu\text{b}/\text{sr}$ )	$\delta\sigma/\sigma$ (%)	$A(\theta)$ ( $\times 100$ )	$\delta A$ ( $\times 100$ )
5.0	5.1	1093	0.8	2.2	1.1
7.5	7.6	757	1.6	- 0.2	1.8
10.0	10.1	408	1.3	4.1	2.5
12.5	12.7	163	2.2	6.6	2.6
14.5	14.7	55	3.8	9.6	4.7
15.0	15.2	43	4.0	41.1	6.5
16.5	16.7	15	7.3	31.0	10.5
20.0	20.3	89	2.8	20.3	3.9
25.0	25.3	281	1.1	10.9	1.5
30.0	30.4	359	1.0	2.0	1.2
35.0	35.5	258	1.2	- 7.8	1.5
40.0	40.5	97	1.9	-31.4	2.9
42.5	43.0	43	3.3	-48.7	5.5
45.0	45.6	28	3.3	-31.1	5.1
47.5	48.1	46	3.2	1.1	3.9
50.0	50.6	75	2.0	12.2	2.7
55.0	55.7	143	1.5	2.9	1.8
60.0	60.7	141	1.5	-13.4	2.0
65.0	65.7	81	2.0	-30.6	3.0